The Role of Motor Primitives in the Control of Movement and Learning

by

Francesca Gandolfo

Submitted to the Department of Brain and Cognitive Sciences
in partial fulfillment of the requirements for the degree of

Doctor of Philosophy in Computational Neuroscience

at the

MASSACHUSETTS INSTITUTE OF TECHNOLOGY

June 1996

Signature of Author .....
Department of Brain and Cognitive Sciences
May 23, 1996

Certified by.....
Dr. Emilio Bizzi
Professor
Thesis Supervisor

Accepted by..
.....
Gerald Schneider
Chairman, Departmental Committee on Graduate Students

The Role of Motor Primitives in the Control of Movement and Learning

by

Francesca Gandolfo

Submitted to the Department of Brain and Cognitive Sciences
on May 23, 1996, in partial fulfillment of the
requirements for the degree of
Doctor of Philosophy in Computational Neuroscience

Abstract

This thesis indicates that movement can be interpreted as a linear combination of motor primitives. Such primitives can be modeled as torque fields, which provide a mapping from the state of the limb to the torques needed to generate the desired behavior. This schema is consistent with psychophysical results, simulations, and physiological findings in the spinal cord.

We used adaptation to viscous loads as a paradigm to investigate how the central nervous system represents outside perturbations. Our psychophysical results are consistent with the hypothesis that the motor-control system builds a model of the environment as a map between experienced sensory input and the output forces necessary to counterbalance external perturbations.

In addition, we found that motor adaptation is local: subjects were able to compensate for perturbations not only over the experienced states, but the adaptation decayed smoothly and quickly with increasing distance from the locations where disturbances were sensed by the moving limb. We found that the extent of local adaptation could be tuned by training.

Furthermore, our experiments indicate that motor adaptation is encoded in intrinsic coordinates (muscles or joints). Consequently, a change in the arm configuration produced effects on learning even though the same end point posture was preserved.

Adaptation is by no means exclusive to humans. Our experiments showed that monkeys were able to adapt to viscous perturbations, and that their pattern of adaptation closely resembled what had been observed in humans.

We developed a model of adaptation based on the constraints of locality, smoothness and representation in intrinsic coordinates—which derived from psychophysics. We simulated the psychophysical experiments adding linearly the torques predicted by the model to the torques necessary to execute unperturbed movements. Simulations results showed that the identified constraints and linearity were enough to successfully reproduce the psychophysical results.

In conclusion, this thesis argues that adaptation and movement can be expressed as a superposition of motor primitives.

Thesis Supervisor: Dr. Emilio Bizzi
Title: Professor

Acknowledgments

First and foremost I thank my advisor, Emilio Bizzi. His comments and suggestions were always insightful. He has taught me a lot, not only about science but also about patience and perseverance in experiments which initially appeared to give more grief than results.

Sandro Mussa-Ivaldi deserves a whole-harted thank you. Not only is he one of the brightest minds I ever had the pleasure to know, but he is also a fair and sympathetic human being. He is sincerely missed in the lab.

Neville Hogan is a very attentive critic. His attention to details and deep knowledge of both the computational and biological aspects of motor control helped me to clarify and organize my thoughts. Mike Jordan has been supportive and understanding and his comments have made my life and experiments simpler. Giulio Sandini has been an advisor for many years, but, above all, he has been a dear friend. He has supported my decisions even when he did not totally agree, putting my interest first. He also came on sabbatical to Boston when I most needed him. Thanks!

My deepest thanks to Margo Cantor, who taught me all I know about primates and keeps the lab running smoothly. Margo and Terry Heyward were instrumental in keeping my sanity during the last days when the things to do were multiplying and time was shrinking.

Needless the say, this thesis could not have been possible without past and present students in the lab, who built some of the hardware and software and who allowed me to keep up with my schedule. They are too many to cite individually, but they all deserve my gratitude.

I am deeply grateful for my friends, who made my life in Boston a memorable experience also from the human perspective.

Last but not least I would like to thank my parents and my husband, who supported me materially and emotionally through the years and made this come true.

Thanks.

Contents

List of Figures

List of Tables

Chapter 1

Introduction

1.1 Motivation

Living beings exhibit an incredible richness of motor behaviors. Walking, reaching for objects, shaking hands—all are actions which we perform effortlessly on a daily basis.

Yet, when we consider the computations involved in the process, we realize that these actions are not at all trivial. On one hand, they involve solving a number of ill-posed problems which range from the planning of a movement, to the translation of the plan into commands executable by the motor actuators, the muscles. None of these transformations are simple, since multiple solutions are possible and the nervous system has to constrain the solution to achieve stable performance.

On the other hand, further complications are caused by the fact that most movements are not simple "hand waving", but rather they involve contacts and interactions with other objects. Therefore, planning a motor action involves not only solving the task constraints, but also integrating interactions with the environment into the computation. For example, we can move with the same ease whether or not we wear a heavy bracelet, and we can move on land and in the water. Although these conditions seem trivial, the computation involved to make it work is not. For example, the torques involved in an unloaded movement are quite different from those to achieve the same movement while holding a load.

Two strategies are possible in order to solve this problem: The motor system could take advantage of the feedback available during movement to correct on-line for the interactions with the environment. Alternately, the environment could be modeled on the basis of the previous experience. The motor commands could integrate in a feedforward fashion a component, dependent on the task to be executed, and also a component compensating for the environment. These strategies are by no means mutually exclusive, and they most likely coexist in the nervous system.

This thesis investigates this feedforward mechanism-the process through which information about the outside environment is incorporated into motor commands.

There are at least two different ways in which this could be achieved: a global minimization model or a superposition scheme. A global minimization model has been proposed by Uno and Kawato [111], according to which, motor commands arise from the minimization of the torque change, i.e. dynamics is embedded into the motor plan. Alternately, a superposition model has been proposed by Shadmehr and Mussa-Ivaldi [105]. In their scheme, a plan is formulated independently from external perturbations: the corresponding torques are computed and correction torques are linearly added to counterbalance the perturbations.

This thesis follows the latter model. We will show that a linear model accounts for the experimental data, and we will present results on the structure of the model of external perturbations. The novelty of the approach is to develop a primitive-based schema for motor adaptation.

This thesis proposes that the problem of movement can be solved by using a linear combination of motor primitives. We propose that these primitives can be modeled as a mapping between the limb's state space (position and velocity) and the torques necessary to counteract the environment.

1.2 Overview

This thesis explores the use of primitives for the execution of movement. Primitives can be hardwired in the nervous system (as in the spinal cord) or can be adapted to

compensate for environmental changes.

The aim of Part One is to present experimental data consistent with the hypothesis that the Central Nervous System (CNS) builds a representation of the outside world [105] and uses it to adapt motor commands to current environment.

Situations requiring adaptation occur frequently during life, as a result of both internal and external changes in the dynamics which the motor system controls. Internal changes can occur on a long-time scale and be permanent (e.g. body growth), or they can be short-lived (e.g. muscle fatigue [77, 30].) The coupling to the external world can be variable too. Tool use, for example, requires the CNS to control a new system composed of the body and the tool itself. This thesis investigates how the nervous system solves the problem of interacting with an initially unknown environment.

The environment can be modeled by the CNS as a mapping between the state of the arm and a set of commands. These commands compensate for the perturbations induced by the environment. This thesis indicates that a viable strategy to execute movements in a perturbed environment is to issue a sequence of motor commands to execute the desired task as if unperturbed, and a set of "biases" to compensate for the effects of the environment. The set of biases can be obtained from the model and is added linearly to the motor commands.

Chapter 2 provides an overview of the methods used in the psychophysical experiments. We present experimental data indicating that subjects adapt to a perturbed environment not only if full sensory feedback is allowed, but also if they are deprived of visual feedback.

Chapter 3 shows how the representation of the environment is updated whenever experience no longer matches expectations. There are at least three ways for the motor-control system to achieve adaptation. First, by representing the perturbing forces as a **look-up table**, that is, as a map that associates these forces to the states (positions and velocities) where perturbations have been experienced. The second approach is to see adaptation as not strictly limited to the visited states but rather to a small region around them. In this case, we would say that adaptation is **local** to

the visited states. Finally, a third hypothesis is that the pattern of forces experienced locally generalizes over the entire arm's workspace. Chapter 3 investigates which alternative is most likely to be implemented by the motor-control system. We found that our experimental data is best explained by a local model.

Chapter 4 investigates the coordinate system in which the map of the environment is represented. Two competing hypothesis are tested: the CNS might model the environment as a mapping between the arm end point position/velocity and the forces experienced on the hand. This coordinate frame is referred to as extrinsic, since it ignores the kinematics of the arm. Alternately, the mapping could reflect the structure of the arm (intrinsic coordinates) and build a correspondence between state (for example joint angles, joint velocity, muscle length) and joint torques (or muscle activation). The experiments reported are consistent with the model in which the map is encoded in intrinsic coordinates. Although at this point we cannot dissociate a muscle-based map and a joint-based map, we have evidence that a map expressed in extrinsic coordinates is in conflict with the experimental findings.

Chapter 5 shows that motor adaptation is present in primates such as macaques. Data from psychophysical experiments on monkeys show patterns of adaptation consistent with what was observed in humans. These findings provide a baseline for future physiological studies.

In conclusion, Part One of this thesis demonstrates that the motor system can adapt to changing environments through local modification of its pre-existing model. The analysis of the changes shows that the motor system interprets the world in intrinsic coordinates.

Our interpretation of the findings on adaptation is that the execution of movement can therefore be thought of as a process in which the "standard" motor command is superimposed on primitives which, in turn, are combined via a superposition process. Whenever the environment undergoes changes, a new primitive is generated and its predicted torques are added to the planned motor command.

Part 2 of the thesis presents a computational model of how a primitives-based schema for movement might be implemented. We present a model of how adapta-

tion can be interpreted in terms of generating compensatory primitives for external perturbations. We then show how these primitives could be approximated using the "spinal cord machinery". In particular, we show that the superposition of effects in the spinal cord is not a property of biomechanics.

Chapter 6 presents a computational model of how primitives for adaptation can be built from experience. Two factors are traded off in the model: accuracy in the capturing of the data, and smoothness. The first requirement follows from the definition of learning, smoothness instead is a biological constraint, given that muscles cannot produce non-smooth torque profiles. Kernel regression has been chosen as a paradigm satisfying both constraints. The mechanism has been simulated and compared to actual data. The simulation closely mimics the results of psychophysical experiments.

A model of movement execution arises in which a set of movement templates or behaviors are stored in the CNS. New movements could be generated by combining existing behaviors.

This model, although only an hypothesis as far as the CNS is concerned, is experimentally sound in the spinal cord [7].

The work of E. Bizzi and collaborators [7, 43, 44, 42] has demonstrated that the spinal cord is not a functionally homogeneous structure with respect to the production of forces, but it is best described as organized into separate patches.

The electrical and chemical stimulation of each patch has been shown to correspond to a behavior. Coactivation of different regions produces a behavior consistent with the linear summation of the costimulated patches. Chapter 7 presents a model of the structure of the cord. It shows that linear summation is not a necessary outcome of the biomechanical structure of the model. Nonetheless, a number of Montecarlo simulations point out that linear summation is a likely consequence of coactivation of different muscle pools.

We are now left with the problem of how to map the primitives resulting from adaptation onto spinal cord behaviors. Chapter 8 presents a network capable of approximating an arbitrary pattern of vectors by a linear superposition of non-linear

vector fields.

In conclusion, this thesis shows that motor execution can be modeled as a coactivation of motor primitives. This hypothesis accounts for psychophysical results and it is consistent with physiological findings.

Part I

Primitives for adaptation

Chapter 2

Introduction

2.1 Background

Two strategies can be devised to adapt to change. The motor system could use a feedback mechanism to correct on-line for the inadequacies of its control schema. This would require a tight control loop between perception and action, mediated by comparison between the desired outcome of a motor command and its actual effect on the system. Although there is evidence that feedback control is used by the nervous system [67, 113], we will show that this model alone is not compatible with the experimental evidence on adaptation to changing external dynamics. Alternatively, evidence has been gathered that the nervous system builds a model [35, 105, 78, 63, 108] of the outside environment on the basis of feedback information and uses the model to update motor commands. Once the adaptation has occurred, this model results in a feedforward control, which, in turn, anticipates the effects of disturbances before they actually occur. Clearly, the two models are not mutually exclusive, and most likely cooperate for the execution of movement. The paradigm we use is adaptation, i.e., we artificially perturb arm trajectories, and then we investigate how the nervous system responds to such perturbations.

The first part of this thesis is aimed at characterizing the way in which the motor system builds a model of the outside environment.

Adaptation is a very general phenomenon, whose occurrence is by no means re-

stricted to the motor system. The phenomenon of adaptation was first described in the visual domain by Helmoltz at the beginning of the century, but it was not until more recently that researchers set to understand the underlying mechanisms. Held et al. [52] showed that it was possible to learn how to compensate for induced visual distortions. When subjects wore prisms which translated the visual scene, they displayed errors in pointing movements. However, with practice, subjects learned to point accurately. As the prisms were removed, subjects missed the targets. This behavior was called **aftereffect**.

Wolpert et al. [122] demonstrated adaptation to nonlinear perturbations in the visual feedback. Subjects executed pointing movements but could not see their arm. They received visual feedback of the position of their hand by observing a cursor moving onto a computer screen. Unknown to the subjects, the curvature of the movement was progressively distorted on the screen. With practice, subjects corrected their arm movements so that the cursor would move onto the screen in a straight path.

Also Flanagan et al. [26] showed that subjects compensated for nonlinear distortions in the visual feedback. Subjects executed pointing movements while watching their elbow and shoulder trajectories displayed onto a computer screen on the x and y axes. With practice, the combined joint trajectory became straight, while the actual endpoint trajectory became curved.

Similar results were obtained by Imamizu et al. [59]. They perturbed the visual feedback so that subjects were shown a movement generated by a virtual arm, the shoulder angle of which was 5/4 of their own, and whose elbow angle was 1/2 of their own. As the subjects moved in straight lines, the display appeared curved as an effect of the kinematic distortion. With practice, subjects learned to move in straight lines compensating for the distortions.

In the auditory domain, Held and Durlach [21] among others, showed adaptation to displacements of auditory cues, resulting in normal auditory localization.

Adaptation to motor perturbations has been reported by Flash et al. [28], who showed that humans can adapt to loads. Shadmehr and Mussa-Ivaldi [105] extended the study to viscous loads. Subjects were asked to execute pointing movements to

visually specified targets. Force perturbations proportional to the movement velocity were applied to the subject's hand. Initially, the trajectories were significantly distorted by the applied forces. After a period of practice within this altered mechanical environment, subjects recovered the original performance to a remarkable degree. In addition, when the mechanical perturbations were removed, the resulting trajectories displayed aftereffects. The presence of aftereffects is an indication that subjects adapted to the novel environment not by a generic strategy, such as making their limb more rigid, but by generating endpoint forces that exactly compensated the applied perturbation. Accordingly, the sudden removal of the perturbation resulted in an equal and opposite unbalanced force that gave rise to observed aftereffects.

Adaptation to motor perturbations has been also reported by Lackner et al. [71]. Their experimental set up consists of a spinning room in which subjects sit at the center of rotation. If no movement is executed, subjects do not perceive anything unusual. As they start to move, Coriolis forces perturb their movements. Once again, with practice, subjects adapt to the rotating environment.

Sainburg and Ghez [99] showed that it is possible to adapt to inertial changes. In particular, they magnified/reduced the interaction forces in the arm by adding a mass, either medially or laterally, with respect to the hand.

In conclusion, adaptation is a phenomenon which has been characterized in many systems. Both humans and primates display an incredible ability to adapt to distortions, both in the perceptual and in the motor environment. The next chapters are aimed at understanding the mechanism behind adaptation.

2.2 Methods

The protocol used for most experiments is described in the following sections. The perturbations (experimental stimuli) used in the study are described in Section 2.2.1; Section 2.2.2 describes the experimental procedure, and Section 2.2.5 describes the hardware setup.

The details of the protocol for each experiment will be described in the relative protocol section.

2.2.1 Experimental stimuli

The perturbations used for this study can be modeled as end point viscous force fields, i.e. velocity dependent forces. [1] Given the subjects' (and manipulandum) end point velocity v, the manipulandum produces an end point force $F = Bv$, where the 2x2 B matrix characterizes the kind of perturbation. Some examples of force fields are shown in Fig. 2-1. Depending on the coefficients of the B matrix, the manipulandum can assist the movement by pushing the subject's arm in the direction of the movement (see Fig. 2-1A). It can similarly resist the motion, by pushing against the subject, and modeling motion in a viscous liquid such as honey. Alternatively, we can generate directions of instability (Fig. 2-1C) or "curl" perturbations (Fig. 2-1B), in which the perturbing force is always orthogonal to the movement direction.

We chose viscous perturbations for their properties:

- They are null at rest.

  $F = B(v = 0) = 0$

  This means that subjects are unaware of the presence or absence of the perturbations until they start moving. Their motor plan depends only on their expectation and cannot be corrected before the onset of movement. The subjects can not therefore replan their movements on the basis of the knowledge that the perturbation is on or not. Moreover, no force bias is necessary for the subject in order to hold still before the movement onset.

[1] We will use the terms perturbations, forces, and fields, almost interchangeably.

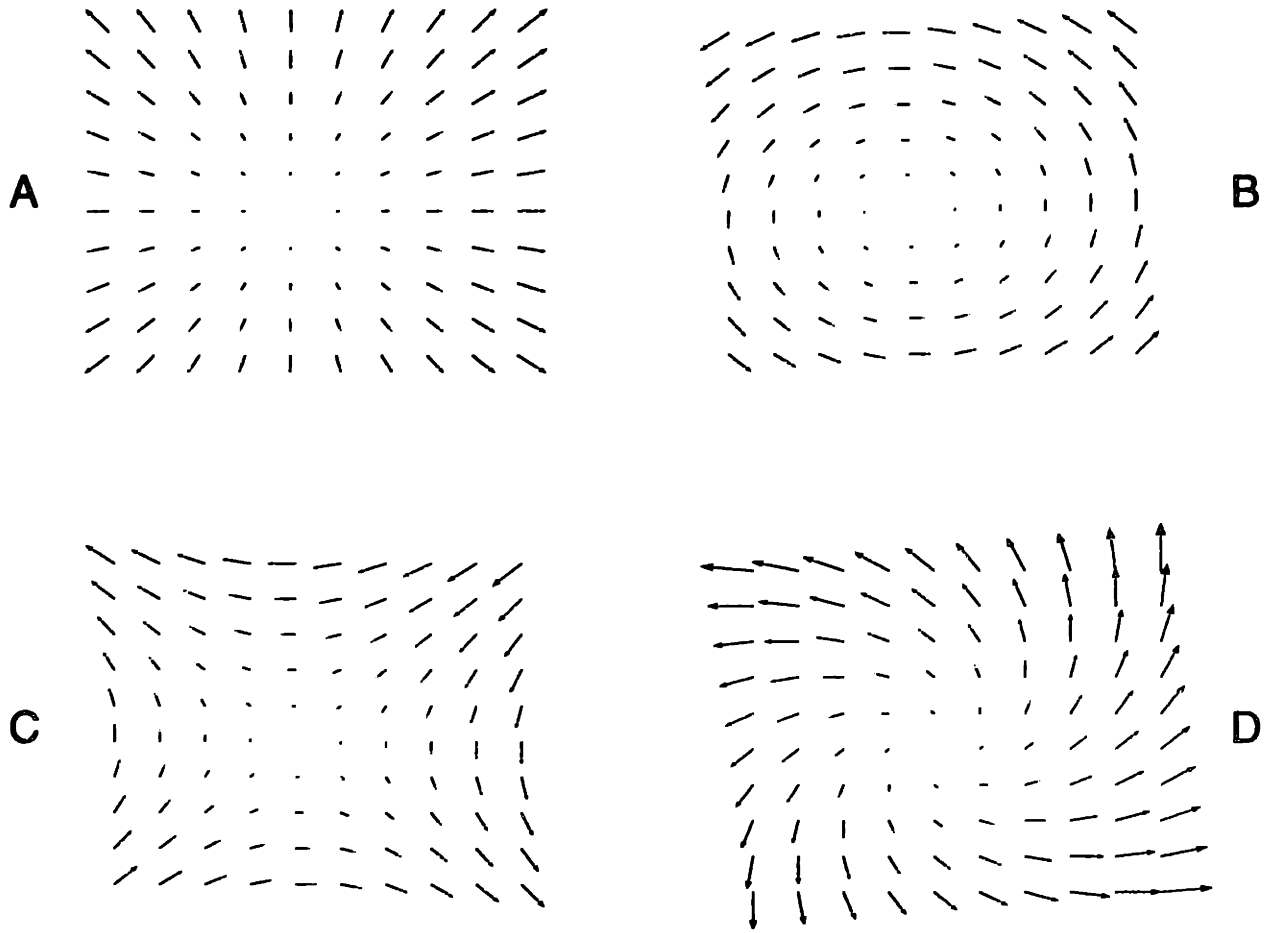

Figure 2-1: Examples of some possible perturbations

- Unlike elastic perturbations, which are commonly experienced in everyday life and are compensated for almost instantaneously, the time course of adaptation to viscous perturbations is in the order of 10 minutes in the experiment presented (but it is a function of the complexity of the field, and of the number of trajectories executed in the field). This makes viscous perturbations an ideal input for studying not only the resulting steady state, but also the transients of the adaptation mechanism.

- The perturbations rely only on the first derivative of motion, which can be easily calculated either in hardware or in software. In the set up for human psychophysics, the velocity data was obtained using tachometers. In the setup used with monkeys, the velocity data was obtained via numerical differentiation.

2.2.2 Experimental procedure

Most of the subjects used for the study were MIT undergraduates. Few subjects were graduate students or staff members. They were all right-handed and in the age group 18-35. They reported good eye sight (or used corrective lenses), no known neurologic disease, and good general health.

No subject knew the purpose of the experiment, even if some subjects participated in more than one experiment. Subjects were paid $5 for each session.

In each experiment, subjects sat in front of a computer screen placed above the manipulandum, a 2 degrees of freedom (d.o.f.) robotic arm. Each subject's right arm was supported by a sling hanging from the ceiling, which kept the subject's elbow approximately in the horizontal plane. A seat-belt strap restrained the right shoulder to limit the motion of the upper body. Subjects held onto the manipulandum with their right hand. A sketch of the set up is shown in Fig.2-2

The task consisted of point-to-point reaching movements. Subjects used the manipulandum as a joystick to move a cursor to visually presented targets. Occasionally, the trajectories of the arm were artificially perturbed using torque motors mounted onto the manipulandum. Perturbation and no-perturbation sessions were alternated,

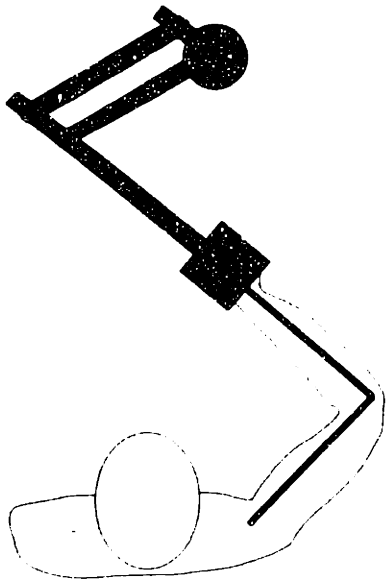

Figure 2-2: Sketch of the experimental setup.

using a protocol already described in the last century by Helmholtz. In his studies on prismatic adaptation, Helmholtz identified the following phases:

1. Pre-exposure performance measure: Data from subjects executing the task in absence of perturbations provided the "typical performance" or **baseline** for each subject;

2. Reduction of effect: as subjects experienced perturbations, their performances were recorded; and

3. Negative aftereffects: removal of the perturbation resulted in a drop in performance with respect to the baseline.

In the baseline condition, no perturbation was present and the manipulandum behaved as a passive joystick. A computer recorded movements to define "prototypical trajectories," which served as benchmarks to evaluate the effects of the perturbations. In our experiment, the baseline condition also had the dual effect of allowing subjects to learn the effects of the dynamics of the manipulandum. We assumed the manipulandum to be "ideal" in terms of viscosity and inertia. An examination of the very first trajectories by naive subjects indicated that this was not the case. Figure

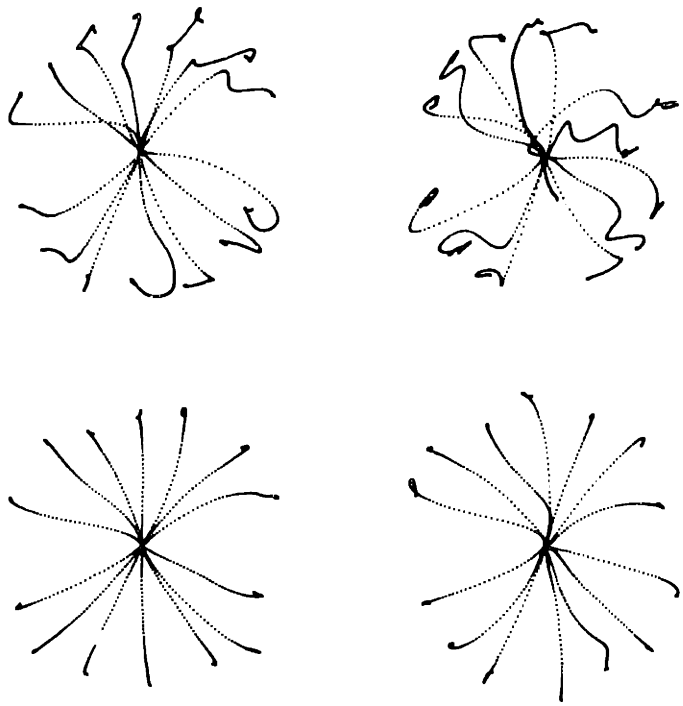

Figure 2-3: The first row shows the first movements using the manipulandum for naive subjects. The dynamic is by no means negligible. The second row shows the same trajectories 192 movements later. Subjects have adapted to the dynamical properties of the manipulandum and to the coupling of their arms to the manipulandum. The first and second columns correspond to data from two different subjects.

2-3 shows examples of such trajectories for two subjects (left and right). The upper panels show the very first distorted trajectories executed while subjects held the manipulandum. The lower panels show that subjects quickly learned how to control the system's inertia.

In the perturbation condition, the torque motors of the manipulandum imposed a force on the end point; Trajectories were initially highly perturbed but, as subjects practiced, the trajectories recovered the baseline shape. During this condition, we randomly interspersed trials in which the perturbation was removed. During these trials, subjects expected a perturbation but experienced none. In this way we were able to test the compensatory strategy to overcome the perturbations. We found distortions in the trajectories, which allowed us to rule out **co-contraction** as a mechanism for adaptation. Co-contraction is a non-specific strategy. Activation of

both flexor and extensor muscles increases the arm stiffness and therefore the impact of the perturbation on the arm. If the perturbation is removed, baseline trajectories should be recovered instantaneously. Instead, we found deviations from baseline in the opposite direction from the perturbation; this phenomenon is known as **aftereffect**, and it is considered a symptom of adaptation.

In the post-exposure condition, we removed the perturbation and we measured the residual effects of adaptation. The time course of the decay of the aftereffects was another correlate of adaptation.

We allowed visual feedback for all trials, both in the perturbation and no perturbation condition. Moreover, visual feedback was allowed in the training and testing condition on the assumption that visual feedback might reduce aftereffects but not enhance them. However, removing visual feedback produced qualitatively similar results to our finding.

2.2.3 A typical experiment

Figure 2-4 shows the outcome of the first set of experiments. The subjects executed pointing movements to 3 targets in the absence of external perturbation. The subjects practiced movements until they achieved a stable performance (baseline) and the desired timing, as seen in Fig. 2-4A. (Note that trajectories were almost straight and velocity profiles are bell-shaped [81].) We asked subjects to move at a constant pace. If they reached the target too fast (less than 450msec), the target square filled with a red color. If they reached the target in more than 550msecs, the targets filled with blue. If the target was reached within the desired time window (500 ± 50 msecs), the target "exploded" and the computer generated a sound.

Subsequently, the torque motors of the robot generated a programmed pattern of force perturbations. The programmed forces were proportional to the subject's hand velocity. Figure 2-1B shows an example of perturbation pattern, in which the force exerted by the manipulandum is plotted as a function of the hand's velocity. Initially, this perturbation highly distorted the subjects' trajectories (see Fig. 2-4B), but as training progressed, trajectories recovered the baseline pattern (Fig 2-4C). On

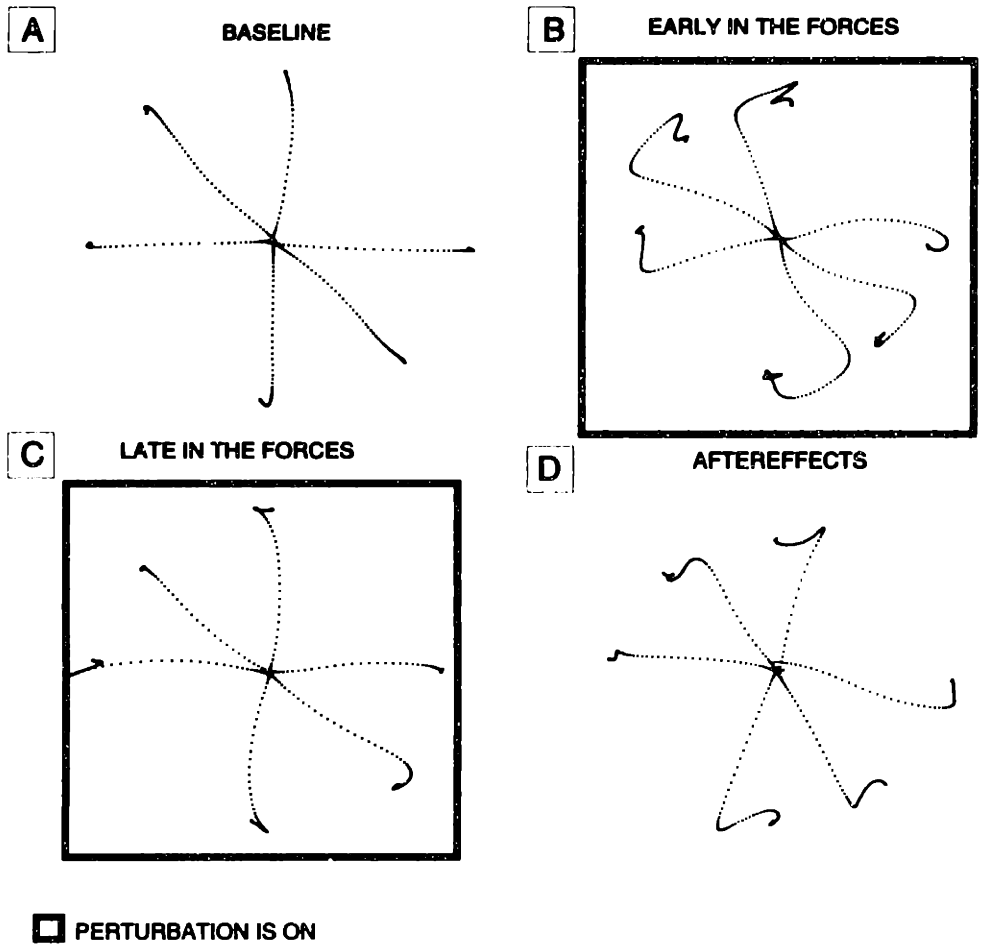

Figure 2-4: Trajectories on a typical experiment include: A) Baseline trajectories, in which the subjects move in an almost straight line; B) Trajectories at initial exposure to a curl field, with high distortions with respect to the baseline; C) Trajectories after having adapted to the field converge back to baseline and are straighter and straighter; and D) Aftereffects resulting from removal of the field. The boxes around the trajectories indicate that the perturbation is switched on.

random trials, we removed the perturbation, and compensatory trajectories, referred to as aftereffects, appeared (Fig. 2-4D).

2.2.4 Data analysis

The objective of the data analysis is to compare trajectories and quantify their similarities.

To quantify adaptation, we measured the similarity of trajectories when subjects were initially exposed to perturbations, and then again after the trajectories converged

back to baseline. The measurement described in [104, 85] is used.

We measured the similarity between two trajectories using the inner product between the velocities of the trajectories. Given a velocity vector v^1 (for the first trajectory) and a vector v^2 (for the second), the similarity measurement can be expressed as:

$$\rho = \frac{Cov(v^1, v^2)}{\sigma(v^1)\sigma(v^2)} \tag{2.1}$$

where:

$$\sigma(v) = \|v - \bar{v}\| \tag{2.2}$$

$$Cov(v^1, v^2) = < v^1 - \bar{v}^1, v^2 - \bar{v}^2 > \tag{2.3}$$

$$< v^1, v^2 > = \sum_i v_i^1 v_i^2 \tag{2.4}$$

and $\bar{v} = < v, v >$.

In the analysis, all measurements compare the trajectory under examination to a prototype or reference trajectory. The reference trajectory is chosen among the baseline trajectories in the following way. We considered a set of 12 baseline trajectories (one set for each direction). A matrix of similarity measures is built by comparing each pair of trajectories. The trajectory which "correlates" best with all the others is the baseline, implying that such trajectory is the best representative of the trajectories in that direction.

For example, the prototypes in Fig. 2-4A had the average score of 0.97; the trajectories in Fig. 2-4B have a score of 0.7; 2-4C 0.94; and Fig.2-4D 0.75.

2.2.5 Apparatus

The manipulandum used in the experiments is a two degrees of freedom planar arm. Its link lengths measure respectively 35.7cm and 33.7cm, and its moment of inertia have been estimated to be about 0.0195 and 0.0037 $Kg.m^2$ [105]. Each joint is activated independently by a JR16M4CH DC torque motor (PMI Corp.) Optical encoders (Teledyne Gurley) and tachometers (PMI) provide status information on the

current position and velocity. A Gateway 2000 90MHz Pentium computer controls the experiment at a rate of 100Hz. For each cycle the computer updates and records the status of the manipulandum and, and updates the perturbation, if necessary. The video display of the subject position is also updated. The movements are approximately 15cm wide, the target is displayed as a 8mm wide square, and the cursor, which indicates the subjects position, is a 2mm square.

2.3 Motor adaptation without visual feedback

Most experiments on adaptation involve both a visual and a motor component [118]. Prismatic adaptation is generally tested by asking subjects to execute pointing movements and the amount of adaptation is measured with respect to motor performance.

The adaptation experiments presented in this thesis, instead, involve a motor perturbation, and the visual feedback shown to the subjects is undistorted and reproduces the subject's behavior. Nonetheless, visual feedback is given in most experiments and there is the possibility that vision might be guiding the adaptation process.

In order to show that adaptation can be achieved independently from the visual feedback, we tested naive subjects, and we asked them to keep their eyes closed through the entire experiment. These subjects had never participated in an adaptation experiment before, had never been exposed to the set up, and had no information as to the purpose of the experiment. This was particularly important, because it ruled out adaptation as a consequence of prior experience and as a result of a cognitive model of the perturbations effect.

We found that subjects adapted to the perturbations, and displayed aftereffects as the perturbations were removed.

2.3.1 Methods

We asked subjects to execute upward and downward movements at a constant pace (500 ± 50 msecs) while keeping their eyes closed. Subjects were told that at an unknown time during the experiment, the motors would try to interfere with their movements. The motors would be switched on and off randomly. Subjects were asked to ignore the perturbations, and continue to move upward and downward as if undisturbed.

Each movement was triggered by a computer generated click 10msecs after the termination of the previous movement. No timing constraint was imposed on the subjects, who were instructed to move at a natural pace.

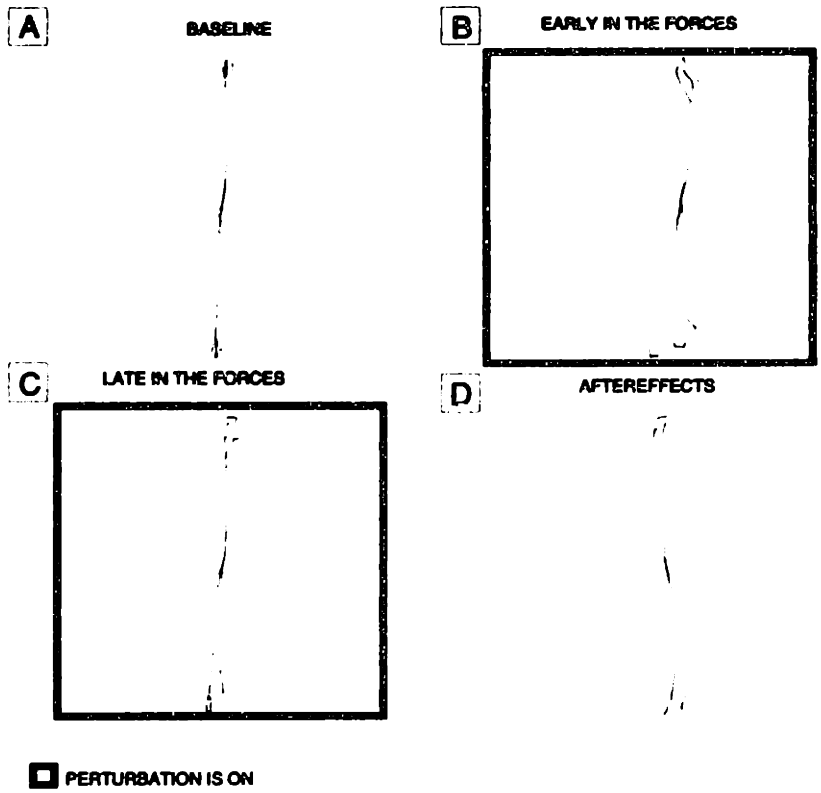

Figure 2-5: Motor adaptation without visual feedback

2.3.2 Results

Subjects executed 100 movements unperturbed. This allowed them to achieve a stable stereotyped performance, as shown in Fig. 2-5A. They were then exposed to a viscous clockwise curl perturbation for 200 movements. Initially, their trajectories were distorted (see 2-5B), but with practice they resumed baseline-like trajectories (see Fig. 2-5C). Randomly, the perturbation was removed, and subjects displayed aftereffects, as shown in Fig. 2-5D.

2.3.3 Discussion

Adaptation in the absence of any visual feedback indicates that vision is not necessary for the adaptation process. Proprioception alone seems to provide enough information for the motor system to be able to compensate for external perturbations.

This finding does not imply that vision has no role in adaptation. Proprioceptive and visual information might be integrated to speed up the process [35, 25, 112].

Chapter 3

Adaptation is local.

3.1 Introduction

How does the motor-control system adapt to new mechanical environments? When we move the arm in a novel environment (for example, when we hold a hammer for the first time), we encounter unexpected forces as the arm goes through a temporal sequence of states (i.e., positions and velocities). As we adapt to this environment, the motor-control system must learn to predict the perturbing forces that the limb will encounter, so as to cancel them out while carrying out the desired movement. There are at least three ways for the motor-control system to achieve adaptation. First, by representing the perturbing forces as a look-up table, (i.e. a map that associates these forces to the exact states where perturbations were experienced). Second, by representing adaptation as not strictly limited to the visited states but rather to a small region around them. In this case, we would say that adaptation is local to the visited states. Finally, a third hypothesis maintains that the pattern of forces experienced locally generalizes over the entire arm's workspace.

To find which option is most likely to be implemented by the motor-control system, we investigated how subjects change their performance after prolonged exposure to a novel mechanical perturbation. Our experiments demonstrate that the motor-control system builds a model of the environment as a map between the experienced somatosensory input and the output forces needed to counterbalance the external

perturbations. In addition, the CNS's ability to compensate for the perturbing forces is restricted to those spatial locations where the perturbations have been experienced by the moving arm. The subjects also are able to compensate for forces experienced at neighboring workspace locations. However, adaptation decays smoothly and quickly, with increasing distance from the locations where disturbances were sensed by the moving limb.

3.2 Background

Our finding that motor adaptation is local, is consistent with the results reported in the visual system.

Poggio et al. [91] studied a hyperacuity task and reported that subjects learned how to perform the task at a particular retinal location, but failed to generalize it at different locations. Performance dropped with distance from the trained area.

More evidence on the locality of visual adaptation has been reported by Fiorentini and Berardi. They tested subjects on learning how to discriminate gratings of different waveforms. They found that "learning is specific for both the orientation and the spatial frequency of the practice stimulus" [24].

The same overall finding of local learning seems to hold not only for low-level processes such as the ones described above, but also for the domain of object recognition. Bülthoff and Edelman [14] tested subjects on recognition of amoeba-like objects when viewed from angles different from the presentation angle. They found that recognition falls off smoothly with distance from the presentation angle.

Ghahramani et al. [36, 35] showed also that visuo-motor adaptation generates local models. They systematically perturbed the visual feedback of the arm location after a pointing movement. Subjects modified their trajectories in order to compensate for the visual distortions. Compensatory strategies were used not only at the locations exposed to the perturbations, but also in a neighborhood of such locations. The observed decay in generalization is similar to the decay we observed in the motor adaptation.

A local adaptation of the visuo-motor mapping was also observed by Roby-Bramy and Burnod. They asked subjects to execute pointing movement to targets displayed onto a computer screen. Subjects used a computer mouse to move the cursor. The mapping between mouse-motion and visual feedback of the motion was rotated by 60 degrees [97]. A "cosine-like" decay of adaptation was observed, when subjects were tested on movements in directions *different* from the trained directions.

The effects of a purely motor perturbation have been reported by Sainburg et al. [98]. They investigated the effects of an inertial perturbation on out-and-back movements, finding that adaptation decayed with distance from the trained location. This is consistent with our findings on viscous perturbations [31].

Studies by Held and Bauer [53] indicate that the mechanism of adaptation we investigated *could* be responsible for the calibration of the visuo-motor map in infants. Held and Bauer found that monkeys deprived of the sight of their bodies during infancy showed poor visuo-motor coordination. Training on a restricted area of the workspace led to little generalization to the rest of the workspace.

Although most of the studies agree in reporting local adaptation, a few studies report contradictory results. Ghilardi et al. [38] presented some evidence that the effects of learning a visuo-motor transformation carry on in the entire workspace. They tested subjects who produced reaching movements in three locations: left of the body midline, centered on the body midline, and right of the midline. They found that the training location induced a significant bias onto the trajectories recorded in the test regions. The phenomenon has been attributed to biases in the representation of hand position depending on experience.

Shadmehr and Mussa-Ivaldi [105] reported broad tuning of adaptation, using the same paradigm as the one used in this thesis. This chapter offers an interpretation which reconciles their experimental findings with our interpretation of local learning.

In conclusion, there is a growing body of literature arguing that adaptation to outside perturbation occurs locally in the nervous system. The literature reported, nonetheless, is mostly descriptive of visuo-motor perturbations. This chapter is aimed at showing that similar results hold for strictly motor perturbations.

3.3 Experiment 1: Generalization across different directions

To estimate the generalization of motor learning, we trained subjects over a region of the workspace and tested for evidence of adaptation by observing the aftereffects both inside and outside this region.

If a global model of adaptation is true, aftereffects should be detected over the entire workspace with a comparable magnitude. If adaptation is local, aftereffects should be detected around the trained locations, and the magnitude of the aftereffects should be proportional to the distance from the trained locations. A look-up table model, instead, predicts no aftereffects outside the trained region.

3.3.1 Methods

We tested fifteen right-handed individuals, ranging in age from 18 to 35 years and with no known history of neuromotor disorders.

We asked subjects to execute movements to targets placed as shown in Fig. 3-1S. Subjects executed pointing movements to 7 directions, equally spaced by 22.5°. The empty circles (Fig.3-1S) represented the training targets (45° and 90°), the filled circles represented the testing targets (0°, 22.5°, 67.5°, 112.5° or 135°). A baseline was acquired in all directions (Fig. 3-1A). In the next session, a clockwise force field (Fig. 3-1F) was used as perturbation. Forces were applied to the two training directions only (Fig. 3-1B) and were applied until the field was learned (Fig. 3-1C). At this point, the test session started. Subjects continued to move to the training targets (two directions), but a test target made random appearances, and subjects moved to this target. Subjects were then re-exposed to the perturbation along the training directions, in order to readapt *before* the next training target was presented. The procedure was repeated, until all the testing targets were presented twice. Aftereffects were recorded along the testing directions (Fig. 3-1D).

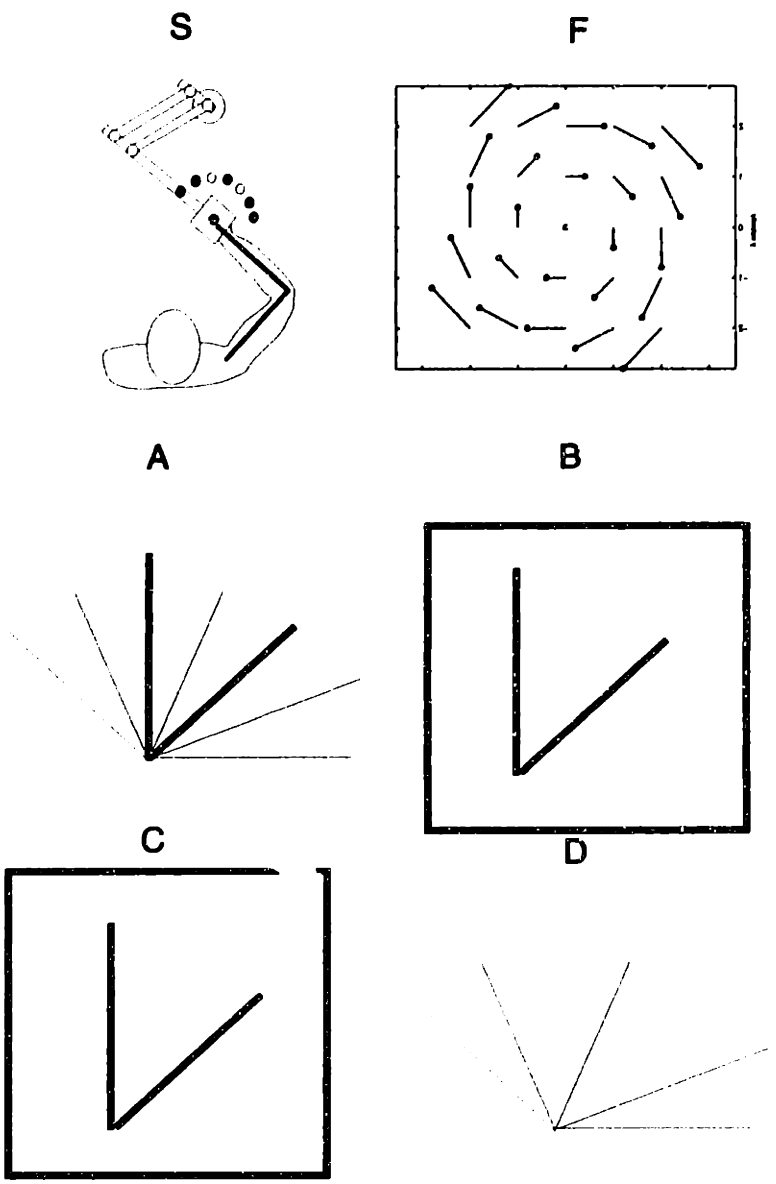

Figure 3-1: Methods for testing the generalization of adaptation. S: set up. The subjects executed pointing movements to 7 directions. The empty circles represented the training targets, the solid circles represented the testing targets. F: a clockwise force field was used as perturbation A: baseline trajectories were acquired along all directions B: forces are applied to two directions only C: forces were applied until the field was learned D: aftereffects were recorded along the testing directions. The thick squares indicate that the perturbation was on for those trajectories.

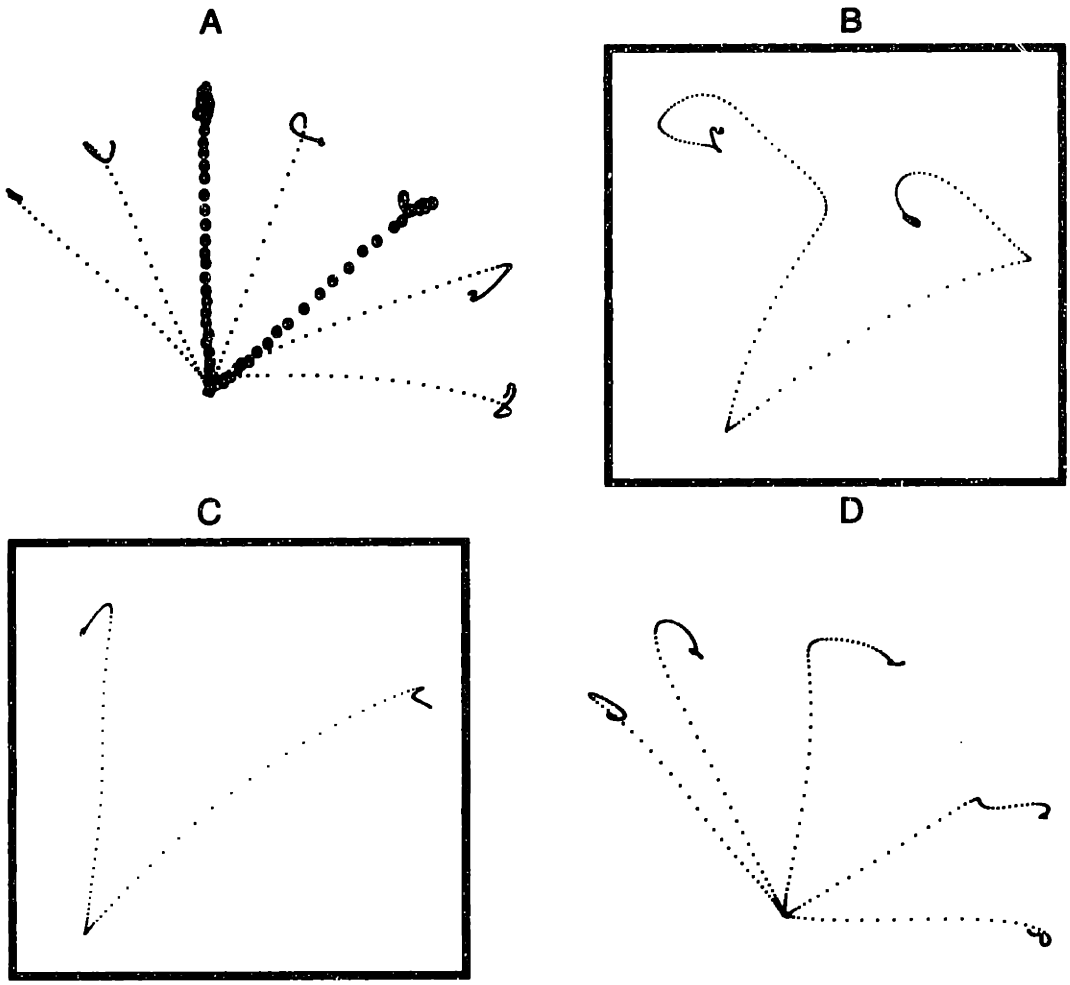

Figure 3-2: Results for subject S11: a clockwise force field was used as perturbation. A: baseline trajectories are almost straight. The dark dots show the directions which will be perturbed B: Trajectories are initially highly perturbed C: With practice trajectories become straight again D: The non-trained trajectories are randomly sampled (without perturbations) for the presence of aftereffects.

3.3.2 Results

Fig. 3-2A shows the baseline trajectories (correlation coefficient 0.95) for a typical subject in the absence of perturbations. Once a stable performance was reached, subjects moved the cursor back and forth from the center to the targets at 45° and 90°, and a clockwise perturbation was applied to the moving hand. This resulted in distortions of these trajectories (Fig. 3-2B). However, after about 400 movements, the original, nearly straight trajectories reappeared (Fig. 3-2C). Fig. 3-2D shows example aftereffects in trajectories to the test targets. (No perturbation was applied during the

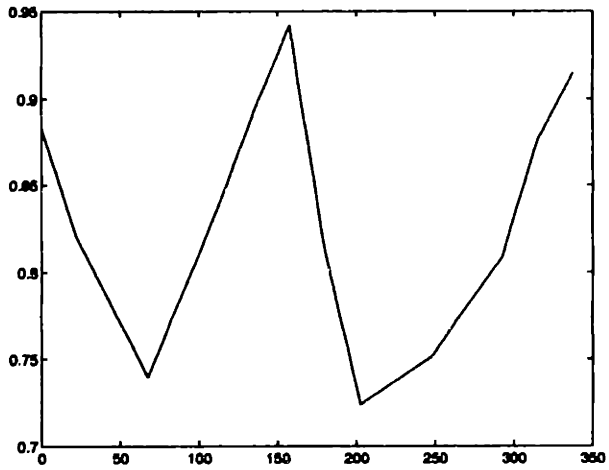

Figure 3-3: Tuning curve of the adaptation. The valley at 67.5° indicates that aftereffects are maximal in the interpolating region. The peak at 157.5° indicates that aftereffects are minimal in the direction farthest from the trained directions.

movements to test targets, and movements to these targets were randomly presented.) The magnitude of the aftereffects decays smoothly with increasing distance from the trained locations. (ANOVA shows a directional effect: $F(11,108)= 5.3$ $p<0.001$, and F test shows a statistical difference between a new trajectory within the training region, and the trajectory that was farthest away from this region.) The tuning curve of the aftereffects is shown in Fig. 3-3. The valley at 67.5° indicates that aftereffects are maximal in the interpolating region. The peak at 157.5° indicates that aftereffects are minimal in the direction farthest from the trained directions.

3.3.3 Is the decay a byproduct of biomechanics?

One possible explanation of the decay in aftereffects is that both the human arm and the manipulandum are not isotropic [87]. Learning might therefore not be equal in all directions, and consequently aftereffects would display a decaying pattern.

To rule out systematic factors associated with particular movement directions, we repeated the experiment using different training directions. Regardless of the training direction, we found a decay of the aftereffects *outside* the training region.

Fig. 3-4 shows trajectories from an experiment in which the trained directions were 0^0 and 45^0. The same qualitative effects as in Fig. 3-2 can be observed.

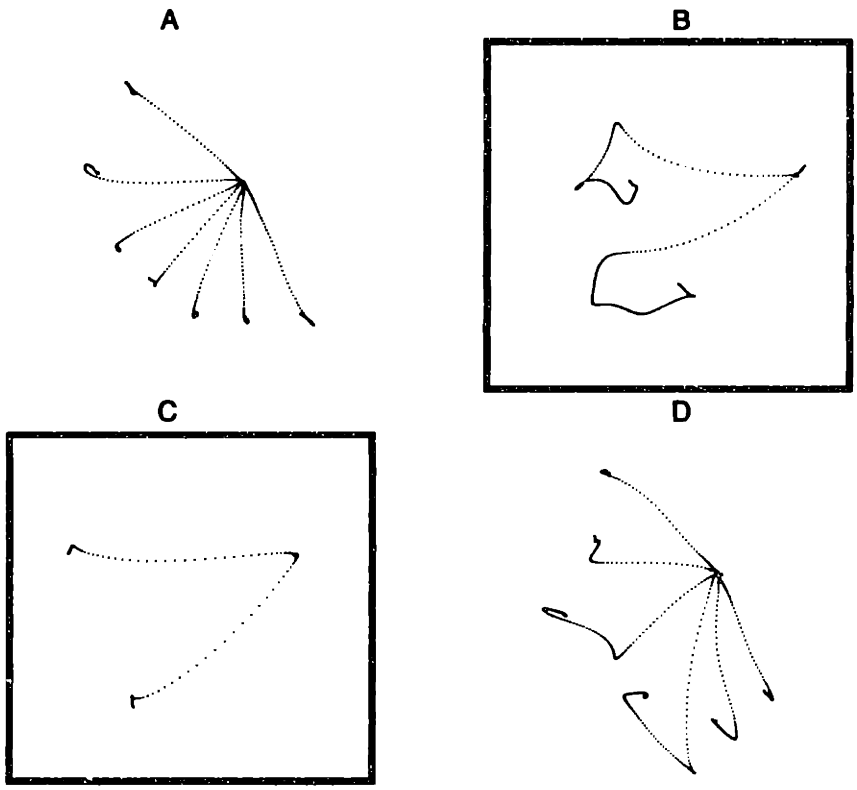

Figure 3-4: Generalization: decaying aftereffects are recorded independently from the trained locations

3.3.4 Discussion

The previous experiment shows results consistent with a local model for adaptation, and not consistent with either a look-up table, or a global model. A look-up table model would predict no generalization outside the trained locations. A global model, instead, would predict no decay of effect away from the trained regions. We found that aftereffects exist outside the trained locations, but their magnitude is modulated by distance from the trained region.

3.4 Experiment 2: Time-varying interference within the same "local" domain

The experiment reported in the previous section proved that motor adaptation has a region of influence which spans outside the trained region.

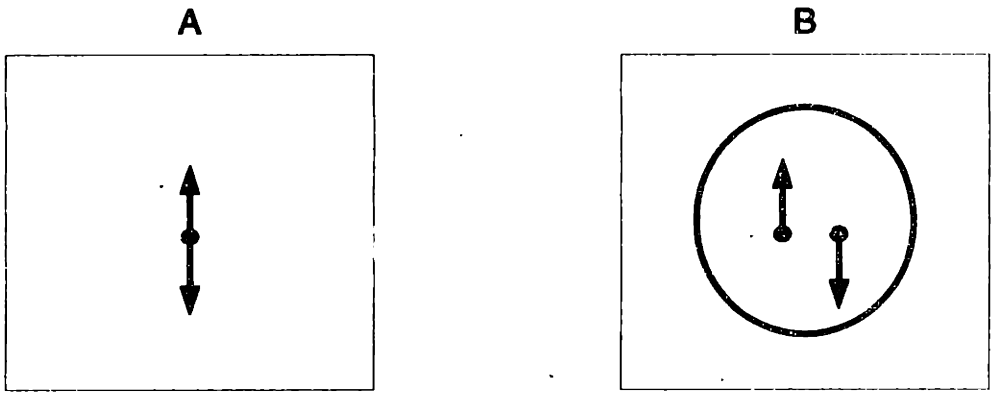

Figure 3-5: Panel A: if a perturbation is such that at a given point it can elicit two different forces, the field is "inconsistent" since it is not possible to predict which of the two forces will be applied. Panel B: each point is associated to a single force. The dark circle represents the resolution of a system. The field appears inconsistent to this system, since two different forces are present below its level of resolution.

It is known from previous studies [9] that if subjects are trained over one force field and subsequently exposed to a different field, they find it harder to adapt to the latter perturbation. This phenomenon is known as **interference** [72, 13]. It occurs when subjects are asked to adapt to conflicting data, since each field needs different compensatory torques.

The test here is to determine whether the same phenomenon can arise when the data presented are not strictly conflicting, but can appear so to the system. In other words, if we present one single field, but the field is designed as not to be locally smooth, would it lead to interference? Mathematically, it need not to do so, since for each point of the state space there is only one corresponding value. Practically, however, if the resolution of the system is limited, the field might be perceived as "inconsistent" (see Fig. 3-5.)

3.4.1 Methods

To ensure that no state could be associated to two different torques, we asked subjects to adopt two different arm configurations. (Chapter 4 will prove that this arrangement corresponds to two different regions of the relevant state space.)

We asked subjects to execute a series of movements, some with wrist posture

A (shown in Fig. 3-6A), some with wrist posture B (see Fig. 3-6B.) These grips induced wrist rotation, defining two distinct sets of joint configurations. Posture (B) was associated with a perturbation, while posture (A) was associated with a no-perturbation condition.

Subjects executed reaching movements to 3 targets, and alternated blocks of 24 trials between which the wrist posture was switched. In the last block of trials, subjects were holding the manipulandum with the B grip but no forces were applied in order to test for aftereffects.

3.4.2 Results

Fig. 3-6 shows trajectories for a typical subject. The first column corresponds to data produced with the wrist posture A, the second column with the wrist posture B. Fig. 3-6C shows that, initially, trajectories were straight in posture A. As the posture was switched, and a perturbation was applied, trajectories become highly distorted (Fig. 3-6D.) As learning progressed, the trajectories executed while grasping with posture (A), which had been exposed to no disturbing forces, appeared to show aftereffects (Fig. 3-6E). This finding indicates that there is interference between the two conditions. With further practice, the interference subsided, and no aftereffects were detected when subjects produced trajectories with the wrist in the A posture (see Figs. 3-6G and 3-6I).

As expected, the perturbation applied in posture B was learned (see Fig. 3-6F and H). We found that trajectories performed with posture B displayed aftereffects when the field was removed. Moreover, the aftereffects persisted even when subjects switched between posture (A) and (B) and, contrary to their expectations, received no perturbations (see Fig. 3-6J.)

Fig. 3-7 shows data for one subject. We plotted correlation coefficient versus trial number. The dotted lines divide blocks of 24 trials. The black boxes indicate trials in the B posture, with the perturbation on. The white boxes indicate unperturbed trials with the A posture. The dotted box indicates the "catch trials", i.e. the trials in the B posture in which, contrary to the subject's expectations, no perturbations

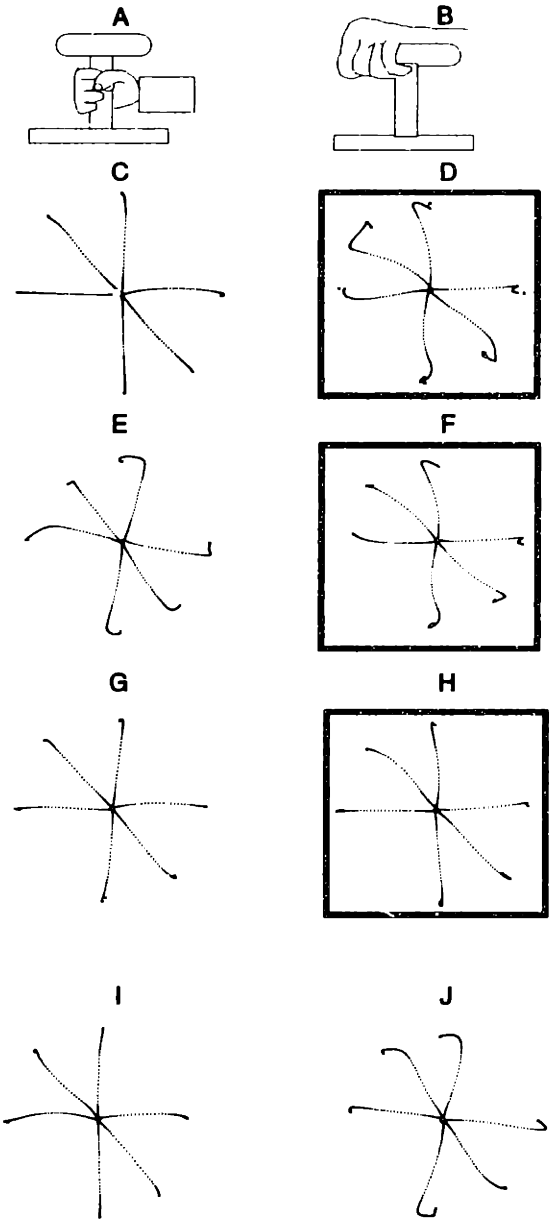

Figure 3-6: Interference between representations is resolved: (A) and (B) show the grips used by the subjects. The first column shows the data regarding the posture (A) which was not exposed to perturbations, while the second column shows the posture (B) which was exposed to a counterclockwise field. (C) and (D) represent the first 6 movements in the first cycle. (E) shows aftereffects in the (A) posture as a result of exposure to the perturbation in (D). As training progresses, the trajectory straightens out, even during the perturbations (F) and (H), and aftereffects (see (G) and (I)) do not affect the non-exposed posture (A) anymore. Aftereffects are present (J) only if the subjects expects a perturbation when switching back to the posture (B).

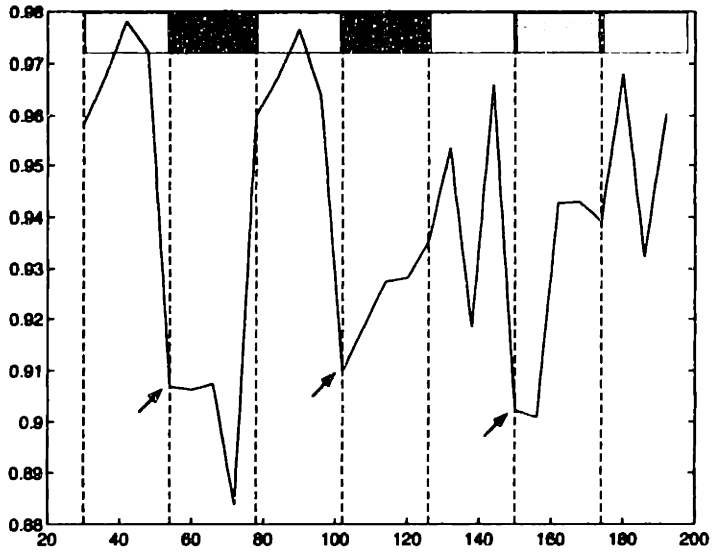

Figure 3-7: Data for one subject. The trial number is on the x axis and the correlation coefficient on the y axis. The dotted lines divide blocks of 24 trials. The black boxes indicate trials in the B posture, with the perturbation switched on. The white boxes indicate unperturbed trials with the A posture. The dotted box indicates the "catch trials", i.e. the trials in the B posture in which, contrary to the subject's expectations, no perturbations were applied. The arrows indicate how the performance drops from unperturbed to perturbed trials.

were applied. The arrows indicate how the performance drops from unperturbed to perturbed trials. Note that in the catch trials, the performance drops because of the aftereffects.

Fig. 3-8 summarizes the results for 10 subjects in the last 8 blocks of trials. Each bin represents how the performance changes when switching between a block with no forces and a block with forces (black bins), or the other way round (white bins). The dotted bin indicates that when subjects expect a perturbation and receive none, their performance in the null field is reduced due to the aftereffects. The shaded area shows an improvement in performance. The white area (negative y axis) indicates a reduction in performance.

3.4.3 Discussion

We observed that interference arises if a field is not smooth in the trained region. Therefore, the CNS tends to smoothly interpolate within a region. However, the

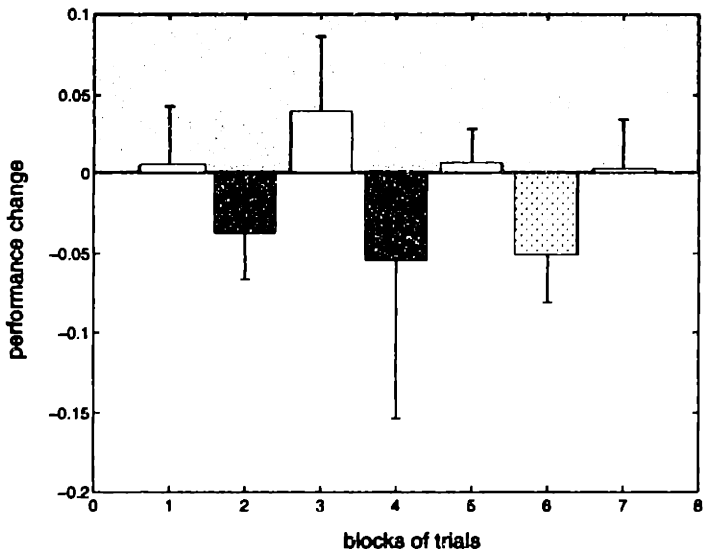

Figure 3-8: Results for 10 subjects in the last 8 blocks of trials. Each bin represents how the performance changes when switching between a block with no forces, and a block with forces (black bins), or the other way round (white bins). The dotted bin indicates that when subjects expect a perturbation and receive none, their performance in the null field is reduced due to the aftereffects. The shaded area shows an improvement in performance. The white area (negative y axis) indicates a reduction in performance.

"spill over" due to the interference fades away if enough practice is allowed. This finding indicates that somehow there is a shrinkage in the region of local influence. The space, which was initially perceived as a unique region, is parsed into smaller portions to accommodate the data.

We conclude that during adaptation, the motor-control system carries out a reconstruction of the dynamical environment by following a process similar to the way in which a statistician could approximate an unknown function from a set of noisy data. The approximation technique, known as "regularization", consists in deriving a function that minimizes the sum of two distinct cost components [40, 110]. One cost component is the approximation error, that measures the distance between the approximating function and the data. The other cost component reflects what is known a priori about the function to be approximated. Typically, this cost component is a measure of smoothness: the unknown function is supposed to minimize the amount of oscillation between data points. The data shown in Figs. 3-6E and 3-6J indicate that at the beginning of the experiment, the motor system assumes that the same pattern

of forces may be present in the two hand postures. This working hypothesis corresponds to a smoothness criterion. However, as learning progresses (Figs. 3-6G and 3-6H), the subject explores the mechanical environment of each posture and recovers the correct movement pattern by producing two distinct compensatory responses.

3.5 Single joint learning

It has been pointed out that there is an apparent conflict between our finding that adaptation occurs locally and Shadmehr and Mussa-Ivaldi's [105] claim that adaptation is broadly-tuned.

In their paper, they report results of an experiment in which subjects are taught a perturbation pattern over a region of the workspace. Subsequently, the subjects are tested for aftereffects over a different region of the workspace. In spite of the distance between the two regions, subjects displayed aftereffects. This prompted these investigators to claim that adaptation is broadly-tuned, and its effects are visible far from the trained locations.

The issue of how to reconcile the above mentioned results with the findings in this thesis has not been conclusively resolved. Nonetheless, we would like to offer an alternative interpretation to the data.

If we assume that, given the redundancy of the arm, the subjects could adapt to the perturbation using mainly their distal joints, we could conclude that the presence of aftereffects in the second region can be attributed to a rotation of the coordinate frame.

We present data indicating that, once exposed to adaptation, the shoulder displays the same pattern of decay seen in previous experiments. Therefore, a decay of aftereffects induced by shoulder rotation should be expected in the generalization across regions of the workspaces.

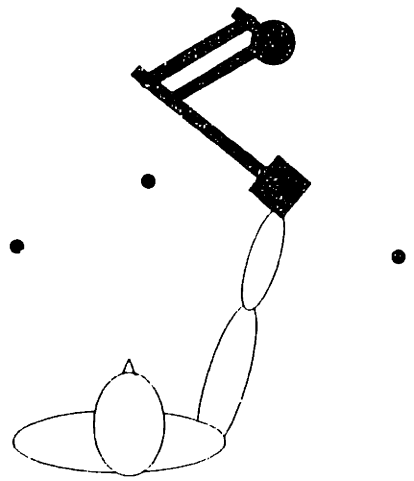

Figure 3-9: Sketch of the subjects' and targets' positions

3.5.1 Methods

We asked subjects to execute reaching movements to 4 targets arranged along a circle centered at the subject's shoulder. The targets arrangement is shown in Fig. 3-9. Subjects were placed so that a fully extended arm was the only configuration satisfying the task.

Four subjects (2 males and 2 females) participated in the experiment. Two subjects were at their first experiment on our apparatus, while the other two had participated in previous experiments. All subjects were naive to the purpose of the experiment. Two subjects participated in both groups of the experiment, so that 3 data sets are available for each experimental group.

All subjects practiced for 192 movements, alternating sequences of 47 movements between the two left-most targets, a movement between the two center targets, and 47 movements between the two right-most targets.

Subjects were assigned to two groups. The first group underwent a training session in which the subject practiced only movements to the two leftmost targets. A resistive perturbation field was associated to these movements. The second group practiced to the rightmost targets, with the same perturbation active.

In the testing session, each group repeated movements to the same targets as in the training session. Randomly, the perturbation was removed and aftereffects were recorded. On other randomly selected trials, a movement between the center

targets was required (under the perturbed condition), and was followed by movements between the targets not trained in the teaching phase. Aftereffects were recorded.

3.5.2 Results

This experiment uses a resistive field as a perturbation. We chose this particular field for two major reasons: First, it is a stabilizing field. Subjects were operating at the edge of their workspace, in a biomechanically disadvantageous position, and we wanted to minimize the possibility of injuries at the shoulder joint. Second, the movements were monodimensional, and a resistive field was the one which did not violate the 1-d constraint and gave easy-to-interpret results. When first exposed to the field, subjects had a tendency to undershoot the targets. As exposure increased, they became more accurate. Aftereffects appeared as target overshoots.

We used the data acquired in the baseline trials to estimate the average path length between any two targets. Doing so, we ruled out differences arising from perceptual and biomechanical effects of operating in different workspace regions.

We then compared the aftereffect's overshoots to the average trajectory, and got a net overshoot score. The same procedure was repeated for aftereffects in the trained and test regions.

Fig.3-10 and 3-11 show some raw data and results for one subject in each group. The upper panel shows instances of raw data. The aftereffects in the trained trajectories are shown to the right of Fig. 3-10 and to the left of Fig. 3-11. The other trajectories represent the aftereffects in the test region. The lower plot represents the overshoot score for the trajectories shown. The first star (x axis =1) represents the score for an aftereffect recorded during the training phase. The second two stars (x axis=2 and 3) are aftereffects recorded during the testing phase in the trained trajectories. The last two stars represent the scores for aftereffects in the testing region.

We compared the difference between the score in the testing and training trajectories, and we found statistical significance both in group 1($p<0.01$ at 95%) and group 2 ($p<0.01$ at 95%). We conclude that the aftereffects in the test and trained

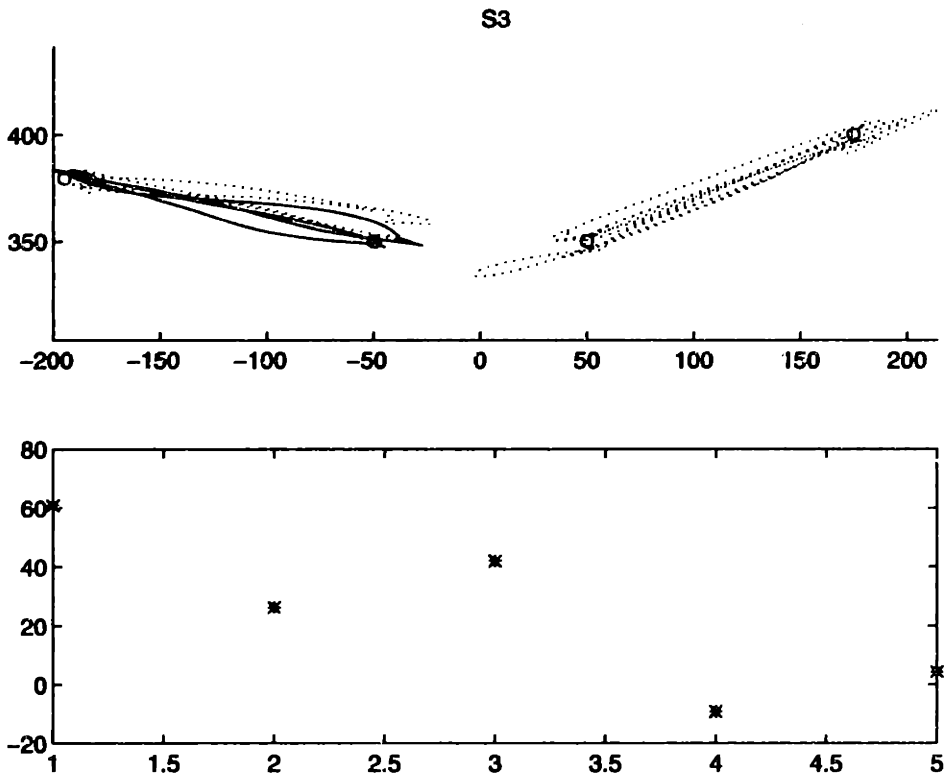

Figure 3-10: The upper panel shows instances of raw data. The aftereffects of the trained trajectories area are shown to the right. The trajectories to the left side of the plot represent the aftereffects in the testing region. The lower plot represents the overshoot score for the trajectories shown. The first star represents the score for an aftereffect recorded during the training phase. The second two stars are aftereffects recorded during the testing phase in the trained trajectories. The last two stars represent the scores for the test aftereffects.

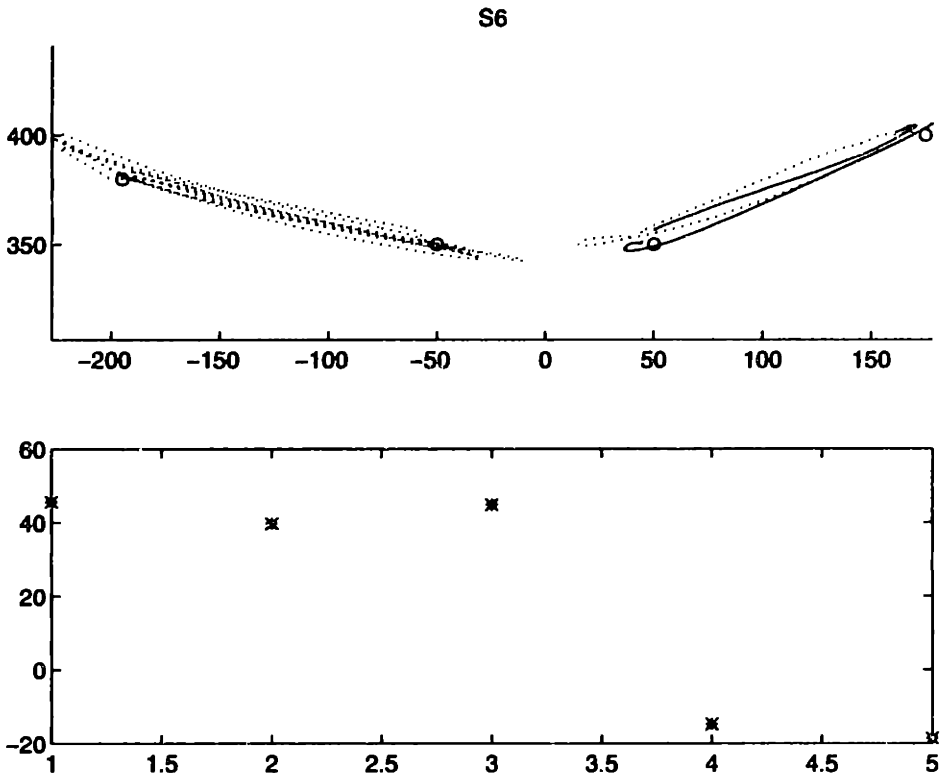

Figure 3-11: The upper panel shows instances of raw data. The aftereffects of the trained trajectories area are shown to the left. The rightmost trajectories represent the aftereffects in the testing region. The lower plot represents the overshoot score for the trajectories shown. The first star represents the score for an aftereffect recorded during the training phase. The second two stars are aftereffects recorded during the testing phase in the trained trajectories. The last two stars represent the scores for the test aftereffects.

region are different, and that the difference is due to the adaptation rather than to a biomechanical or perceptual error.

3.5.3 Discussion

We tested adaptation on a single joint: the shoulder. We found that the shoulder follows the same local pattern of adaptation as the other joints.

Although we do not have any conclusive evidence, we use the generalization of the shoulder as indirect proof that the transfer of aftereffect observed by Shadmehr et al. *could* be attributed to the fact the the shoulder does not have a dominant role in adapting to the experimental task.

3.6 Bimanual transfer

One of the predictions of a local model is that it should not transfer to the contralateral arm. In order to test this hypothesis, we ran the following experiment.

3.6.1 Methods

Subjects were tested in the baseline condition, both with the right dominant arm and with the left non-dominant arm. Subjects practiced until the time constraint could be reliably satisfied using either arm.

Subjects were then exposed to a perturbation pattern while moving with the right arm. They practiced until trajectories recovered the baseline shape. They then switched to the left arm and were tested for aftereffects. They then regrasped the manipulandum with their right arm, to test for aftereffects.

Trajectories whose correlation coefficient with respect to the baseline was lower than 0.9 were considered as aftereffects.

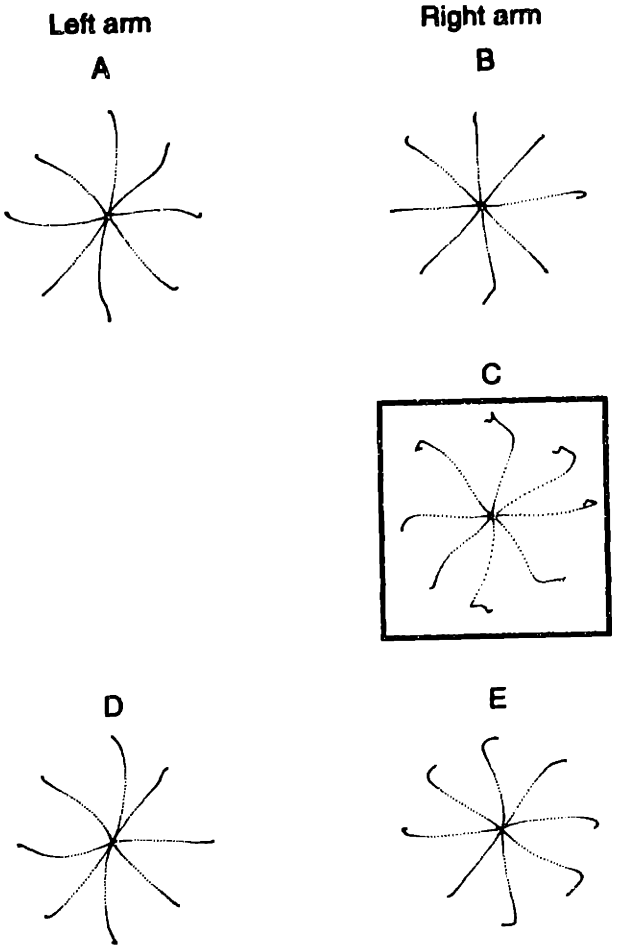

Figure 3-12: Bimanual transfer: (A) left-arm baseline (B) right-arm baseline (C) right arm: trajectories exposed to a clockwise curl perturbation (D) there is no transfer of aftereffects to the left arm (E) aftereffects recorded in the first movements back to the right arm

3.6.2 Results

No aftereffect was observed when switching from the right arm, which had learned to adapt to a perturbation, over to the left arm, which had not been exposed to a perturbation.

When subjects switched back to moving with their right hand instead, aftereffects were detected, eliminating the possibility that arm switching time might have extinguished the effect for the left arm.

We found no task-related effect of transfer, with the exception of what is known as **isochrony principle** [58]: the task imposed an accurate timing and the learning of the timing on one arm facilitated the learning on the contralateral arm.

3.7 Discussion

While many investigators have studied the adaptation of the visual and auditory systems [118], the motor-control system has received less attention. In fact, most of the observed sensori-motor recalibration (for example, in the vestibulo-ocular system) has been attributed to reorganization of a visuo-motor map[71].

The most important finding reported in this chapter is that motor adaptation occurs locally, consistently with the observations in the visual system.

Chapter 4

Motor adaptation is encoded in intrinsic coordinates.

4.1 Introduction

A consistent result in all studies of visuo-motor adaptation is that, with practice, perturbed trajectories converge back to their unperturbed shape. This fact suggests that there is something special about the unperturbed path [29, 27] and that one of the goals of the motor system is to reproduce such shape.

This view argues for the separation of planning from execution of a movement. Planning would be dominated by visual cues, and kinematic constraints only might play a role in it. Dynamics instead, could be accounted for by the "execution" subsystem, which is in charge of translating the plan in motor commands to send to the muscles. In spite of its appeal, the separation of planning and execution is not a universally accepted idea [111, 114], and theories combining these stages have been proposed.

This chapter is aimed at investigating whether motor adaptation follows a pattern of generalization in extrinsic coordinates, as if dominated by visual cues, or if it is a process closer to the dynamics of the system, and can therefore be best described in intrinsic coordinates (muscles or joints). If the former is the case, a change in the arm configuration should produce no effects on learning, provided the same end point

posture is preserved. If, instead, intrinsic coordinates play a role in adaptation, we should observe arm configuration-dependent effects.

4.2 Experiment 1: Two end point fields can be represented as a single field in intrinsic coordinates

If adaptation to a perturbation occurs in extrinsic coordinates, the configuration of the joints during movements should not have any influence in the adaptation process. The following experiment shows that this is not the case: changes from one arm configuration to another are enough to elicit aftereffects of a field previously learned in the latter configuration.

This finding leads to the idea that instead of representing fields in end point coordinates, the CNS represents them in intrinsic coordinates (see Fig. 4-1). Therefore, in order to accommodate two perturbations sharing the same end point space, it is sufficient to build one map in intrinsic coordinates, provided that different configurations are adopted for the different perturbations.

4.2.1 Methods

We asked subjects to grasp the manipulandum using the two postures, A and B, as shown in Fig.4-2. These two postures induce a rotation of the elbow and shoulder joint. Overall the arm is in two different configurations, even if the path of the manipulandum has not changed.

We asked subjects to alternate between the two postures, switching from one to the other every 24 movements.

A clockwise field was presented whenever the subject grasped the handle in posture A and a counterclockwise field was presented in posture B.

Subjects shifted back and forth every 24 movements, between the two postures for 2 sessions of 192 movements each. A minute break was given between sessions.

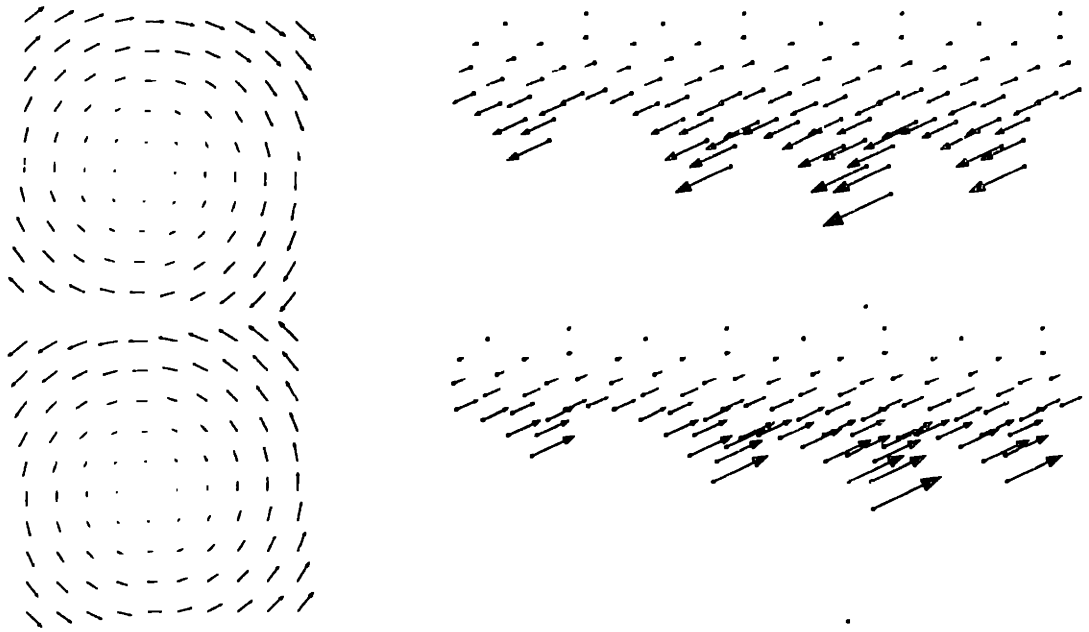

Figure 4-1: Field representation in extrinsic and intrinsic coordinates. The left panels show two curl fields. The x axis is the x velocity, the y axis the y velocity. The right panel shows the corresponding torque fields. Shoulder and elbow velocities are represented on the horizontal and vertical axis

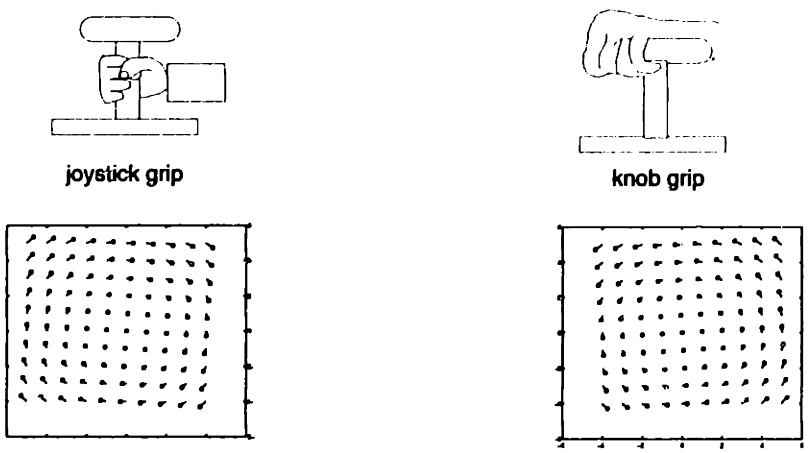

Figure 4-2: Postures and associated perturbations used in the experiment

Every time the posture was switched, the perturbation was switched as well.

In the last two 24-movements blocks, perturbations were not presented and subjects were tested for aftereffects.

4.2.2 Results

Fig. 4-3 shows the results for a typical subject. The baseline trajectories are almost straight for both arm configurations (see Fig. 4-3A and B).

As the perturbation session starts, movements were at first perturbed (see fig. 4-3C and D); however, subjects were eventually able to learn how to compensate for both perturbations (see fig. 4-3 E and F).

We then removed the forces, and subjects continued switching between the two hand postures. We observed that the aftereffects were specific to the field to which subjects had been exposed in each posture. For example, if they adopted posture A, in absence of forces, the observed aftereffects (Fig. 4-3G) were consistent with the field experienced in A. Moreover, once the aftereffects disappeared in posture A, subjects displayed strong specific aftereffects (Fig. 4-3H) as a result of switching over to the posture B, even in the absence of further exposure to forces.

4.2.3 Discussion

There are two possible interpretations of this result. In the first interpretation, the motor system is adapting to a joint-based representation of the force field. The two different configurations of the arm correspond to two different patterns of joint angles, and the two force fields correspond to two separate mappings between joint angles and joint torques. These mappings do not interfere with each other because the two sets of joint angles are separate. In the second interpretation, the motor system is able to learn two different endpoint force fields, and then switch between them by using a sensory cue, such as the arm configuration. We tested this second hypothesis by requiring our subjects to use sensory cues other than the joint angles for switching between two different endpoint fields.

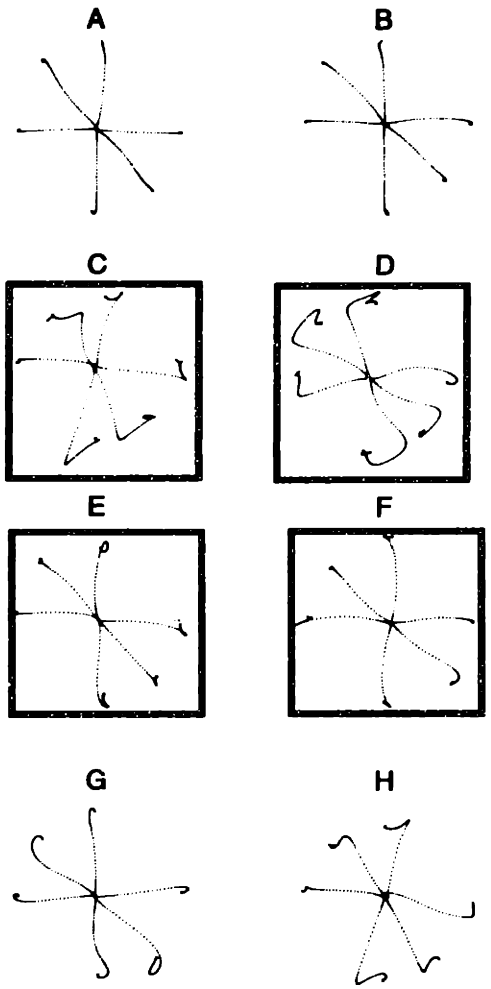

Figure 4-3: (A) and (B) represent the baselines obtained in each posture respectively. (C) and (D) show trajectories distorted by exposure to the perturbations (clockwise for one posture and counterclockwise for the second.) As learning progresses, the trajectories straighten out (E) and (F). (G) shows the aftereffects when subjects switch posture and perturbations are removed: They are consistent with the field expected in posture A. After washout of the aftereffects, if the posture is changed, new aftereffects emerge (H), once again consistent with the field expected in posture B.

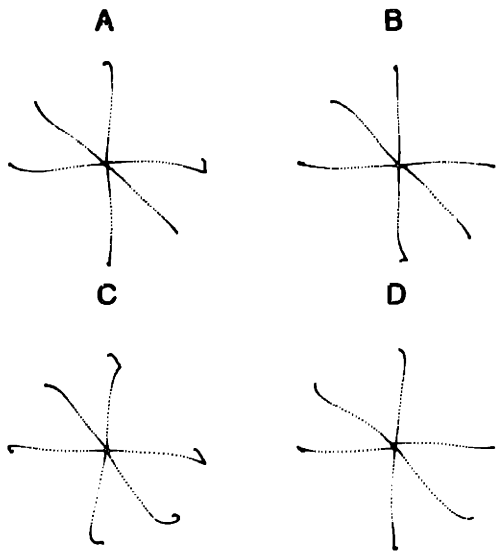

Figure 4-4: Experimental results. Baselines were collected in the red light condition and in the green light condition (panels A and B). Aftereffects were detected only after perturbations were removed (C), and switching the color of the room illumination did not elicit new aftereffects (D).

4.2.4 Experiment 2: A visual cue

We first tried classical conditioning with a visual cue. The two perturbations were no longer associated to different postures, but to the color of the room light. When the first perturbation (clockwise force field) was on, the room was flooded with green light. As the perturbation changed (counterclockwise force field), the room was flooded with red light.

We used exactly the same protocol as in the previous experiment, alternating blocks of 24 movements. When we tested for aftereffects, we found a dependence on the field which was experienced last, and not on the field corresponding to the current light color. See Fig. 4-4C. Furthermore, after the aftereffects were extinguished, no aftereffects could be elicited by a change in illumination (Fig. 4-4D)..

4.2.5 Experiment 3: A proprioceptive cue

Since a visual cue did not induce adaptation, we modified the experiment once more by asking the subjects to use two different thumb postures when moving in the fields, as shown in Fig. 4-5. In this case the overall arm posture was not altered, and only

Figure 4-5: Proprioceptive cues

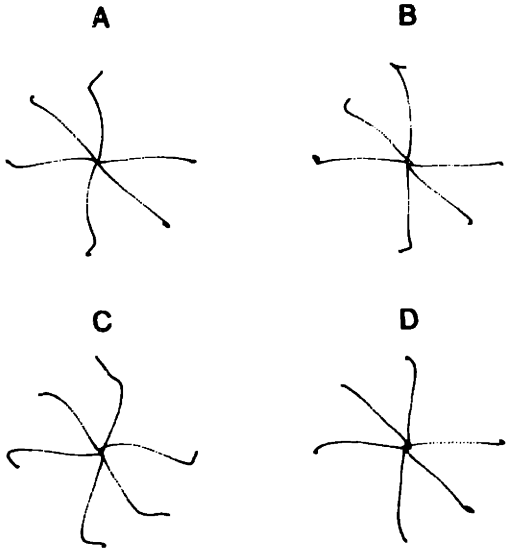

Figure 4-6: Experimental results. Baselines were collected with both thumb positions (panels A and B). Aftereffects were detected only after perturbations were removed (C), and switching thumb posture did not elicit new aftereffects (D).

the hand grip was slightly changed. As with the light experiment, it was not possible to elicit aftereffects by changing the cue thumb position.

Figure 4-6 shows the results for a typical subject. Baselines were collected with both thumb positions (panels A and B). Aftereffects were detected only after perturbations were removed (C), and switching thumb posture did not elicit new aftereffects (D).

4.2.6 Discussion

Both the experiments with the visual cues and with the different thumb positions strongly suggest that motor adaptation can only be affected by factors that are physically involved in compensating the changes of the environmental mechanics.

Clearly, neither the visual cues nor the thumb orientation had any mechanical relation with the forces experienced by the motor system. In this regard, they were abstract and symbolic cues. By contrast, the change in arm configuration associated with switching from position A to position B had a *direct* effect on the pattern of joint torques induced on the limb by the force perturbations. Therefore, our experiments are consistent with the hypothesis that the internal model of the environmental mechanics is represented in intrinsic coordinates. In this system of coordinates, the two experimental conditions (field A associated with posture A and field B with posture B, as shown in Fig. 4-2) can be regarded as a single mapping between torque and limb configuration.

4.3 Experiment 4: How does the system interpolate between different perturbations?

The previous experiment shows that two fields can be efficiently learned by associating them to two different postures. Although we have some evidence of temporary interference between the two configurations, we still do not know what the CNS representation is like in the interpolating postures.

In order to test what happens at interpolating postures, we ran the following experiment.

4.3.1 Methods

We asked subjects to move to 7 targets, equally spaced by 22.5° (see Fig. 4-7). A clockwise curl perturbation, field A, was applied for trajectories at 45° (see trajectory labeled (A) in fig. 4-7). A counterclockwise perturbation, field B, was applied for trajectories at 135° (indicated as (B) in fig. 4-7).

A baseline was acquired on all the movements, in order to test for artifacts in the trajectory curvature due to the dynamics of the manipulandum and its coupling with the human arm.

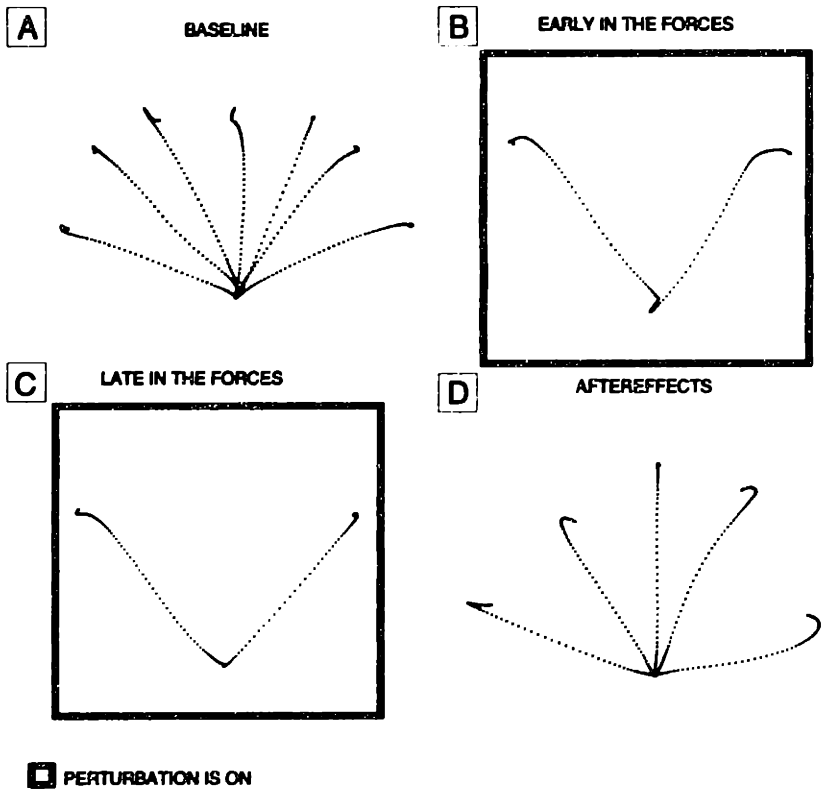

Figure 4-7: A) Baseline trajectories B) a counterclockwise field perturbs trajectories at 45°. A clockwise field perturbs trajectories at 135°. C) With practice, trajectories become straight D) Aftereffects

During the training session, field A was introduced first and randomly removed to probe for aftereffects on all the experimental directions. Field B was subsequently introduced, and the same procedure was repeated. Last, both fields were active at the same time, and aftereffects for their combined presence were recorded.

4.3.2 Results

As subjects were exposed to the first field at 45° only, aftereffects were observed around the trained location. This is consistent with the findings in Chapter 3. Similarly, field B induced adaptation on trajectories around 135°.

In the testing session, both fields were active (see Fig. 4-7B), each along their training direction. The aftereffects in the testing locations appeared to be decaying rapidly, and to be selective for the closest field. In the position equidistant from both fields, we found that the aftereffects seemed to subside. (see Fig. 4-7 D).

4.3.3 Discussion

The two fields used in the experiment were a clockwise and a counterclockwise curl field. These fields have the same structure, but the perturbing forces are rotated by 180°. If the fields are superimposed, they cancel out at each point.

In the experiment described, the fields were practically superimposed, but, by effect of the local decay, the relative strength of each field depended on the distance from the direction in which they had been applied. Only around the center of the interpolating region, the fields were present with equal strength, thus cancelling each other out. This can be seen in in Fig. 4-7D.

This schema is consistent with the idea that a single map can represent both perturbations. The map smoothly incorporates data from both perturbations. Theoretically, there should be some interference in the map, since both fields affect the trajectory at 90°. Practically, given that the perturbations are opposite, no compensatory forces are the best compromise for the field along the trajectory at 90^0.

4.4 Is generalization task specific?

The previous experiments show how the effects of adaptation are also transferred to movements which were never exposed to perturbations. However, all the movements considered belonged to the same class of reaching movements.

The following experiment investigates whether this transfer is a property of movements in the same class, or whether it is a more general phenomenon, affecting any movement spanning an adapted area of the state space.

In order to test which hypothesis is correct, we trained subjects on a perturbation pattern, while executing reaching movements. We then tested whether there was any transfer of aftereffects over a circle drawing task[1].

[1]This work has been done in collaboration with Michael Conditt, Northwestern University, Chicago Il

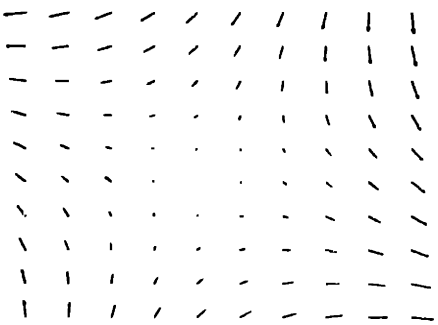

Figure 4-8: Perturbation used in the experiment. We chose an anisotropic perturbation to emphasize the distortions on the circle

4.4.1 Methods

We trained subjects to execute pointing movements to 8 equally spaced targets and to draw circles over approximately the same region. The circle had to be completed in a fixed time, and a bounding box was displayed to give a reference as to the circle size.

During the testing phase, we applied a perturbation while subjects were executing pointing movements. We then removed the perturbation, and asked the subjects to draw circles to test for indirect aftereffects, i.e. aftereffects induced by adaptation on a different task.

Subsequently, we trained subjects to draw circles while exposed to the same perturbation as during pointing movements. As the subjects adapted to the perturbation, we removed it, and tested for direct aftereffects, i.e. aftereffects induced by adaptation on the same task.

4.4.2 Results

Fig.4-9 shows the results for a typical subject.

Panel A shows a set of circles produced *before* the subjects were exposed to any perturbation.

Panel B shows the distortions induced by the perturbation on the reaching movements. The perturbation we used (see Fig. 4-8) is a saddle point, whose anisotropies ease the detection of distortions on circle drawing.

Panel C shows the indirect aftereffects. Clearly, the circles are strongly distorted by the adaptation to the perturbation. We measured the eccentricity of the best fitting ellipse, and found a significant difference with respect to the baseline circles.

When subjects were asked to produce circles under the perturbation condition (Fig. 4-9D), the resulting trajectories displayed a strong skewing in the opposite direction. However, as the perturbation was removed, the trajectories showed direct aftereffects (Fig. 4-9E), which were qualitatively similar to the indirect aftereffects. It is currently not possible to quantify the differences, since it is still unclear how to compare the amount of learning to which the subjects had been exposed while executing reaching movements, with the amount of learning while drawing circles.

Panel F shows the performance on circle drawing once the aftereffects have washed out. The circles now strongly resemble those recorded during the baseline trials, indicating that the distortions previously discussed were not a byproduct of fatigue or a change in strategy.

Fig. 4-10 shows the changes in eccentricity induced by previous experience of the perturbation active while drawing circles (dashed line), or active while executing reaching movements (solid line). The dotted line indicates the eccentricity measured during non-perturbed baseline trials.

4.4.3 Discussion

Adaptation produces effects that generalize across tasks. Under the conditions explored, the circle and the reaching movements could not define different motor contexts. Therefore, the nervous system did not build multiple maps which could subsequently be evoked by different movements. Instead, a single map was generated and applied for each movement.

Our experiments imply that motor learning effects can be detected when movements involve the same set of configurations employed while learning, irrespective of the task being performed. Therefore, learning *might* occur at a motor level which is shared by the different tasks.

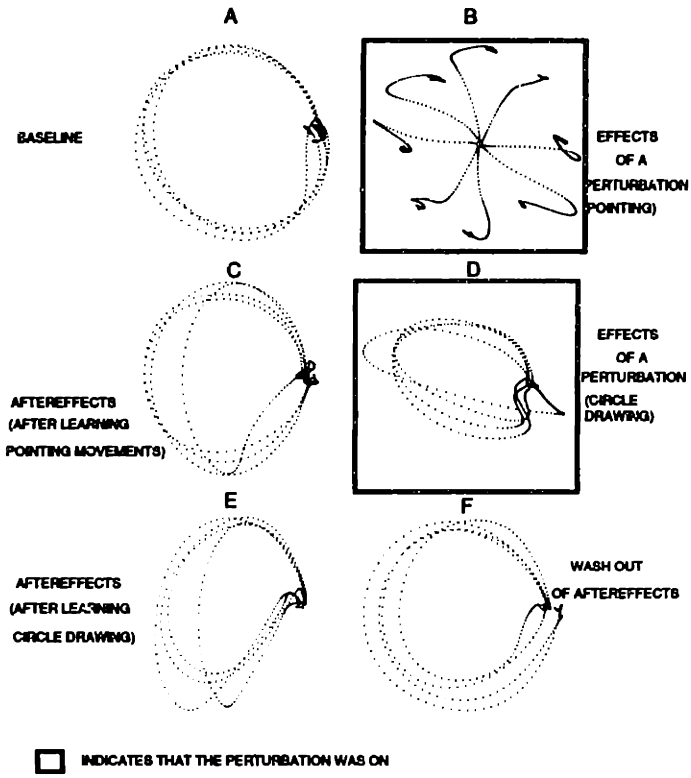

Figure 4-9: Transfer of aftereffects from pointing movements to circle drawing. Superimposed traces represent subsequent trials. A) represents the baseline for circle drawing. D) shows the effects of learning a field during pointing movements. F) shows the effects of the force field on circle drawing. G) aftereffects on circle drawing produced by the learning of the field while drawing circles. J) circle drawing after the aftereffects have washed out.

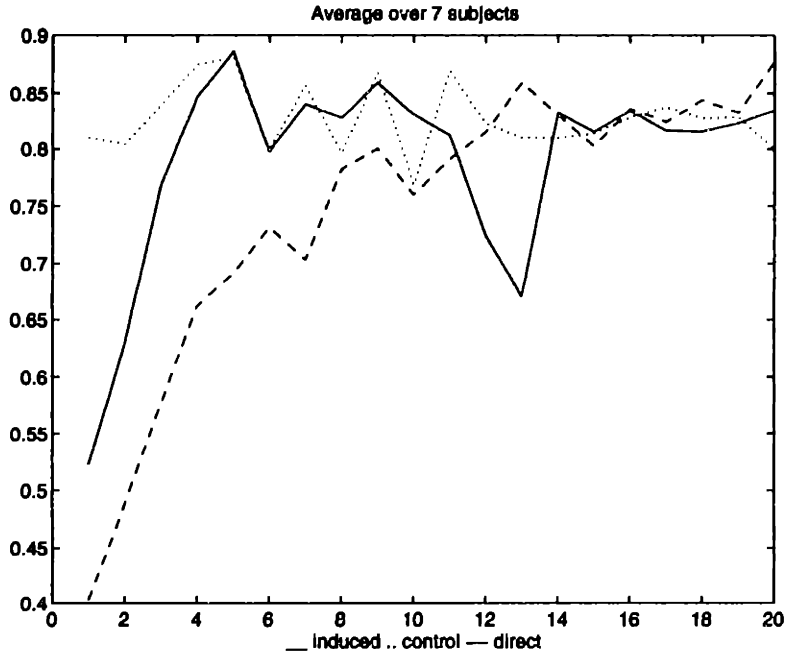

Figure 4-10: Eccentricity as a function of trials. Dotted line: eccentricity measured on control circles. Solid line: distortions induced by having previously moved in a field while executing reaching movements (induced indirect aftereffect). Dashed line: distortions induced by having previously moved in a field while drawing circles (direct aftereffect)

4.5 Discussion

This chapter has shown that adaptation occurs in intrinsic coordinates.

This finding draws an interesting parallel between visual perturbations (which have their main effects in extrinsic coordinates), and motor perturbations. Wolpert et al. have found that subjects compensate for visual distortions in the trajectory feedback by altering their movements so as to restore their natural visual appearance. The pattern of generalization of the distortion was consistent with adaptation in extrinsic space.

Our results indicate that indeed subjects do tend to modify their trajectories so as to achieve straight paths in visual space. Nonetheless, the pattern of adaptation is consistent with an intrinsic representation of the perturbation.

This schema is consistent with a separation between planning and execution, in which planning is dominated by the visual domain, and the execution level compen-

sates for the system dynamics in order to carry on the plan.

The execution level *could* be composed of a strategy to execute plans "under normal circumstances" (for example by combining pre-existing primitives), and a mechanism to compensate for changes: Adaptation. Under this hypothesis, whenever a change occurs in the environment, a new primitive could be generated to compensate for the changes. This primitive is used whenever a movement is generated, since the environment is assumed not to change in relation to the specific actions taken.

Chapter 5

Monkey Psychophysics

5.1 Introduction

The previous chapters have shown that humans succeed in adapting to external perturbations by modeling them.

In order to understand how this process is implemented in biological systems, it is necessary to change methodology and address the question from the physiological point of view.

The first step in this direction is to establish if the effects observed in human behavior are reproducible in primates. The aim of this chapter is to present data indicating that monkeys are able to adapt to viscous fields, and that the pattern of adaptation closely resembles that which has been observed in humans.

5.2 Experimental set up

A quasi-replica of the human set up has been assembled. Some changes have been introduced to simplify the neural recording procedure which will take place in the second part of the project.

The monkey manipulandum is a 2 degrees of freedom planar arm. Its link lengths measure 20 and 23cm respectively. Its design is a scaled replica of the human manipulandum. Each joint is activated independently by a E.G.G. motor driven by

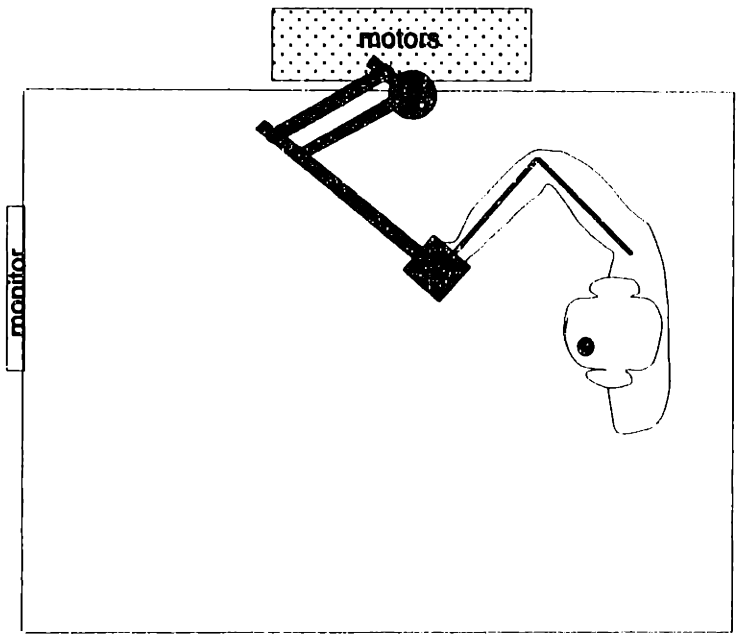

Figure 5-1: A sketch of the setup used for monkey psychophysics: The monkey sits at 90° with respect to the manipulandum and faces a computer monitor onto which the targets are displayed

PMI amplifiers. Potentiometers provide information on the position of the arm and velocity data is computed using a hardware filter developed in house.

The manipulandum is controlled by a Gateway2000 90MHz Pentium computer. The communication with the peripherals (encoders/amplifiers/juicer) is done through a Computer Boards DAS 1602/12 D/A and A/D board.

The system is controlled at a frequency of 100Hz. For each cycle, the position and velocity of the manipulandum joints are updated. If necessary, a suitable perturbation torque is computed and a signal is sent to the amplifiers which provide the motors with the appropriate current. If necessary, a command is sent to the solenoid controlling the juice supply (the monkey is rewarded for its work with drops of apple juice). The status of the system is saved into a buffer and it is periodically downloaded to a file.

The two major differences between the hardware of the human manipulandum and the monkey manipulandum are the following:

- the size of the monkey apparatus is reduced, since the arm length of our monkeys is smaller than humans.

- the monkeys sit at 90° with respect to the manipulandum. This modification was dictated by the need of keeping the animals head perfectly vertical during neural recordings. The presence of the elbow motor above the manipulandum "shoulder" prevented us from putting the computer monitor there. We decided then to rotate the monkeys by 90° freeing ourselves from the constraints imposed by the motors.

Figure 5-1 shows the setup.

The software was developed under the Borland C++ environment. The control loop is written in C++, as an interaction of state machines. The target, reward, and data management, are each independently organized by a separate state machine.

The interface to the D/A board is written in C, and the timing software was written in assembly language by E. Todorov.

5.3 Experimental paradigm

Three Monkeys (Macaca Nemestrina) are currently under training. Data from two male monkeys (B. approx 11Kg. and M. approx 8Kg.) are presented here. The monkeys are water deprived during the week, and received a drop of apple juice (approx 0.3-0.5 ml) for each correct trajectory. A trajectory was considered correct if the cursor reached the target within the given time limit (1sec), and if the cursor (3 pixel) was kept within the target (14 pixels) for 1sec. If the monkey failed to reach the target on time, or did not execute the hold period, no reward was given and the next target appeared. Targets were organized in star-like pattern at a distance of 10cm from the center. Outward targets appeared pseudo-randomly. The return trajectory was always predictably toward the center.

The protocol is consistent with the human experiment. Initially, a baseline was acquired in absence of external perturbations. A force field was then selected, and the animal learned how to move in it. When the trajectories were back to their baseline shape, the perturbation was removed and aftereffects were recorded. Aftereffects washed out after few trials of re-exposure to the baseline condition.

5.3.1 Data analysis

Unlike humans, monkeys often loose concentration and get distracted. Their inconsistency makes it impossible to extract a reliable baseline as a function of few randomly selected trajectories. In order to avoid time consuming and biased visual inspection of the trajectories used for the computation of the baseline, we developed an algorithm which fully automates the process.

For each trajectory, we consider the velocity vectors. This approach eliminates the bias of the starting point. All trajectories in a movement direction (in absence of external perturbations) are pooled together, and averaged. The inner product between each trajectory and the average is computed. The trajectory with the least score is rejected as an outlyer. The procedure is repeated until the average trajectory is considered a good representative of the trajectories in that direction. Our criterion is that the remaining trajectories correlate at least 0.95 with the average trajectory. The advantage of this procedure is that it automatically eliminates outlyers, converging on the "true" average movement. The algorithm could fail if, for example, the monkey had two independent strategies which were alternated. The algorithm would try to converge to the mean of the two clusters, which lies outside both clusters and possibly it would not converge. We propose this analysis method nonetheless, because our trajectories are "well-behaved", in the sense that they form a single cluster with a number of random outlyers.

Once a baseline has been identified for each direction, it is used a reference trajectory. Scores for each trajectory are computed by inner product, following the same algorithm as in the human experiment analysis.

5.3.2 Experiment 1: does adaptation occur in non-human primates?

The first issue we confronted was whether the macaque is a good animal model for motor adaptation. In order to address the issue, we tested whether monkeys are able to adapt to a single force field.

We gathered baseline trajectories, exposed two animals to force fields, and recorded aftereffects.

We found that when animals are initially exposed to a perturbation pattern, their trajectories are initially perturbed similarly to what is recorded with human subjects.

Progressively, the trajectories converge back to baseline, displaying adaptation. The monkey receives no incentive for adaptation. The reward is administered whenever a target is successfully reached, and the timing of the task is such that a distorted trajectory is often rewarded.

When the perturbation is removed, humans and monkeys alike display aftereffects. It is therefore possible to conclude that monkeys adapt selectively to force fields, and their convergence to baseline trajectories is not simply a result of co-contraction.

Fig. 5-2 shows an example of adaptation. The upper left panel (A) shows baseline trajectories. The upper right panel (B) shows early trajectories in the field, still highly perturbed. The lower left panel (C) shows adapted trajectories. The lower right panel (D) shows aftereffects generated by unexpectingly removing the perturbation. Fig. 5-3 shows the perturbation used in the session. The right panel shows the performance of the monkey. The axis indicates samples trajectories. The y axis indicates the correlation coefficient. The black thick rectangle identifies the trials when the perturbation was switched on.

5.4 Experiment 2: Retention

Humans not only adapt to external environment, they also form memories [9] which allow for improved performance over subsequent days.

We tested whether monkeys display similar retention, or whether they are unable to carry on memories from one session to the next.

We tested monkey B. over subsequent days. The monkey underwent the same procedure as described in the previous experiment. The perturbation pattern was not changed from one day to the other.

We found that indeed, experience is carried on from one day to the next.

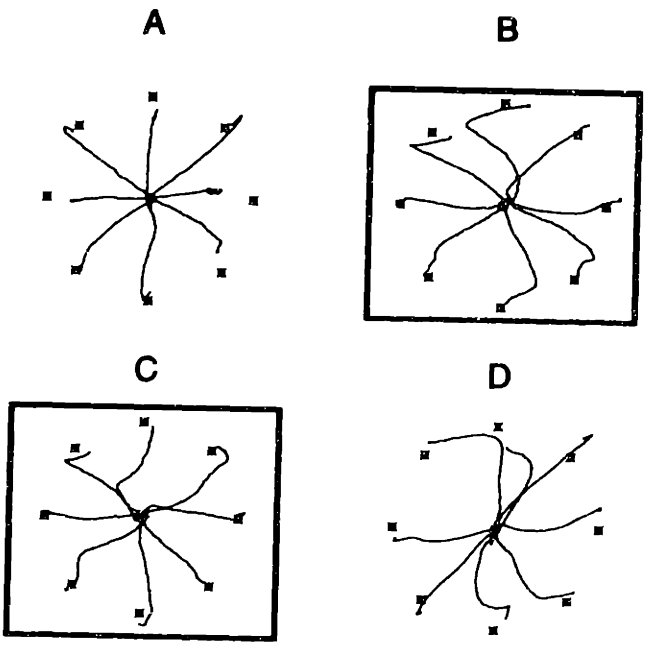

Figure 5-2: Data from a day of training in monkey M.

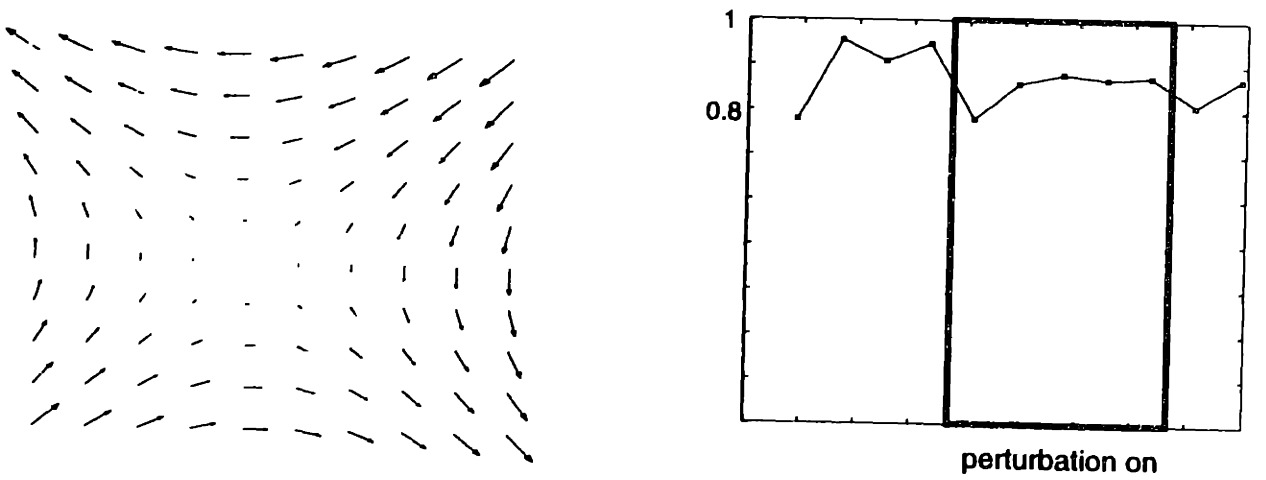

Figure 5-3: Left panel: the viscous perturbation Right panel: the learning curve

On one hand, the starting performance level in a field is higher with different days of training. In other words, switching on a field produces less and less perturbations as the training days increase.

On the other hand, the final performance level increases with the number of days of training and the top performance plateau is reached faster with subsequent exposure to the field. This indicates that the monkey is primed for the field, and, in addition to remembering the field from the previous days, its daily learning rate is accelerated by practice.

One example of this behavior is shown in fig. 5-4. Three consecutive days of training are represented on the x-axis, separated by a vertical line. The y-axis represents the correlation coefficient for each movement. Each * is the average of 8 movements. A regression through the data has been computed for each day. In order to eliminate outlyers, only data within one standard deviation from the median have been considered in the regression. The lines indicate the trend in the behavior of the animal, showing a progress in adaptation for each subsequent day.

5.4.1 Experiment 3: Interference

We have shown that it is possible for non-human primates to adapt to a perturbation and that the memory of what was learned is carried on across subsequent days. The amount of training also correlates with the ease with which monkeys can switch between the perturbation and no-perturbation conditions. As the training progresses, the amount of interference is greatly reduced.

We set to investigate whether this ability to switch between different environments depends on the particular nature of one of them, the natural gravitational field, or whether it is a more general mechanism of the adaptation system.

In order to investigate this issue, we rephrased it as: can primates learn more that one force field?

We repeated the protocol described in Experiment 1 with the following modification: after exposure to a perturbation, instead of removing it and testing for aftereffects, we changed the perturbation pattern to a new one (shown in Fig 5-5).

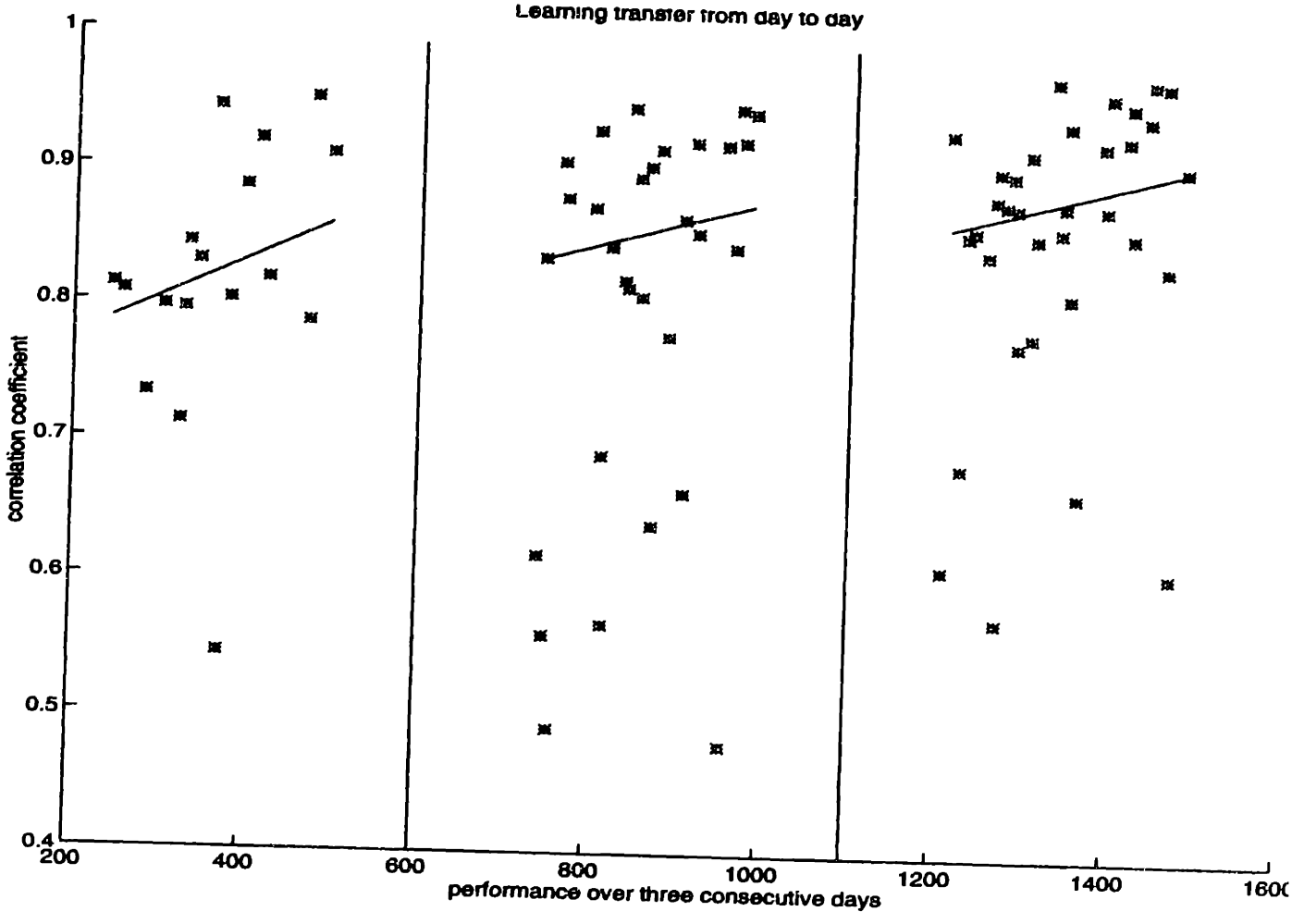

Figure 5-4: Retention: the vertical lines divide the session recorded over 3 consecutive days. Averages of subsequent trials are represented on the x axis, and their correlation coefficient is shown in the y axis. The regression lines for each day represent the trend in the learning.

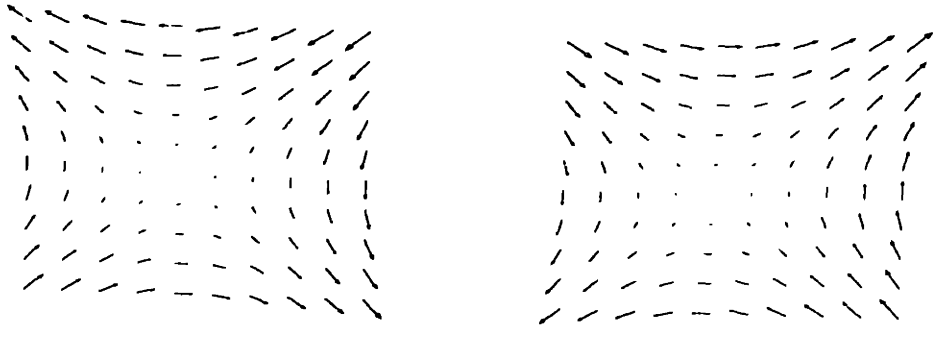

Figure 5-5: The left panel shows the first perturbation given within a session. The right panel shows the perturbation given after the first has been learned.

The first finding is a confirmation of what Brashers-Krug [10] observed in humans: Two competing perturbations administered in sequence compete for resources. This is normally referred to as "interference". Therefore, the second field is learned less efficiently than the first, i.e. it needs more training to obtain the same performance level.

Fig. 5-6 shows the different time scales of learning for the two perturbations. In each plot, the straight solid line represents the 1.0 correlation coefficient line. The dashed line shows the 0.9 level. The plots should be read from bottom up, and each plot is offset by a unit to improve readability. The lowest plot shows the evolution of the baseline, as the animal starts an experimental session. Each open circle represents the mean value for the day, and the bar represents one standard deviation. The circles are connected by solid lines to emphasize the trend. 8 days (4 in one week and 4 in the next) were considered. The average baseline day lies mostly within the 0.9 threshold.

The second plot (labeled as "field A") shows the evolution of adaptation to the first field. The monkey starts from an average correlation coefficient of 0.8, and within 8 days it reaches a daily average of 0.9.

The third plot ("field B") shows that the performance drops, due to exposure to the second field. Nonetheless, the mean performance increases dramatically as the animal practices. Eventually, the animal reaches the same mean performance both in field A and B.

The fourth plot ("baseline final") shows that after washout of the aftereffects, the monkey regains a stable performance. This is an important control which rules out changes in strategies or fatigue, which could account for poor performance on some days.

5.4.2 Interference and local models

The phenomena of interference can be easily explained in terms of a local model in which information is incorporated on the basis of experience. When the subjects experience the first field, their representation of the environment can be described as a *tabula rasa*, a null map. No information is available, therefore no bias is present.

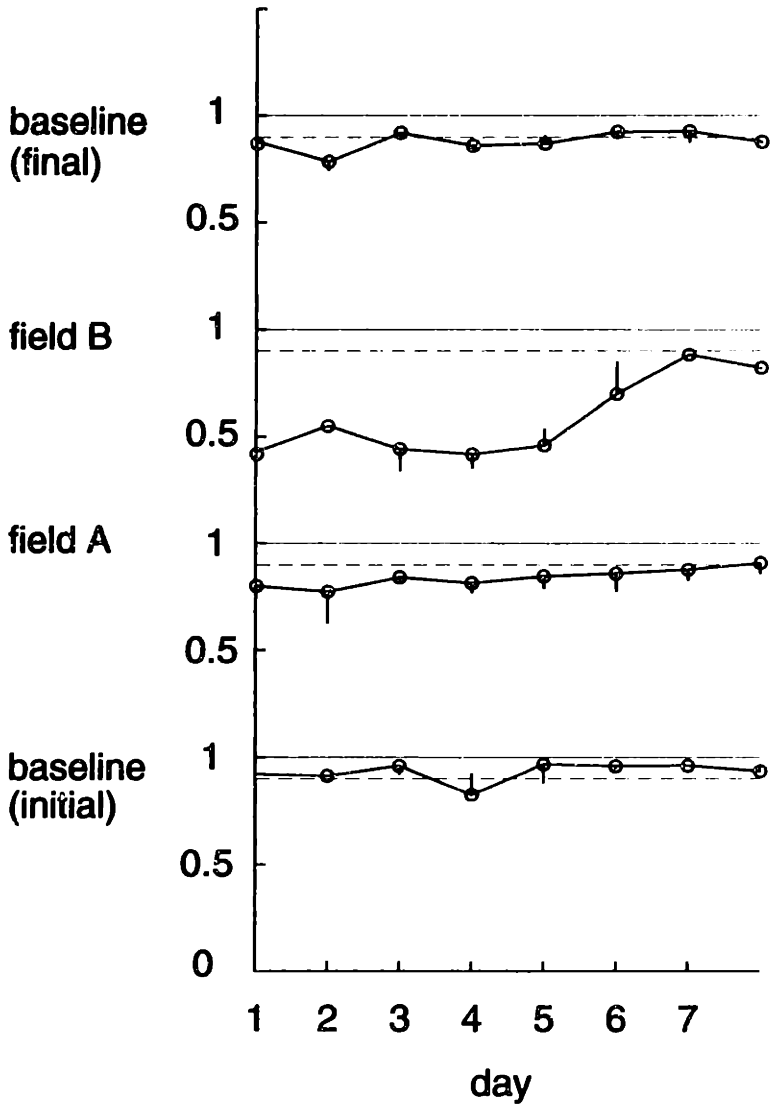

Figure 5-6: Interference between two fields. The bottom plot represents the evolution of the baseline over 8 days. The second and third plot show the adaptation to the first and second field over time. The fourth plot shows the last trajectories in absence of perturbations and after washout of the aftereffects.

As the first perturbation pattern is learned, the environment model becomes biased towards the perturbation for which it is learning to compensate.

As the second perturbation is introduced, the compensatory commands are still tuned towards the first pattern. The model must first recover from the bias, and then learn how to cope with the second perturbation pattern.

Eventually, both perturbation patterns are learned and retained. This process can be modeled as a separation of maps, as shown in humans. The motor system learns to recognize the two perturbations as separate entities and instead of trying to fit both of them onto a single map, it develops separate representations for each. This phenomenon has been modeled in the humans [10] using the hierarchical networks developed by Jordan and Jacobs [62].

5.5 Conclusions

We have shown that humans and non-human primates alike adapt to dynamical perturbations of the external environment. They compensate for aftereffects using a perturbation specific strategy (as opposed to cocontraction), retain learning across subsequent days, and display interference if different patterns are presented one after the other.

Macaques are therefore a good animal model for motor adaptation.

This allows us to widen the investigation to the neural substrate of motor adaptation.

Part II

A model of motor primitives

Overview

Part 1 has shown that motor adaptation leads to the formation of an internal model of the outside environment. Such model is local and it is best expressed in intrinsic coordinates.

Part 2 presents a computational model of how the representation of the environment is incorporated in the motor system. We will show that the environment can be modeled as a motor primitive which is linearly added to the unperturbed motor plan.

Chapter 6 shows that the nervous system builds a smooth map which associates the state of the arm and the compensatory torques necessary to counterbalance the perturbations induced by the environment. We describe a mechanism for the formation of maps to adapt to external perturbations based on Kernel Regression, a smooth interpolation technique. We show that the proposed mechanism can reproduce the psychophysical results presented in the previous chapters.

We are left with the problem of how to implement these motor primitives, in other words, of how to translate the torques specified by the primitives into motor commands interpretable by the muscles. Investigations by Bizzi and collaborators [7, 43, 44, 42] has demonstrated that the spinal cord is not a functionally homogeneous structure with respect to the production of forces.

The electrical and chemical stimulation of each patch has been shown to correspond to a behavior. Coactivation of different regions produces an end point behavior consistent with the linear summation of the costimulated patches. Chapter 7 presents a model of the structure of the cord. It shows that linear summation is not a necessary outcome of the biomechanical structure of the model. Nonetheless, a number

of Montecarlo simulations point out that linear summation is a likely consequence of coactivation of different muscle pools.

The implementation of motor primitives can therefore be modeled as a coactivation of spinal cord primitives.

The only step missing is how to do the actual approximation of the "adaptation" field to the spinal primitives. Chapter 8 presents a network capable of approximating an arbitrary pattern of vectors by a linear superposition of non-linear vector fields.

Chapter 6

A computational model of motor adaptation

6.1 Introduction

The previous chapters have presented constraints on how an internal model of the outside environment is represented in the CNS. This chapter is aimed at modelling the learning process which occurs in the nervous system. We postulate that the nervous system builds a smooth map which associates the state of the arm (position and velocity) and the compensatory torques necessary to counterbalance the perturbations induced by the environment.

After reviewing some evidence that maps are ubiquitous in the brain, we describe a mechanism for the formation of maps to adapt to external perturbations.

We show that the proposed mechanism can reproduce the psychophysical results presented in the previous chapters.

6.2 Brain and Maps

The concept of representation has received great attention in the medical and neuroscience community. Early in the century, neurologists like Broadmann and Penfield [11, 89] discovered that the brain was not a homogeneous structure but could be

subdivided cytoarchitectonically and functionally in different areas. They used microstimulation of the human brain in the preparation for surgery to relieve patients of epileptic seizures. This microstimulation led to the identification of body maps in the brain. Penfield found that if primary somatosensory cortex (S1) was stimulated, sensations could be evoked in the contralateral part of the body in an orderly fashion, and he described the corresponding somatotopic map known as "homunculus".

Further investigation by Kaas et al. [64, 65] among others, showed that somatosensory cortex is far more complex than what Penfield described. A number of maps, at least four, have been identified in subregions of S1 which are now know as Broadmann areas 3a, 3b, 1 and 2 [123, 76].

A topographic organization is by no means exclusive of S1. An early description of primary motor cortex (M1) by the neurologist J.H. Jackson [61] indicates that seizures involving M1 progress in an orderly fashion through the body indicating the presence of a map which is stimulated as the seizure wave progresses along the cortex. More recently, a variety of microstimulation studies [3] and recordings from cortical neurons [34, 32, 102, 2] have characterized M1 at different levels. A "motor homunculus" has been described, similarly to the findings in S1. Detailed studies have indicated that anatomically [19, 100, 101], projections from M1 to muscle pools are not one-to-one and a single muscle has multiple representations in M1. M1's structure is therefore more complex than a simple cortex-to-muscle map.

Functionally, studies by Georgopoulos et al. [34, 66, 16] indicate that M1 neurons are responsive to the direction of motion. In contrast, Scott [103] prefers not to map the activity of M1 onto a single coordinate system. He presents evidence that the activity of M1 is best interpreted initially within an extrinsic coordinate system but, as the movement progresses, the activity becomes more correlated with intrinsic coordinates. Dynamics has also been shown to correlate with M1 activity: Evidence has been collected about M1 response to external loads [66, 33, 22]. Therefore, although anatomical studies reveal a clear distributed mapping between cortical patches and muscles, its functional significance is still matter of debate.

Somatotopic maps have been characterized all over the brain. In premotor areas,

Rizzolatti et al. [75, 95] found multiple representations of the body. Similarly, the cerebellum [1, 106, 109, 60] and its nuclei as well as the basal ganglia [47] have been shown to be topographically organized.

Although an abundance of information is available on how the CNS represents the body, both from the physiological and the genetic point of view [96, 18], less is known about how the outside environment is encoded in the brain.

Gross and Graziano found neurons in premotor cortex which seem to provide a representation of the space near the body, which might be useful for the visual control of reaching [49]. These neurons were characterized as having both a somatosensory and a visual receptive field. Both receptive fields were in register and corresponded to the same region of the external space. Cells with similar characteristics were found in areas 6, 7b and VIP [48].

The most extensively investigated aspect of the representation of external space is object recognition. Clinical observations on patients undergoing unilateral anterior temporal lobotomy exhibited specific visuo-perceptual deficits [79, 80]. Lesions in inferotemporal cortex led to impairment in pattern recognition [50]. Recent investigations by Poggio et al. propose [74, 15, 90] that the actual representation of objects is composed by a number of 2-D views and not by a 3-D reconstruction. Physiological evidence supporting this theory has been presented by Logothetis et al. [73]. They showed that a population of inferotemporal neurons responds with high selectivity to individual views of previously-seen objects. A tuning curve of the cell response to different views has been observed, indicating a preference for some views.

The representation of extracorporal space has also been investigated by Wilson and McNaughton [121, 120], who studied the activity of hyppocampal cells as rats moved in a known environment. They also investigated how the representation of external space develops through exploration of an unknown environment. They found evidence that the animal position and movement in the maze can be predicted using a population code.

6.3 The model

Chapter 2 has demonstrated that learning is local to the trained regions. Learning is not instantaneous, but it follows a typical time course of the order of 10-15 minutes in normal subjects. The amount of aftereffects detected correlates positively with the training time and with the similarity of the trajectories in the field with respect to the baseline trajectories. Chapter 3 has shown that learning is best described in intrinsic coordinates and it affects all movements, independently from those which were used to adapt to the environment.

In order to comply with these constraints, the model we present is structured as a map between state space and torques. The state variables considered are joint positions and velocities. These variables are biologically measurable [37].

Initially, the map is null, since we assume that no compensation is necessary in the unperturbed condition and, for example, the gravitational offset has been accounted for elsewhere, for example in another map. As the arm starts to move and it is exposed to a perturbation, a discrepancy is experienced between the expected outcome of the motor command and the actual movement. The map is therefore updated. The constraint on locality and the time course of learning prompted the choice of Kernel Regression as an update method [51, 88, 117] since it trades off accuracy in data reproduction and smoothness.

6.4 Kernel Regression

Kernel regression is a closed form algorithm which smoothly approximates a function from sampled data. The kernel chosen in the simulation is a gaussian kernel.

We defined a mapping $T(q)$ from state space $\mathcal{Q}$ to output torques $\mathcal{T}$. We initialized the simulation to a null map ($T(q) = 0$) at each data point. Given the kernel width σ, the smoothed value t of the map in the q point is equal to:

$$t(q) = \frac{\sum_{i=1}^{n} T(q_i) e^{-\frac{\|q-q_i\|^2}{\sigma^2}}}{\sum_{i=1}^{n} e^{-\frac{\|q-q_i\|^2}{\sigma^2}}} \tag{6.1}$$

Each data point is smoothed with the neighbouring points. The balance of the smoothing is incorporated into the width of the kernel σ. σ controls the degree of smoothing but also how fast the system can learn a mapping. The larger the selected σ, the higher the smoothing, the more the sampled data is blurred with the neighbours. In order to sharpen the data representation, the data must be presented multiple times to the system.

6.5 The simulation

A dynamic simulation of a 2 degrees of freedom arm was developed using MATLAB. Straight trajectories to the desired target were planned using minimum jerk [29, 27] as a model. The necessary torques were computed using a dynamic model of the arm [124]. The following equations of dynamics were implemented:

$$\tau_1 = M_{11}\ddot{\theta}_1 + M_{12}\ddot{\theta}_2 + h_{122}\dot{\theta}_2^{\,2} + 2h_{112}\dot{\theta}_1\dot{\theta}_2 \tag{6.2}$$

$$\tau_2 = M_{21}\ddot{\theta}_1 + M_{22}\ddot{\theta}_2 + h_{211}\dot{\theta}_1^{\,2} \tag{6.3}$$

Where:

$$M_{11} = m_1 l_g 1^2 + I_1 + m_2(l_1^2 + l_{g2}^2 + 2l_1 lg2C_2) + I_2 \tag{6.4}$$

$$M_{12} = M_{21} = m_2(l_{g2}^2 + l_1 l_{g2} C_2) + I_2 \tag{6.5}$$

$$M_{22} = m_2 l_{g2}^2 + I_2 \tag{6.6}$$

$$h_{122} = h_{112} = -h_{211} = -m_2 l_1 l_g 2S_2 \tag{6.7}$$

and $C_2 = \cos(q_2)$ and $S_2 = \sin(q2)$

For each time step, a torque ($\tau_{dynamics} = [\tau_1 \tau_2]$) necessary to execute the movement was computed. The arm control ($\tau_{control}$) consists of two terms: the arm dynamics and a visco-elastic term. The latter term defines an equilibrium around the desired trajectory ($[q_e; \dot{q}_e]$). Therefore, $\tau_{control} = \tau_{dynamics} + K(q - q_e) + B(\dot{q} - \dot{q}_e)$. A term τ_{model} was added to the computed torque to accommodate the input from the map

Manipulandum simulation parameters		
Description	Symbol	Value
link 1 (L_1) length	l_1	0.357
link 2 (L_2) length	l_2	0.337
L_1 center of mass	l_{g1}	$l_1/2$
L_2 center of mass	l_{g2}	$l_2/3*2$
L_1 mass	m_1	0.024
L_2 mass	m_2	0.024
L_1 inertia	I_1	0.0141
L_2 inertia	I_2	0.0188

Table 6.1: Simulation parameters used for the 2 d.o.f. manipulandum

Human arm simulation parameters		
Description	Symbol	Value
link 1 (L_1) length	l_1	0.33
link 2 (L_2) length	l_2	0.34
L_1 center of mass	l_{g1}	$l_1/2$
L_2 center of mass	l_{g2}	$l_2/3*2$
L_1 mass	m_1	1.93
L_2 mass	m_2	1.52
L_1 inertia	I_1	0.0141
L_2 inertia	I_2	0.0188

Table 6.2: Simulation parameters used for the human arm [105]

model of the outside world. Initially this term was always zero, since no model of the environment was available. $\tau_{environment}$ is the projection of the external perturbation onto the joints. The simulation moved the arm according to the following relationship:

$$\tau = \tau_{control} + \tau_{model} + \tau_{environment} \tag{6.8}$$

The parameters for the simulation of the manipulandum are shown in table 6.1. The parameters for the simulation of the human arm are shown in table 6.2 [105].

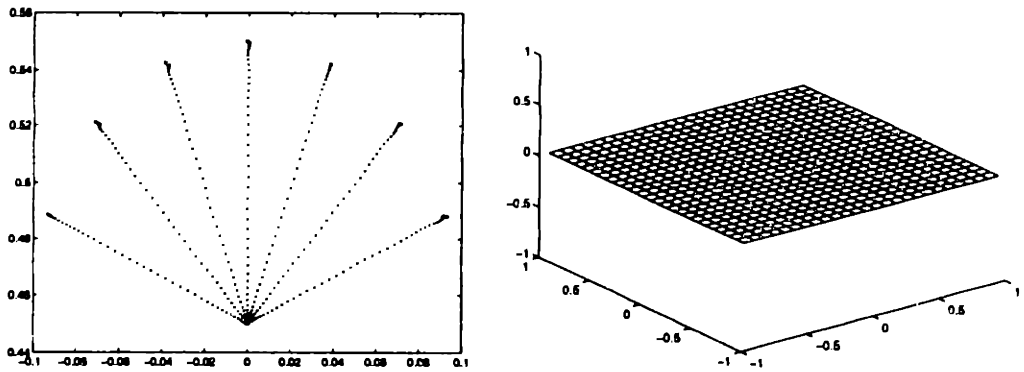

Figure 6-1: Simulated baseline trajectories appear virtually straight (left panel). Initially the model of the external world is null, since no experience has been gathered so far.

6.6 Simulation Results

6.6.1 Experiment 1: Generalization

The generalization experiment reported in Chapter 3 on humans was repeated onto the model.

Initially, τ_{model} was zero as no experience had been gathered by the system. A set of baseline trajectories was acquired in absence of external perturbations ($\tau_{environment} = 0.$) Fig. 6-1 shows the output of the simulation. The left panel shows the baseline trajectories, the right panel shows the initial null map. The x axis represents the shoulder joint velocity, the y axis the elbow joint velocity. The z axis represents the magnitude of the torques.

A clockwise curl perturbation is then fed into the system when the model arm moves straight upward. Initially the trajectory is highly perturbed. Fig. 6-2 shows the first trajectory. The right panel shows a superposition of the $\tau_{environment}$, which distorted the baseline trajectories, and the null map.

As more practice is allowed, the map is refined and trajectories become straighter (see Fig. 6-3.)

We then tested the model on neighboring trajectories to test for aftereffects. We found that aftereffects are present in neighboring directions and, as seen in human subjects, their effects decay with distance from the trained locations (fig. 6-4.)

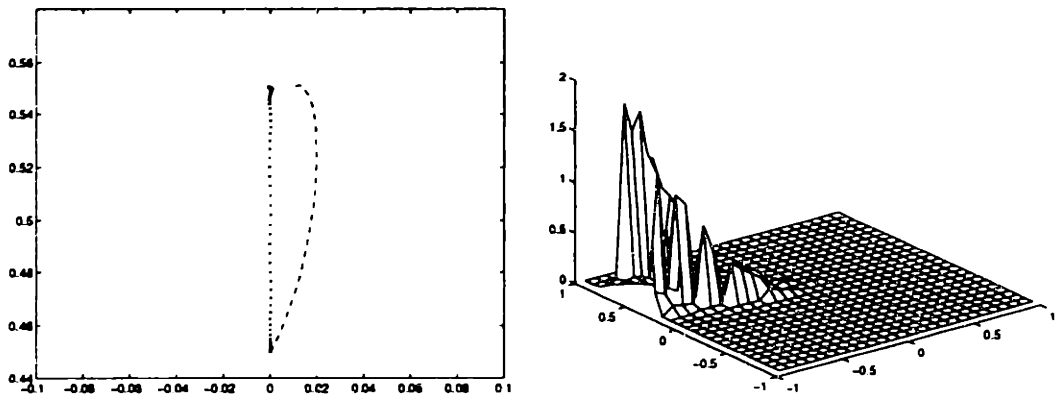

Figure 6-2: Left: Trajectories are initially highly perturbed. The dotted line is the baseline trajectory. The dashed line the perturbed trajectory. Right: The environmental torques which distorted the trajectories are superimposed to the null map

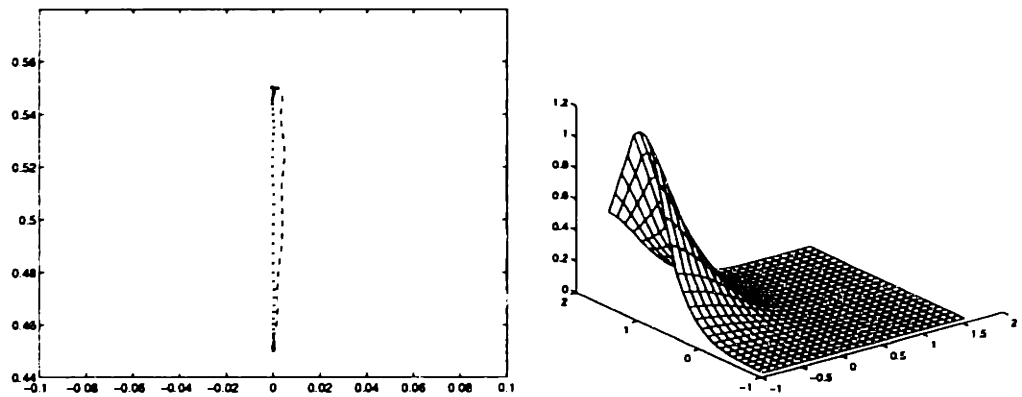

Figure 6-3: As learning progresses, the trajectory becomes straighter and the map better approximates the expected perturbation

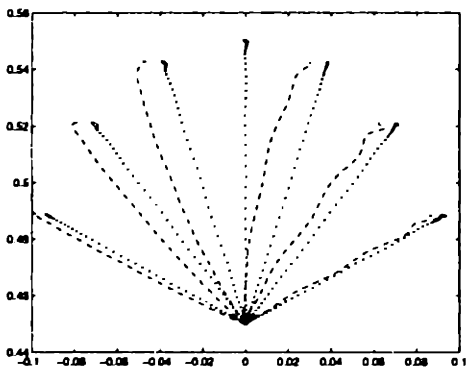

Figure 6-4: Aftereffects induced by learning the upwards trajectory

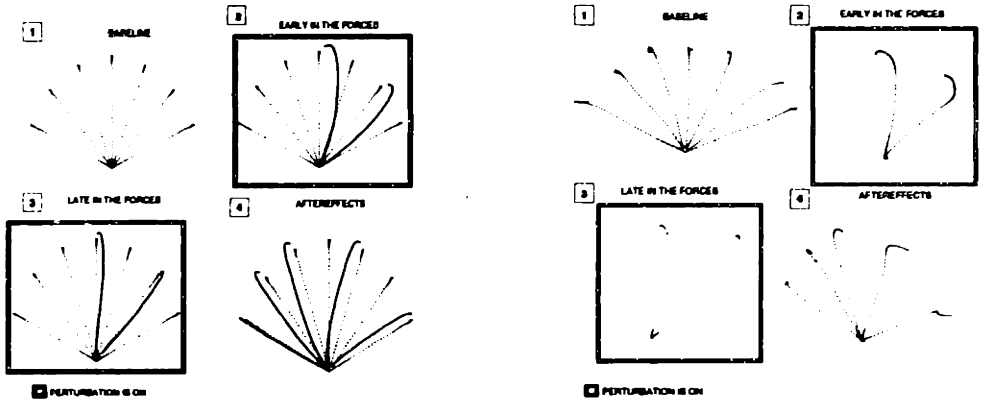

Figure 6-5: Generalization experiment. Left: model results. Right: human data

Fig. 6-5 compares the generalization data for the model and the human data. To replicate the psychophysical experiment, the model has been trained both in the 45° and in the 90^0 direction.

6.6.2 Experiment 2: Interpolation between two fields

Chapter 4 has shown that if two fields are learned over different arm postures, the generalization pattern in between the two postures follows a smooth interpolation. We repeated the experiment using our model.

The simulated arm was used to generate baseline trajectories (see Fig.6-6A).

A clockwise curl perturbation was applied to trajectories oriented at 45^0, a counterclockwise curl field to trajectories at 135^0.

The simulated arm practiced one trajectory at 45^0 and one at 135^0 and then the sampled data was incorporated in the map. The two trajectories were then further practiced. Fig.6-6B shows the trajectories after initial exposure to the perturbations.

Once both perturbations have been learned (Fig.6-6C), the simulation was tested for aftereffects in the interpolating and extrapolating region (Fig.6-6D).

The map modelling the perturbations is shown in Fig. 6-7. The x and y axis represent shoulder and elbow velocities. The z axis plot the magnitude of the compensatory torques.

As predicted, we found similar results (Fig. 6-8) to those observed in humans.

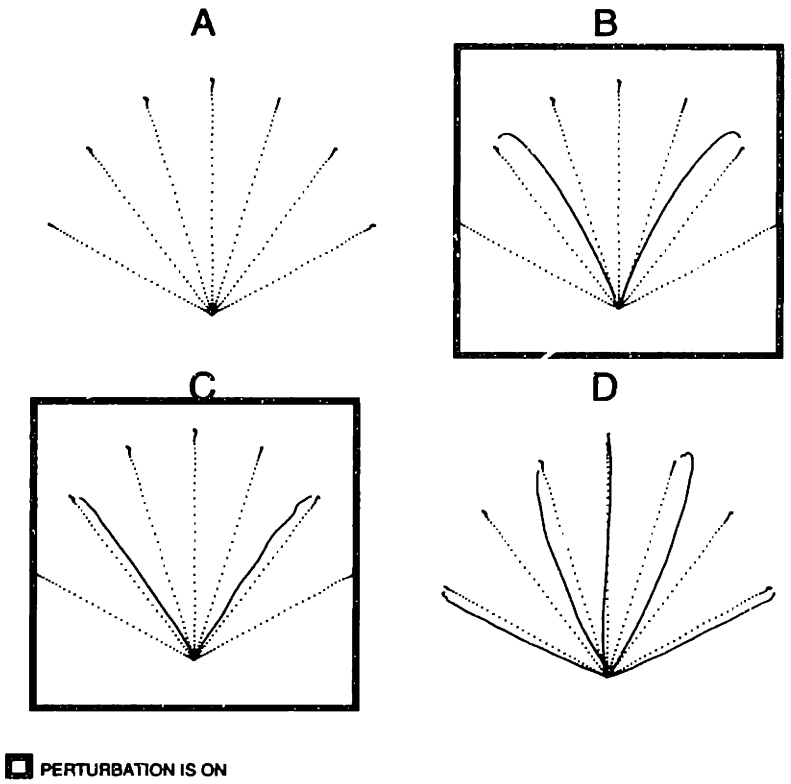

Figure 6-6: Simulated experiment: 1) baseline trajectories. 2) trajectories after initial exposure to the perturbations 3) trajectories after prolonged exposure to the field 4) aftereffects due to the removal of the perturbation. Dotted lines represent the baseline trajectories and the dashed lines represent the trajectories after adaptation

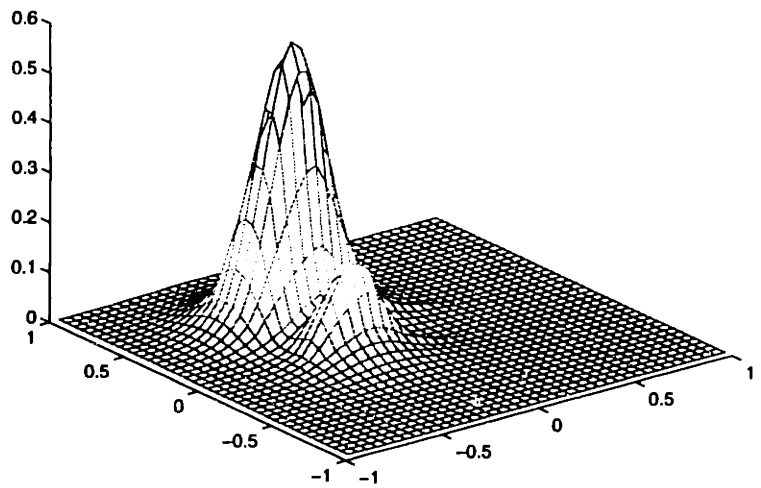

Figure 6-7: Model of the environment after adapting to the perturbations. The x and y axis represent shoulder and elbow velocities. The z axis plot the magnitude of the compensatory torques.

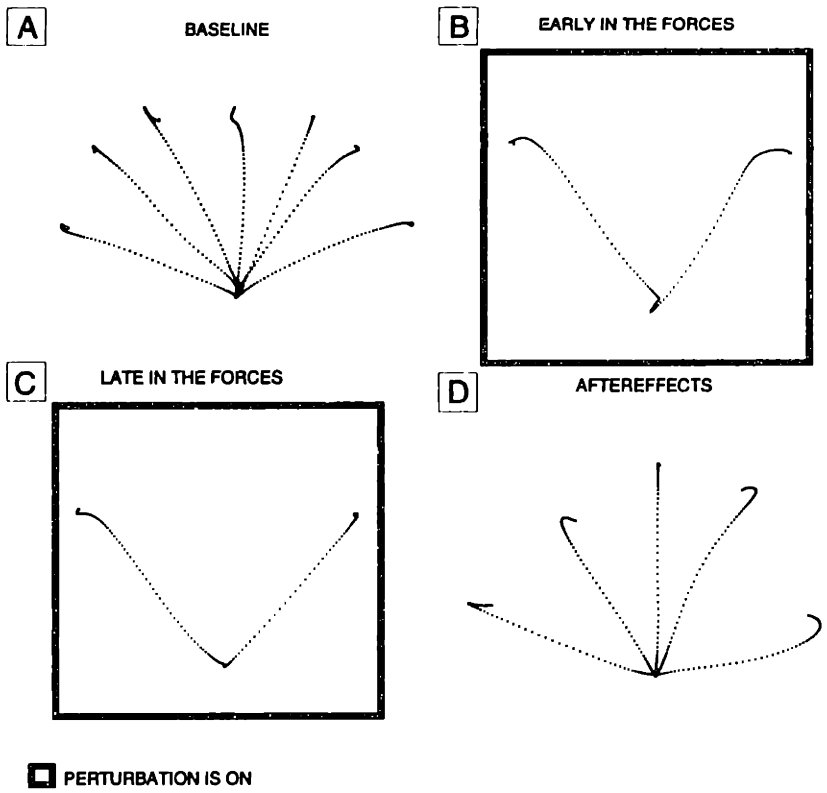

Figure 6-8: Interpolation results in a human psychophysics experiment

Namely, a smooth interpolation between aftereffects specific for one field and those specific for the other.

6.7 Future development of the model

The power of kernel regression is the ability of capturing not only the "spatial" characteristics of the experimental data, but also the time course of learning. Since the sampled data is smoothed by the "experience" previously encoded in the model, kernel regression requires multiple trials for learning how to approximate the data. Moreover, it offers a close form solution and requires no training, making it extremely appealing from the computational standpoint. Nonetheless, it requires a primitive for each data point, which is inefficient from the data storage standpoint and potentially unrealistic from the biological perspective.

A more realistic model could be achieved using Hyper Radial Basis Functions (HRBF) [41, 39]. Although the results are similar qualitatively to kernel regression,

HRBFs are more economical in terms of storage in that the primitives are allowed to migrate towards the areas of low smoothness in the data and they can release the isotropy constraints to accommodate elongated data sets using a low number of primitives. Future work will include the implementation of the HRBF model. Although it is hypothesized that the predictions will be consistent with the predictions from kernel regression, HRBF will show how the anisotropy of intrinsic space coexists with the anisotropy of the sampling space during normal behavior.

6.8 Conclusions

We have presented a model that accounts for the experimental data. We have been successful in reproducing the psychophysical findings by running the same experiments in simulation.

An aspect of the model which can be easily overlooked is its time course of learning. Models of adaptation have been previously presented [10] which can probably satisfactorily account for some of our results. These models, though, use backpropagation-based algorithm for learning. Such design allows the model to decouple two important parameters: learning rate and kernel size, which determines amount of generalization.

The model presented here, instead, does not allow independent control of the two parameters: the only "free variable" we can control is the kernel width. A large kernel implies a large amount of generalization but a long learning horizon, since the smoothing effect prevails over accurate reproduction of the sampled data. On the contrary, a small kernel allows for very fast learning, but poor generalization capabilities.

Our model finds a compromise between the two conditions which is consistent with human data.

This model can be used to predict the results of experiments involving motor adaptation.

Chapter 7

A model of the spinal cord

7.1 Introduction

Adaptation can be modeled as the summation of a compensatory torque field to the preplanned movement. The next step in the realization of a movement is the mapping of the "high level" primitives onto commands interpretable by the muscles, the CNS actuators. These commands must be able to produce the desired movements but they also have to ensure the stability of the system with respect to external perturbations. This problem is by no means trivial and it has received great attention in the robotics community.

A number of researchers have demonstrated the possibility of controlling a robot's passive behavior as a way to achieve purposeful and stable interactions with the environment [55, 17, 46]. A practical way to specify the passive behavior of a system is to control the field of forces that the system must apply to its environment in response to externally imposed states. This field of forces constitutes a generalization of local impedance.

Implicit in the idea of controlling passive behaviors are certain assumptions regarding the very basic definition of a vector field. In particular, given two passive behaviors expressed by two impedance fields, the vector summation of these fields must define another passive behavior. More precisely, in the context of impedance control [55] the property of vector summation can be reformulated as follows. We

say that a manipulator has the **vector–summation property** when the following condition is verified:

if two (or more) force fields add vectorially in generalized coordinates, then their images in end-point coordinates also add vectorially and the fields' sum in end–point coordinates is the image of the fields' sum in generalized coordinates. Here, we use the term "end–point" in a broad sense to indicate the site of mechanical interaction between a manipulator and its environment.

The vector–summation property is important because it insures that what matters for controlling interactions is the behavior of a manipulator at the interface with its environment and that, for this purpose, the details on the kinematic structure (the mapping between configuration and end–point space) can be neglected. In practical terms, the vector–summation property allows one to program the impedance of a manipulator by combining the end–point fields generated by a set of independent controllers. In this context, a controller is a device that determines how a system should react to a state imposed by the environment. Functionally, we characterize a controller as a force field. Previous investigations [83, 86] have shown that the passive behaviors generated by a set of independent controllers can be described as a set of basis fields (the vectorial equivalent of basis functions) spanning a linear functional space of achievable behaviors. In this context, the task of generating a desired impedance field can be dealt with using the techniques of functional approximation.

The vector–summation property is always satisfied in a non–redundant kinematic mechanism that is in a system whose transformation from configuration to end–point position is one-to-one and invertible. But, what happens when the number of configuration variables exceeds the number of end–point position variables? Simple geometrical reasoning makes it clear that in this case vector summation of the end–point impedance fields is no longer a valid assumption. Just consider two linear springs connected in series: one end is attached to ground and the other end is the "end–point" of the system. This is a kinematically redundant system whose configuration variables are the two lengths, l_1 and l_2, of the springs and whose end–point variable is the net length, $l = l_1 + l_2$. Clearly, the net end–point stiffness of this

system is not the sum of the two springs' stiffnesses but rather their geometric mean.

Being aware of this inherent non-linearity of redundant kinematics, one may still ask to what extent the vector-summation property may approximate the net behavior of a redundant manipulator. The answer depends presumably on the manipulator's kinematics. We have addressed the issue of vector summation by simulating the combination of random end-point force fields in a simple redundant manipulator. This manipulator incorporates some aspects of biological limbs: there are three revolute joints operated by a number of muscle-like actuators. These actuators behave as tunable springs and act as flexors or extensors about one or two joints. Briefly, our method consisted in simulating the end-point fields generated by activating two distinct groups of muscles chosen at random, first one group at a time and then simultaneously. Then, we derived a statistics of how the fields obtained from the simultaneous activation matched the vector sum of the two fields generated by the independent activation of each group.

Our results indicate that (a) as expected, the summation property does not hold for a redundant manipulator; (b) however vector summation provides an adequate approximation of the net endpoint field in the large majority of cases; (c) accordingly, the linear superposition of end-point fields can be used to obtain good approximations of desired passive behaviors; (d) by carrying out the simulation of random patterns of activation it is possible to determine which combinations of actuators should be eliminated to avoid or minimize nonlinear effects. In summary, our findings suggest that the linear summation properties that apply to the end-point forces generated by a non-redundant manipulator can be extended without a great loss of accuracy to describe the passive behavior of a redundant mechanism. To the extent that this approximation is acceptable, one may be able to successfully control interactive tasks by focusing on endpoint variables, without being concerned with the cumbersome details of inverse kinematics.

7.2 The summation problem

One way to control the interactive behavior of a manipulator is by specifying an impedance field at the interface between the manipulator and its environment. For simplicity, we focus on the static component of the impedance field, that is on the mapping from position to static force. Let us start by considering a generic manipulator structure operated by M actuators. We indicate by q a generic point in the manipulator's configuration space and by Q the corresponding generalized-force vector. We label the elements of multi-dimensional objects (vectors, matrices, points, etc) using subscript indices, while superscript indices are used to label different instances of such objects. Thus, for example, Q^i is the generalized force vector generated by the i-th actuator and Q^i_j is the component of this force along the j-th generalized coordinate.

The steady-state behavior of an actuator is described by a generalized-force field in configuration space. We assume that this force field is modulated by a real-valued control variable, u. More formally, the (static) mechanical behavior of the i-th actuator is fully described by specifying the vector-valued function

$$Q^i(q, u_i) \quad ; \quad i = 1, \ldots, M.$$

We assume that this function is continuous and differentiable in the regions of interest.

We consider a control structure partitioned into a set of controller modules (Fig. 7-1). Each controller module delivers a single control signal to a group (or synergy) of actuators. This organization is consistent with some recent observations on the of the frog's spinal cord [8, 45]. These observations suggest that the interneuron in the spinal gray matter act by recruiting wide populations of motoneurons innervating different skeletal muscles.

In formal terms, we define a **controller**, c, as a pair $\{I^c, u_c\}$ where I is a collection of distinct natural numbers belonging to the set $\{1, \ldots, M\}$ and $u \in R$. We indicate with $\mathcal{C}$ the set of all controllers.

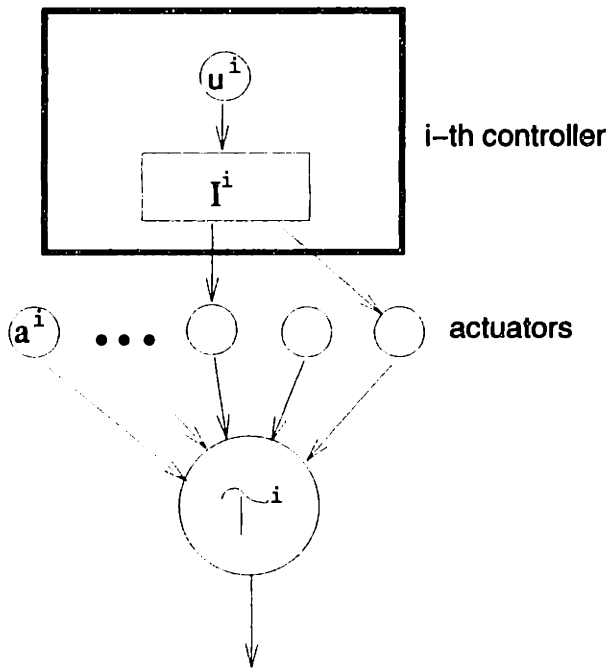

Figure 7-1: A controller module

The **controller field** is the field of generalized forces

$$\tau^c(q, u_c) = \sum_{i \in I^c} Q^i(q, u_c)$$

This notation emphasizes the fact that controllers, like actuators, are fully characterized by the fields of generalized forces that they generate. The **net generalized-force field** generated by the entire set of controllers is then given by

$$Q(q) = \sum_{c \in \mathcal{C}} \tau^c(q, u_c).$$

Let's now assume that the manipulator interacts mechanically with its environment at a site (the **end–point**). Let's also assume that the position, x, of the end–point is related to the configuration by a continuous and sufficiently differentiable[1] mapping, $x = \mathcal{L}(q)$. The Jacobian of this mapping is the matrix $J(q) = \frac{\partial \mathcal{L}}{\partial q}$. Then, for any controller, c, the controller field in generalized coordinates, $\tau^c(q, u_c)$, maps in

[1]In order to insure continuity and the existence of derivatives, one may have to restrict the analysis to a limited region of the workspace.

the **end–point controller field** $\phi^c(x, u_c)$. Similarly, the net generalized–force field, $Q(q)$, maps into a **net end–point field**, $F(x)$.

With this notation, the vector–summation property corresponds to requiring that

$$F(x) = \sum_{c \in C} \phi^c(x, u_c). \tag{7.1}$$

The summation property allows us to control the end-point impedance knowing only the end-point field of each control module. When the vector–summation property is satisfied, the end–point impedance becomes the necessary and sufficient a–priori information about the controlled structure. That is, given:

- two manipulators A and B
- two sets of independent controllers generating the same set of end–point controller fields
- access to the controllers input
- access to the end-point impedance field
- no other information

it is impossible to discriminate between A and B if the vector–summation property holds.

7.2.1 Non-redundant manipulators

A manipulator is said to be *non–redundant* when the dimensions of the end–point space match the dimensions of the configuration space. In this case, wherever the Jacobian is not singular, the net end–point field is linearly related to the net generalized–force field, that is:

$$F(x) = (J^t)^{-1}(q)Q(q). \tag{7.2}$$

The linearity of the above expression implies the vector–summation property.

7.2.2 Redundant manipulators

In a redundant serial mechanism there are more configuration variables than end-point coordinates. For each end-point position there are infinite configurations. Then, given two distinct controllers, c_1 and c_2, the force vector generated at the same end-point location by each controller, may correspond to generalized-force vectors at different configurations. As a consequence, the vector-summation property can no longer be given for granted. The end-point elastic field is related non-linearly to the generalized force field in configuration space.

In order to establish whether or not the vector summation property holds for a given system one must be able to derive the end point field generated by an arbitrary combination of controllers. Unfortunately, a closed-form expression (such as Eq. 7.2) for the end-point field is not generally available with a redundant manipulator. However it has been shown [84] that the end-point field generated by a set of elastic actuators can be derived numerically by iterating the following procedure.

Step 1 Compute the equilibrium configuration, q^0, (the configuration that results in zero generalized force) and the equilibrium point, $x^0 = \mathcal{L}(q^0)$;

Step 2 Displace the end-point by a quantity dx;

Step 3 Increment the end-point force by

$$dF = (J(K - \Gamma)^{-1} J^t)^{-1} dx \tag{7.3}$$

where:

$$\Gamma_{ij} = \sum_k \frac{\partial^2 x_k}{\partial q_i \partial q_j} F_k. \tag{7.4}$$

and K is the stiffness matrix. Note that the term Γ is zero at the first iteration (at equilibrium) but it is non-zero subsequently.

Step 4 Update the configuration by adding:

$$dq = (K - \Gamma)^{-1} J^t (J(K - \Gamma)^{-1} J^t)^{-1} dx \tag{7.5}$$

Step 5 Repeat from step 2 until the desired target position is reached.

The precision of the above procedure is affected by the magnitude of each step. In our simulations, we impose an upper bound to the magnitude of dq and vary dx adaptively to satisfy this constraint. This procedure has been proved to be integrable and to yield the inverse kinematic of a passively displaced redundant manipulator [84].

7.3 A statistical approach

As we have already stated, it is not possible to make a general claim regarding the vector–summation property in an arbitrary redundant system. However, one may use the procedure outlined at the end of the previous section to test the vector–summation property in a probabilistic sense for a particular manipulator architecture. To this end we define a **random controller** as a pair $\{I, u\}$, where u is a real number and I is a random collection of distinct numbers chosen within the set $\{1, \ldots, M\}$. In other words, a random controller is established by coactivating a random pattern of actuators.

Once a manipulator's structure has been defined, it is possible to estimate the probability that a set of N random controllers has the vector summation property. One way to do this is to compare the net end–point field generated by these N controllers with the vector sum of each controller field. An exhaustive exploration of all settings of N random controllers acting on M actuators is subject to a combinatorial explosion. An obvious remedy to this problem is to explore the space of possible controller settings by using a Monte Carlo method. Essentially, this method involves (a) generating a number of random controller settings, (b) estimating the fields corresponding to both sides of Equation (7.1) and (c) evaluating a random variable that measures to what degree the vector–summation property (Equation (7.1)) has been fulfilled. In order to implement step (c) we need a rigorous measure of similarity between two vector fields.

7.3.1 Field comparison

The random variable that captures the degree of similarity between net end-point field and the vector sum of the controller fields is a measure of vector–field correlation. Let's consider two vector fields, A and B, sampled at a set of discrete locations $x = (x^1, .., x^N)$. We define operationally the inner product of the sampled fields $< A|B >$ as:

$$< A|B >= \sum_i \sum_j A_j(x^i) * B_j(x^i) \tag{7.6}$$

The reader may verify that the above expression satisfies the formal requirements for the inner product. Accordingly, the norm of a field A is:

$$\| A \| =< A|A >^{1/2} \tag{7.7}$$

Given this inner–product structure, the similarity between two fields A and B can be expressed by their spatial correlation defined as:

$$\mathcal{S}(A, B) = \frac{< A|B >}{\| A \| \cdot \| B \|} \tag{7.8}$$

$\mathcal{S}$ satisfies Schwartz 's inequality: $-1 \leq \mathcal{S} \leq +1$. Therefore $\mathcal{S}$(A,B) can be considered as a measure of the cosine of the "angle" between the two fields. If $\mathcal{S}$(A,B) is equal to ± 1, then A and B are proportional to each other. In particular, if $\mathcal{S}(A, B) = 1$, the relevant topological properties, such as the equilibrium point and the pattern of vector convergence and divergence, are the same for both fields. We also define the coefficient $\mathcal{P}$ as the ratio of the norms of the fields A and B:

$$\mathcal{P}(A, B) = \frac{\| A \|}{\| B \|} \tag{7.9}$$

For two fields, A and B, to be identical it is both necessary and sufficient that $\mathcal{S}(A, B) = \mathcal{P}(A, B) = 1$.

7.4 A simulation

We have applied the statistical analysis described in the previous section to a computer model of a planar redundant robot with three rotational joints (Fig. 7-2 and Fig. 7.1). The robot is equipped with 10 muscle-like actuators. In analogy with biological limbs, these actuators are organized in agonist/antagonist pairs for each joint.Multi-joint actuators are provided to couple the first two links and the last two links.

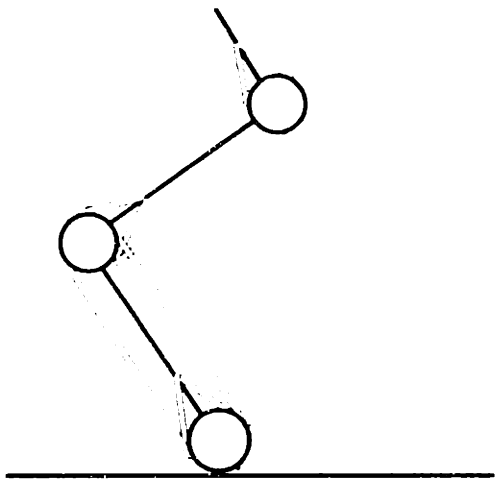

Figure 7-2: Sketch of the modeled redundant manipulator. The dashed lines illustrate the topology of the muscles' connections. In the simulation, double-joint muscles "ran along" the linkages in order to insure constancy of moment arms.

7.4.1 Actuators' model and controllers

At steady state, each actuator generates a force depending upon an activation variable and on the "muscle's" length. This force is translated by a moment-arm matrix into a corresponding vector of joint torques. For simplicity we consider a constant moment-arm matrix. We call flexors and extensors the model muscles having positive and negative moment arm, respectively.

Each simulated muscle is assumed to generate a force f depending on the muscle length and the net activation variable α:

$$f = fp(l) + \alpha fa(l) \tag{7.10}$$

where

- l is the length
- fp is the "resting" component of the force– that is that component that can be measured when the activation variable, α, is zero.
- fa is the active component of the force

In this simulation, we use a linear form both for the active and the passive component, that is:

$$f = Kp(l - l0p) + \alpha Ka(l - l0a) \tag{7.11}$$

where $l0p$ and $l0a$ are rest-length parameters and Kp and Ka are stiffness parameters. We do not place any a–priori constraint on the sign of the muscle forces. Therefore, unlike real muscles, our model's muscles may push and pull.

According to Equations 7.10 and 7.11, when all the activation variables are zero, the simulated arm is expected to stay in a "natural" equilibrium posture determined by the resting elastic properties of its muscles. The activation of one or more muscles results in a shift of this equilibrium posture. This model behavior is consistent with biological findings suggesting that tuning of spring-like muscles underlies the control of posture, movement and mechanical interaction [23, 69, 6, 54, 87].

We implemented the modular controller structure described in section 7.2 by establishing that each controller, c, delivers a signal, u_c, to a set of muscles, determined by the entries of a binary vector, I_j^c. If $I_j^c = 1$, then the controller c is connected to the muscle j. If $I_j^c = 0$ the controller is not connected. The net activation, α_m, for the m-th muscle is determined by summing all the control signals received from the connected controllers:

$$\alpha_m = \sum_i I_m^i u_i$$

To compute the end-point field for a given configuration of controllers, the first step is to derive the position of the equilibrium point. This can be done in closed form by solving for $Q_i = 0$.

The robot is placed in the equilibrium configuration so that the end point force is zero. The end point of the arm is then passively displaced to a set of locations on the vertexes of a 3 by 3 regular grid and the restoring forces are computed using Eq. 7.3.

For each point the integration starts from the equilibrium position in order to minimize the numerical error.

7.4.2 Resting, active and total forces

The separation of muscle force into an active and a resting component leads naturally to a similar separation of the end–point field into an active and a resting component. The **resting field** is the force field $Fp(x)$ generated by the passive mechanical properties of the manipulator when no controller is active ($u_i = 0$ for all controllers.) We call **total field**, Ft, the end–point field that is generated by the entire set of muscles when any of the controller is active ($u_i \neq 0$ for some controller). The amount of force added by the activated muscles to the background of resting forces is expressed by the **active field**,

$$Fa = Ft - Fp$$

In our simulation, the vector summation hypothesis is equivalent to the requirement that the active fields produced by the activation of two or more controllers, with $u = 1$, add vectorially. For example, calling $Fa^1(x)$, $Fa^2(x)$ and $Fa^{1\&2}(x)$ the active fields produced respectively by the first controller, the second controller and both, we want to test whether:

$$Fa^{1\&2}(x) = Fa^1(x) + Fa^2(x) \tag{7.12}$$

7.4.3 Monte Carlo method

We have investigated the vector–summation property by simulating the behavior of 2, 3 and 4 independent controllers.

Each simulated experiment followed six steps:

1. the resting end-point field was computed

2. each controller was activated independently and the total field generated by each controller was computed

3. all the controllers were simultaneously activated and the total field was computed

4. the active fields were derived by subtracting the resting field from the total field

5. the active fields from the individual controllers stimulations added to each other.

6. this sum was compared to the active field of the coactivation of all the controllers

The comparison was performed using the correlation coefficient $\mathcal{S}$.

7.4.4 Results

We have run three Monte Carlo simulations each one involving 10000 trials. We used a uniform random number generator so that the probability of an actuator to be connected to a controller was .5 for each actuator and for each controller. At each trial, we randomly generated a whole connection matrix "I" and we tested the summation property by following the steps described above.

In the first simulation we tested the combination of two controllers. Fig. 7-3 presents the results of this simulation. The first plot shows a sample of the equilibrium points generated by the random controllers and by their coactivations. These equilibrium postures covered a substantial portion of the work space. The second plot shows the subset of the first plot corresponding to the controller coactivations alone. Note that also these equilibrium points are scattered in the same region of the workspace. This fact reflects the absence of a bias towards the coactivation of muscles acting in antagonistic configuration (flexor–extensor) about the same joints. In fact, if such a bias were present one would expect a clustering of equilibrium points within a smaller region of workspace.

The third plot is the frequency histogram of the correlation coefficient $\mathcal{S}$ across trials. More than 90% of trials resulted in a coefficient included between .97 and 1.

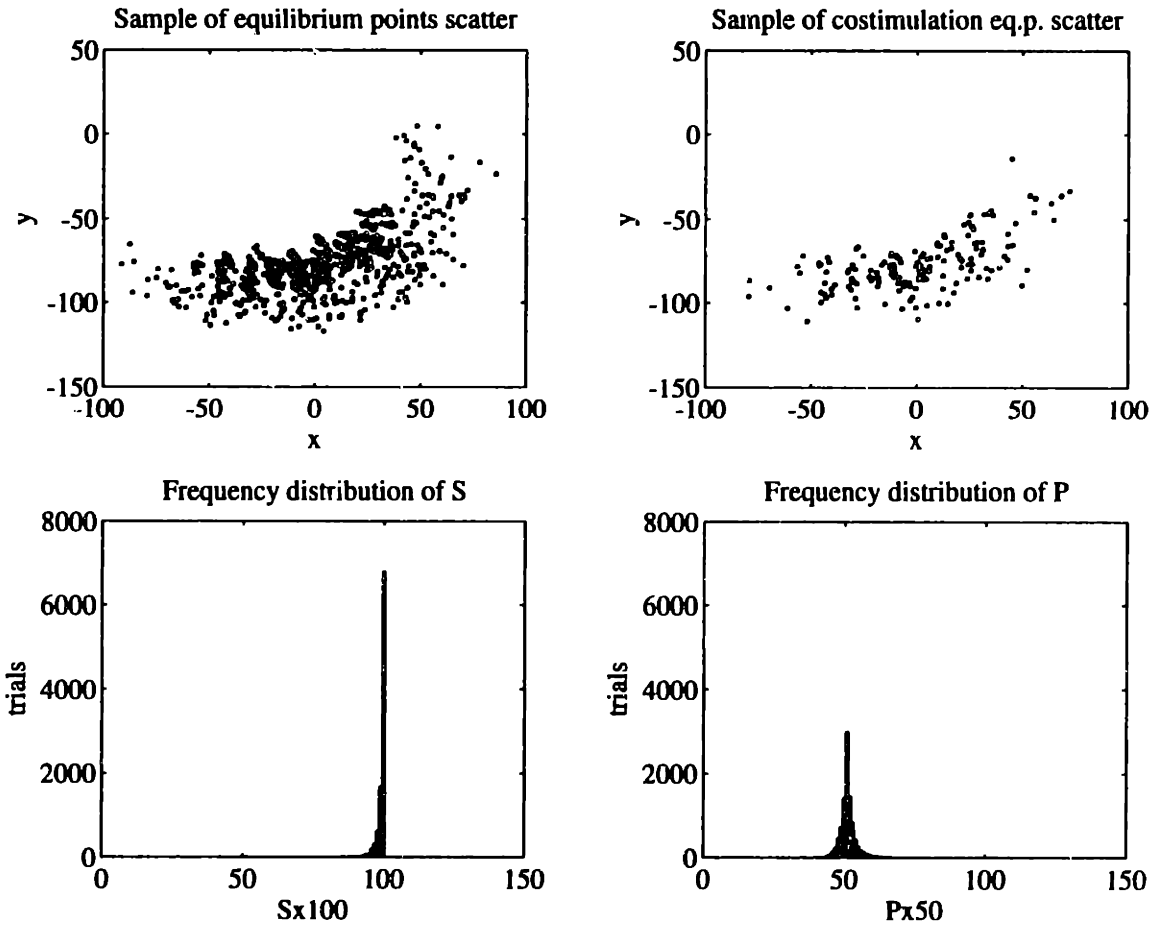

Figure 7-3: Equilibrium points scatter and distribution of $\mathcal{S}$ and $\mathcal{P}$ in the Monte Carlo simulation using 2 controllers. The manipulator's shoulder is placed in (0,0) and the links' lengths are 60, 60 and 30 units.

Such a sharp peak indicates that in the great majority of cases, the sum of the fields was proportional to the costimulation field.

The last panel of fig 7-3 shows the distribution of the parameter $\mathcal{P}$ (ratio of norms) among the fields whose $\mathcal{S}$ value was larger than .9 In more than 70% of cases the ratio of norms was between 0.8 and 1.2. Therefore, one may state that the costimulation field and the sum of the fields were not only proportional but substantially equal in the majority of the random trials. These results indicate that for the simple redundant structure used in this example, it is possible to choose a set of controllers such that the vector–summation property is satisfied.

How is the vector–summation property affected by the presence of an increasing

number of control modules? To address this question we performed two more sets of Monte Carlo simulations involving the combination of three and four controllers. We found that the statistics of the summation hypothesis were qualitatively similar to those shown in Fig. 7-3. Moreover, the data shown in Tab. 7.2 indicate that the likelihood of the summation is quite stable with respect to the number of controllers.

7.5 The approximation problem

We have found that the vector–summation property holds at least approximately for our simulated redundant mechanism with two or more controller modules. Is this a sufficient condition for implementing a desired end–point impedance as a linear combination of controller fields? The problem of approximating with a non–redundant manipulator an arbitrary end–point field by combining controller–fields has been recently formulated as follows [86]. First, one must specify a desired end–point field by giving a set, $\{\tilde{F}^j, x^j\}$ $(j = 1, \ldots, D)$, of D force vectors $\tilde{F}^j$ at D end–point locations, x^j. The desired vector pattern can be specified with variable accuracy by changing the number, D, of sample vectors. Then, given a set of linearly–independent end–point controller fields, $F^1(x), F^2(x), \ldots, F^K(x)$, the desired end–point patterns can be approximated by solving for the control inputs, $u_1, u_2, \ldots, u_k$, the D linear vector–equations:

$$\sum_{i=1}^{K} u_i F^i(x^j) = \tilde{F}^j \tag{7.13}$$

With a N–dimensional end–point space, these vector equations give rise to $D \times N$ scalar equations.

In our simulation, we considered two types of vector patterns, both expressed by four sample–vectors (Fig. 7-4a and7-5a). In the first pattern, the sample vectors converge to a stable equilibrium point. Thus, they specify a position controller. In the second pattern the four vector are parallel and have equal magnitude. This case corresponds to the specification of an ideal force–controller. In both cases, the desired pattern gives rise to eight scalar equations. We considered how the pattern vectors could be approximated by linearly combining four controller fields. To this end, we

derived the standard least squares solution for u_i in (7.13).

We derived the end-point field approximation to the desired pattern under three different conditions. First we considered a non–redundant planar manipulator with 2 joints. In this case, the vector summation property holds exactly and any error in the approximation should be attributed to the least–square solution. (Fig. 7-4b and 7-5b) Then, we considered the approximation with the redundant manipulator of Fig. 7-2. In one case (Fig. 7-4c and 7-5c), we used four controllers that had been found to satisfy the vector–summation property ($\mathcal{S} = 0.99 \quad \mathcal{P} = 0.94$). Finally (Fig. 7-4d and 7-5d), we considered another set of four controller that instead violated the condition for vector–summation ($\mathcal{S} = 0.78 \quad \mathcal{P} = 1.10$).

The structure of the controllers used in the approximation task is described in tables 7.3 and 7.5.

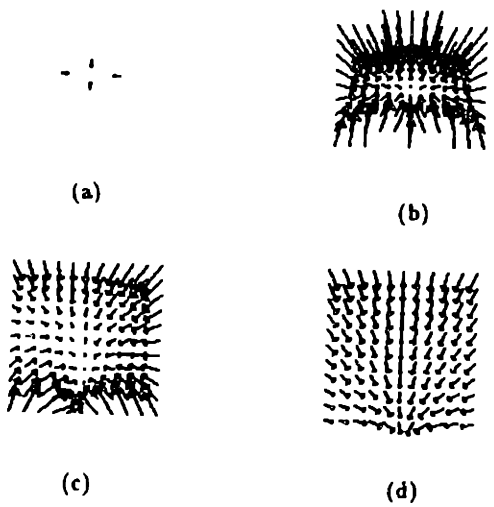

Figure 7-4: Approximation of a position control.

Also in these cases, the approximation captures the topological properties of the pattern to approximate. Quantitatively, though, it is clear that in Fig. 7-4c the equilibrium point is much closer to its desired position than in Fig. 7-4d. Moreover, when the system has the summation-property, it seems also capable of a better generalization outside the area delimited by the data points, resulting in a smoother end–point

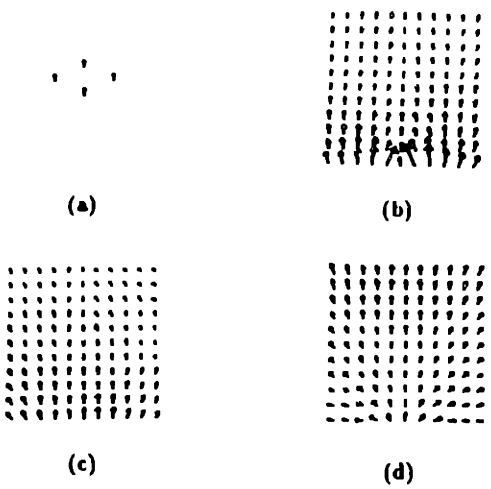

Figure 7-5: Approximation of a force control.

field.

7.6 Conclusions

Kinematic redundancy has been widely recognized to be a key feature for endowing a manipulator with dexterity– that is with the ability to cope with a variety of tasks in a variety of environments [119, 4, 57, 116] At the very least, "extra" degrees of freedom would allow a robot's arm to reach a point in space in many different ways, thus providing multiple solutions to the problem of finding a path for the end–point while avoiding obstacles. But the advantages of redundancy aren't limited to kinematics. Redundancy can be exploited for programming a manipulator's end–point inertia, the latter depending strongly upon joint configuration [56]. In this way, the manipulator would be able to control the end–point position while providing at the same time an adequate response to a predicted impact with the environment. Unfortunately, the advantages brought by redundancy come at a price. Redundant kinematics is obviously more complex and local solutions to the inverse–kinematics problem may be ill-behaved [70, 107, 84].

In this chapter, we have considered the challenge posed by kinematic redundancy to the control of impedance. As we have just stated, the extra degrees of freedom can be used for achieving a wider repertoire of end–point impedances. At the same time, however the possibility of linearly combining end–point impedances is generally lost with a redundant manipulator. This problem arises because two different settings of the manipulator's impedance result not only in two different fields of forces at the end–point, but also, eventually, in two different set of configurations throughout the reachable space. This lack of linearity might pose a serious problem for impedance control [55]. In fact, impedance control is based upon the key idea that what ultimately matters in the control of mechanical interactions is the impedance of the manipulator *as seen through the point of contact with the environment.* In this respect, the presence of redundant degrees of freedom seems to threaten the possibility of describing the behavior of a controller solely on the basis of its end–point field: this end–point field might indeed be affected by the presence of other controllers acting simultaneously and independently upon the same manipulator.

We have developed a formal approach to this problem based upon the definition of the "vector–summation property". The vector summation property expresses the fact that the superposition of vectors in configuration space implies the superposition of the image of the same vectors in end–point space. The vector–summation property is characteristic of any non–redundant manipulator. The major result of our investigation is that in a redundant manipulator this property is not exactly satisfied but it can be approximated with a surprisingly high degree of accuracy. We reached this conclusion after simulating a large number of controller combinations in a model of a redundant three–joint planar manipulator. In each simulated trial we compared the end–point fields obtained from the simultaneous activation of two or more controllers with the vector sum of the end–point fields generated by the same controllers in isolations. We found that the vector sum and the simultaneous activation yielded very similar fields (correlation higher than 0.9) in more than 98% of cases.

Our findings suggest a practical way for designing a set of controllers yielding summation of end–point fields with a redundant manipulator: one simply needs to

eliminate the relatively few controllers that do not follow the vector–summation property. Once the "bad controllers" are eliminated it should be possible to program a desired end–point field as a linear superposition of the end–point fields generated by the remaining controllers. To test this approach, we investigated the approximation of two kinds of fields related to two radically different control schemes: position control (a convergent pattern) and force control (a parallel pattern). We compared the performance the approximations obtained using four controllers in three distinct conditions: (1) non-redundant kinematics, (2) redundant kinematics with four controllers that closely approximated the vector–summation property and (3) redundant kinematics with four controllers that violated the vector summation property. We found that in the first two cases, the desired patterns were well approximated, both topologically and numerically. In contrast, in the third case the approximating field did not reproduce the desired features.

In conclusion, our findings indicate that the presence of redundant degrees of freedom need not to be an obstacle to the vectorial combination of the end–point fields generated by a set of independent controllers. We suggested a simple process for designing a control system which follows the rules of vector summation. This process is loosely reminiscent of Darwinian evolution as random controller combinations are generated and those not fulfilling a given conditions are eliminated. By using only the surviving controllers, a robot may control the mechanical interactions with its environment without being needlessly concerned with inverse–kinematics computations.

actuator type	joints involved	rest length		stiffness	
		Resting	active	resting	active
f s	1	-1.	-1.8	-1.	-1.
e s	1	-29.	-0.2	-1.	-1.
f s	2	-25.	-0.2	-1.	-1.
e s	2	-1.	-1.8	-1.	-1.
f s	3	-1.	-1.2	-1.	-1.
e s	3	-15.	-0.2	-1.	-1.
f m	1-2	-2.	-1.8	-1.	-1.
e m	1-2	-6.	-0.2	-1.	-1.
f m	2-3	-11.	-0.2	-1.	-1.
e m	1-2	-2.	-1.8	-1.	-1.

Table 7.1: Muscle parameters. Actuator type: f=flexor, e=extensor, s=spanning one joint, m= spanning two joints. Joints involved: 1= "shoulder", 2= "elbow", 3= "wrist".

No. of controllers	No. of trials	%>.9
2	10000	98.50
3	10000	98.65
4	10000	97.81

Table 7.2: Percentage of actuator pools giving rise to $\mathcal{S} > .9$ during the Monte Carlo simulation

actuator	joint	c1	c2	c3	c4
f s	1	0	1	1	1
e s	1	0	1	0	0
f s	2	1	0	0	1
e s	2	0	1	0	0
f m	1-2	1	1	1	0
e m	1-2	0	0	0	1

Table 7.3: Controllers settings used in the non redundant example. First column: "f" and "e" indicate respectively flexor and extensor, "s" and "m" indicate respectively single- and multi-joint actuator. Second column: 1= "shoulder", 2 = "elbow". Subsequent columns: 1 indicates controller-actuator connection, 0 indicates no connection.

actuator type	joints involved	Sum				Non-sum			
		1	2	3	4	1	2	3	4
f s	1	1	0	0	1	1	1	0	0
e s	1	0	1	0	1	0	0	0	1
f s	2	1	0	0	0	1	1	1	0
e s	2	0	0	0	0	0	1	0	0
f s	3	1	0	0	0	1	1	1	1
e s	3	0	1	1	0	0	1	1	0
f m	1-2	0	0	0	0	1	1	1	1
e m	1-2	1	1	0	0	0	0	0	0
f m	2-3	0	0	1	1	1	0	1	1
e m	2-3	0	0	0	1	1	1	1	0

Table 7.4: Controllers settings used in the redundant example. Same notation as Tab.7.3. The number 3 in the second column indicates the wrist joint.

Chapter 8

Field Combination Network

The previous chapters have shown that adaptation can be achieved through the construction of a primitive, meant as a torque field, which compensates for the environmental perturbations. This primitive could be "implemented" through approximation via spinal fields. This chapter investigates a mechanism to do so, and more generally, the problem of reconstructing continuous vector-valued mappings by the linear superposition of local vector fields.

The issue of approximating and representing vector–valued mappings emerges in a number of important computational problems. Some of these problems are related to the analysis of optical flows– the fields of velocity vectors associated with the motion of an observer. For example, how is it possible to separate rotational and translational components and to determine the "center of expansion" of an optical flow? Problems of field combination also arise in control theory. For instance, one may express a control law as a field of generalized forces over the state space of a manipulator. One issue is then how to achieve an arbitrarily specified control law from the superposition of independent controllers, each one tuning a local non-linear field. Still other issues of vector field representation arise in areas of research that are not related to brain science or cybernetics, such as weather forecasting. In this case, for example one faces the problem of reconstructing a wind flow field from a number of sparse samples [115].

A field-approximation problem that is shared among these different areas of in-

vestigation can be stated as follows. Given a set of vectors at a set of points find a vector–valued map that approximates these vectors at the sampling points while at the same time providing a smooth estimate of the underlying field at non-sampled locations. This problem is formally identical to the ordinary approximation of a scalar map. One may be tempted to treat each component of the approximating map as an independent scalar entity, to be represented as a combination of scalar basis functions. However, a disadvantage of this "component–based" approach is that the values assumed by a vector component are contingent upon the arbitrary choice of a coordinate system. In contrast, most if not all the interesting properties of a vector field do not depend on such a choice. For example, a vector field may contain a point attractor or it may be characterized by a circulating pattern. These interesting properties involve *relations* among components, such as the relation defining the curl and the divergence of a field. One way to capture the invariant properties expressed by these relations is to use vector fields instead of scalar functions as computational primitives.

Following this point of view, Mussa-Ivaldi [82] has recently suggested a method for extending to vector fields the paradigm of function approximation by the superposition of scalar basis functions. Essentially, this method consists in deriving from a known set of scalar basis functions, a corresponding set of vector fields that have been named *basis fields*. A set of vectors can be approximated by the linear superposition:

$$F(x) = \sum_{i=1}^{K} c_i \phi^i(x) \tag{8.1}$$

where $\phi^i(x)$ are K distinct basis fields[1] and $c_i \in \Re$ are weighting coefficients.

The above expression is formally identical to the representation of a scalar mapping as a sum of basis functions. We propose a neural network architecture for vector-field approximation that is based upon the linear combination of basis fields (8.1). This general idea, of course, is not new. The reconstruction of scalar map

[1] We adopt the convention of using superscript indices to label different multidimensional *objects* (points, vectors and matrices). In contrast, we will indicate the *components* of a multidimensional objects (e.g. the coordinate of a vector or the elements of a matrix) by subscript indices.

by combining basis functions is already a well–established theoretical framework for a wide class of multilayer networks [12, 92, 5]. However, we would like to stress a point of departure of our approach from the current design of basis–function networks. Basis–function networks are usually intended to store a *finite* number of scalar maps. Each map is provided by a set of connection weights that correspond to the coefficients c_i of Equation (8.1) (in its scalar version). These connection weights are learned from a set of examples of the map that has to be stored. In contrast, our network architecture, that we call "field combination network" (FCN), is capable of storing a continuous repertoire of maps[2]. In other words, the purpose of FCNs is not to approximate this or that vector field from this or that set of examples. A FCN is set up to learn the task of approximating *any* set of vectors presented at a given set of sampling points. We will show that this goal is achieved by considering the combination coefficients, c_i, in (8.1) not as connection weights but as *signals*. These signals modulate via a set of "product units" [20] the outputs of the units implementing the basis fields.

We represent the problem of field reconstruction as an auto–association problem: the primary task of a FCN is to match an input pattern of sampled vectors with an output field that at the sampling points is "as close as possible" to the input vectors. We show that this task can be achieved by a network that (a) projects the input vectors into a coordinate system defined by the basis fields and then (b) linearly combines these projections with a set of appropriate weights. The output of this network are the desired signals that modulate the basis fields. Thus, we can conclude non only that the vectorial combination of basis fields is a powerful method for reconstructing a variety of non-linear vector mappings but also that the task of finding the appropriate combination parameters can be solved once and for all by a simple auto–associative network.

[2]Of course this is strictly true for an ideal analog computer. With a finite–state machine the number of stored fields is bound to be finite as well. However, here we are implying that in a FCN a relatively small set of connection weights can store a very large number of fields.

8.1 Vector–field approximation

We are concerned with the representation of N–dimensional vector fields defined over some domain $\mathcal{E}$ of $\Re^N$. These vector fields are collections of N real–valued maps with the important assumption that such a collection belongs to a vector space– that is that the operations of addition and scalar multiplication are defined.

The goal of vector field approximation can be stated as follows. Let us choose M distinct points in $\mathcal{E}$: $x^1, x^2, \ldots, x^M$. We will call these points *sampling locations.* Now, suppose that we are presented with one N-dimensional vector at each sampling location. So, we have M such vectors $v^1, v^2, \ldots, v^M$ that we may call the "data". These data are samples of some unknown field, $\hat{F}(x)$. Then, we consider a known family of vector–fields, $F(x \mid c_1, c_2, \ldots, c_K)$, parameterized by K real numbers, c_i. The goal of vector–field approximation is equivalent to the goal of scalar approximation [94], namely: find a set of values for c_i that minimize the distance between $\hat{F}(x)$ and $F(x \mid c_1, \ldots, c_K)$.

In the case of a scalar map, the approximating function may be represented and parameterized as a weighted sum of non–linear basis functions, $g_i(x)$:

$$f(x) = \sum_{i=1}^{K} c_i g_i(x).$$

This approach is particularly significant since it has been shown that the form of the basis functions can be directly related to the presumed properties of the unknown map [92, 93]. Mussa-Ivaldi [82] has proposed to extend the same approach to vector–field approximation, by representing the approximating field as a weighted sum of *basis fields*, $\phi^i(x)$ (Eq. 8.1).

Basis fields can be directly derived from scalar basis functions by taking advantage of a well–known theorem of potential theory [68]. This theorem states that any continuous vector field, $F(x)$, can be expressed as the sum of two fields,

$$F(x) = C(x) + S(x). \tag{8.2}$$

The first field, $C(x)$, is *irrotational* and the second field, $S(x)$, is *solenoidal.* We remind that an irrotational field is defined as a field having zero curl and a solenoidal field is a field with zero divergence, that is: $curl(C) = \nabla \wedge C(x) = 0$ and $div(S) = \nabla \cdot S(x) = 0$. The symbols $\wedge$ and ∇ indicate, respectively, the external product and the differential operator $\sum_{i=1}^{N} \partial/\partial x_i$. In the above expressions, we have implicitly assumed that the metric of the input domain, $\mathcal{E}$, is Euclidean. For simplicity we will maintain this assumption throughout the paper. However, the main results can be applied with some precautions (in the expression of the differential operators) to the more general Riemannian metric.

We now proceed with a brief account of the derivation of basis fields from basis functions. In this derivation we will assume that one set of scalar basis functions, for example Gaussians, multiquadrics or splines, has been chosen. We indicate these functions as $g_i(x)$. Following the field–decomposition theorem, we will derive from these scalar basis functions a set of irrotational basis fields (IBF) and a set of solenoidal basis fields (SBF).

8.1.1 Irrotational basis fields.

Let us start from the assumption that the approximating field, $F(x)$, has only an irrotational component. An equivalent way to state that the field $C(x)$ in (8.2) is irrotational is to postulate the existence of a *scalar* potential function, $U(x)$, such that $C(x)$ is the gradient of this function:

$$C(x) = \nabla U(x). \tag{8.3}$$

Then, it is possible to represent the approximating potential as a weighted sum of scalar basis functions:

$$U(x) = \sum_{i=1}^{K} c_i g_i(x). \tag{8.4}$$

The above expression cannot be used for finding an approximation because the data supplied in our problem are not scalar values for $U(x)$. However, one may take advantage of the fact that the gradient is a linear operator and combine Eqs. (8.3)

and (8.4) to express the irrotational approximating field as

$$C(x) = \sum_{i=1}^{K} c_i \varphi^i(x) \tag{8.5}$$

with $\varphi^i(x) = \nabla g_i(x)$.

Unlike equation (8.4), equation (8.5) can be directly used for vector–field approximation by relating the vector data to the values of $C(x)$ at the sampling points. The fields $\varphi^i(x)$ are irrotational basis fields derived as gradients of scalar basis functions. A particular class of IBFs is derived by taking the gradient of radial basis functions (RBFs). A generic RBF has the form $g_i(x) = h(\| x - t^i \|)$, where the parameter t^i is a center of symmetry. The corresponding gradient field is $\phi^i(x) = ((x - t^i)/ \| x - t^i \|)(\partial h/\partial \| x - t^i \|)$. For any point, x, the vector $\phi^i(x)$ is directed toward the center, t^i. Thus, the basis fields obtained by taking the gradients of RBFs have central symmetry.

Note that the point at which $g_i(x)$ reaches a maximum is also the point at which the corresponding basis field vanishes, thus exerting the least influence. This observation suggests that a good strategy for placing the centers of the basis fields in vector approximation needs not to be that of placing the centers at the data points, as is often the rule of thumb with scalar basis functions.

8.1.2 Solenoidal basis fields.

Now, let us consider the solenoidal field $S(x)$ in (8.2). It is easy to prove that *in the Euclidean metric, a solenoidal field is obtained from an irrotational field when the latter is multiplied by an antisymmetric matrix.* This statement provides us with a very simple way to generate solenoidal basis fields from basis functions. First, take the gradient of a basis function to obtain an irrotational field. Then, multiply this irrotational field by some antisymmetric matrix, A. The resulting field

$$\psi^i(x) = A \nabla g_i(x) \tag{8.6}$$

is solenoidal, that is $\nabla \cdot \psi^i(x) = 0$. Note that in 2D, there is essentially one anti-symmetric matrix- that corresponds to a 90 degree rotation operator. In contrast, in higher dimensional spaces it is possible to generate a larger number of linearly independent antisymmetric matrices. Thus, we can say that in general from a set of K scalar basis functions it is possible to generate K_S ($\geq K$) solenoidal basis fields as in (8.6).

8.1.3 Complete field representation

Putting together the sets of IBFs and SBFs we obtain a general representation for a continuous field as:

$$F(x) = \sum_{i=1}^{K} c_i \varphi^i(x) + \sum_{i=1}^{K_S} d_i \psi^i(x) \tag{8.7}$$

The task of field approximation is to determine the coefficients c_i and d_i given a set of data presented at a set of sampling points. Note that, once this problem is solved, the basis field representation provides a powerful framework for extracting important features from the pattern of data. For example: (1) The solenoidal and the irrotational component can be immediately separated; (2) The divergence and the curl of the total field can be readily estimated from the known divergence and curl of the IBF and SBF, respectively; (3) The irrotational component of the field can be integrated from the known set of scalar basis functions $g_i(x)$ that have been used to generate the IBFs. Note in fact that the coefficients c_i in (8.4) and (8.7) are the same. Then, once the irrotational component is estimated also the corresponding potential is also obtained as a byproduct.

To simplify our notation, in the remaining sections we will use expression (8.1) instead of (8.7) with the implicit assumption that the basis field $\phi^i(x)$ can be either conservative or solenoidal.

8.2 Basis fields as a coordinate system

A direct way for using Eq. (8.1) in a field approximation problem consists in equating the field combination to the data, and then solving algebraically for the unknown combination parameters, c_i. With M vectorial data we have M vector equations

$$\sum_{k=1}^{K} c_k \phi^k(x^j) = v^j \tag{8.8}$$

for $j = 1, \ldots, M$. Each one of these vector equations can be explicitly decomposed in N (dimension of the vector space) real-valued components. Thus, we end up with $N \times M$ "scalar" equations in K unknowns. A discussion of this rather straightforward algebraic method can be found in Mussa–Ivaldi (1992).

In this paper we take a different path. We would like to start by pointing out what we consider to be an unsatisfactory aspect of the above mentioned approach, namely the coordinate representation of the input pattern. The numerical components of the scalar equations derived from (8.8) have to be specified in some arbitrary coordinate system. In contrast to the use of such an arbitrary coordinate system, we would like to represent the pattern of input data– i.e. the vectors v^i– *in the coordinate system that is inherently specified by the basis fields.* To this end, for each basis field, $\phi^i(x)$, we define the projection of the data–set $v^1, v^2, \ldots, v^M$ on $\phi^i(x)$ as:

$$\Lambda_i = \sum_{j=1}^{M} < \phi^i(x^j) | v^j > \tag{8.9}$$

where operator $< u|v >$ is the inner product between two N-dimensional vectors u and v. This operation is a form of "vector–filtering" of the sampled data, carried out by taking the inner product of the field $\phi^i(x)$ with each input vector. If the data were sampled continuously, the summation could be replaced by an integration.

Given the definition (8.9), it is easy to show that the least–squares solution to (8.8) is

$$c_k = \sum_{i=1}^{K} [\Phi]^{-1}_{k,i} \Lambda_i \tag{8.10}$$

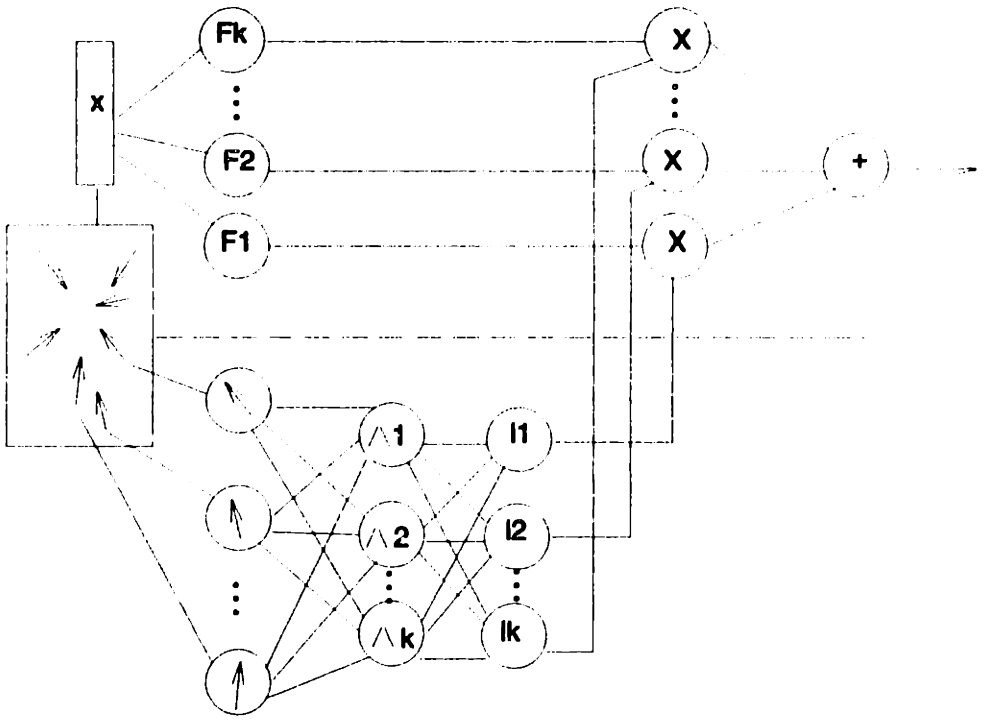

Figure 8-1: Field Combination Network.

where the matrix $[\Phi]^{-1}$ is the inverse of the $K \times K$ matrix

$$[\Phi]_{l,m} = \sum_{j=1}^{M} < \phi^l(x^j) | \phi^m(x^j) > . \tag{8.11}$$

If the number of basis fields is equal to the number of data components (that is if $K = MN$) then Eq. (8.10) yields the exact solution of (8.8). Equation (8.10) is the vectorial counterpart to the solution for the combination coefficients in scalar basis function networks.

Equations (8.1) and(8.10) provide a simple paradigm for representing and reconstructing vector fields. This paradigm can be directly translated into a network architecture that we call "field combination networks" (FCN) (Fig. 8-1).

The input space of a field combination network is a spatial domain, $\mathcal{E}$ with M fixed sampling points. An input vector, v^i, is presented at each sampling point. The purpose of the the network is to reconstruct the vector field over the entire spatial domain, $\mathcal{E}$. The network is divided into two subnetworks: a basis–field network and a modulator network.

1. The basis–field network (Fig. 8-1, upper part) takes as input a representation of a point in $\mathcal{E}$. This input is delivered to a set of units (labelled F_i in Fig. 8-1), each one implementing the input/output map of a basis field, $\phi^i(x)$. These basis–fields units are not network units in a conventional sense: they do not generate a scalar signal but a collection of N such signals, one for each vector–field component. The outputs of the basis–fields units are multiplied (via product units) by a set of coefficients that are continuously generated by the modulator network.

2. The job of the modulator network (Fig. 8-1, lower part) is to generate the combination coefficients corresponding to a set of vectors presented at the sampling points. The input vectors are "projected" by a set of K units (labelled Λ_i) implementing the filtering operation (8.9). Then the outputs of these projection units are combined by another set of K units (Labelled L_i)implementing the linear transformation.

$$c_i = \sum_{j=1}^{K} w_{i,j}\Lambda_j. \tag{8.12}$$

   The coefficients $w_{i,j}$ correspond to a set of connection weights that effectively implement the inverse of the basis–field correlation matrix Φ (8.11). We will discuss a simple learning rule for these coefficients.

In essence, the purpose of FCNs is to acquire the ability to combine vectorial modules (the basis–field units) in order to generate arbitrary continuous fields that are specified by a discrete set of samples. Thus, vector–field approximation is expressed as an auto–association task: the output of the network must try to match the input vectors at the sampling points. Naturally, the network does more than that as it "completes" the input pattern outside (or within) the sampling points.

We would like to add a remark concerning information storage. In a "standard" basis–function network (e.g. see Bishop, 1989) with K basis functions, $K \times M$ weights are required to store M different mappings. Each mapping is stored by K connection weights. In a field combination network with K basis fields, there are $K \times K$ connection weights (in the modulator subnetwork). The number of distinct mappings that

are stored by these weights depends upon the resolution of each "parameter line", c_i. for example, if all the parameter lines have the same resolution of L bits, then the field combination network can generate 2^{KL} distinct output fields.

A learning rule. As we have mentioned above, the connection weights, $w_{i,j}$, (Eq. (8.12)) yielding the least-squares solution for the system (8.8) are obtained from the inverse of the basis-field correlation matrix Φ. On way to calculate them through an iterative procedure is to use the following learning rule:

$$\Delta w_{l,m} = \eta \left((\sum_i \Phi_{i,l}^2) w_{l,m} - \Phi_{m,l} \right) \tag{8.13}$$

where η is a learning-rate parameter. This learning rule is derived by minimizing the cost function

$$J = \frac{1}{2} \parallel \Phi W - I \parallel^2$$

where the norm of a matrix A is defined as $\parallel A \parallel^2 = \sum_{i,j} A_{i,j}^2$. This learning procedure is a simplified form of gradient descent and is computationally advantageous with respect to matrix inversion when the number of basis-fields is large and when a coarse approximation of the pseudoinverse may be acceptable.

8.3 Example

The following example illustrates the performance of our network and of the learning algorithm (8.13). The input space is shown in Fig. 8-2 as a square planar domain covered by a regular grid. We consider a set of 20 sampling points. A pattern of vectors presented at these sampling points is shown in Fig. 8-2A. The basis-field subnetwork is composed of 32 units implementing an equal number of basis fields. The locations of the basis-field centers are indicated in Fig. 8-2B. Each center location is shared by an irrotational and by a solenoidal basis field. These irrotational and solenoidal fields were derived as described in Section 2 from a set of bivariate Gaussians with variance $\sigma = 1.67$ (in grid-step units). Therefore, there was a significant degree of overlap between contiguous basis fields. Fig. 8-2C shows

the Hinton's diagram of the connection weights corresponding to $W = \Phi^{-1}$ (Moore–Penrose solution). Each weight is represented by a square with area proportional to the weight size in absolute value. Empty and filled squares represent, respectively, positive and negative weights. Fig. 8-2D shows the approximating field for the set of examples shown in Fig. 8-2A, corresponding to this least squares solution. Fig. 8-2E and F show, respectively, the irrotational and the conservative component of the approximating field. Note that these components correspond to a pattern converging at a single point and a pattern circulating around a different location. The learning algorithm (8.13) can be used to derive an acceptable, although not optimal, approximation field after a relatively small number of iteration. This number of iterations depends on the dimension of the weight space– that is on the square of the number of basis fields. The weight matrix obtained after 3002 iterations of the learning rule is shown in Fig. 8-2G. Learning started from an initial random state of the connections. After 3002 iterations, some of the features of the least–squares matrix have begun to develop, although the overall patterns of Fig.8-2C and G are still fairly different. Fig. 8-2H, I and L show the total approximating field, its irrotational and solenoidal components obtained at this early stage of learning. This approximation is visibly less accurate (and smooth) than the least–square approximation. However one can see that the most relevant qualitative features of the least–square approximation have already emerged.

8.4 Summary and Conclusions

Vector–field approximation can be formulated as an auto–association problem: given a set of (input) vectors at a number of sampling locations, the task is to find a mapping whose output reproduces "at best" (for example, in the sense of least squares) the input vectors at the same sampling locations. We investigated a network architecture, the "field combination network" that is capable of performing this auto–association task. Field combination networks are based on the idea of representing a vector–valued mapping as a combination of local basis fields [82]. Basis fields are the

vectorial equivalent of basis functions: their linear combination defines a vector space of continuous fields. Starting from a set of scalar basis functions one may derive two classes of basis fields: (a) irrotational basis fields and (b) solenoidal basis fields. These two classes provide a rich vocabulary for expressing a broad repertoire of continuous vector–valued mappings. In a field reconstruction network, the task of learning this whole repertoire is accomplished by inverting a square matrix expressing the mutual correlation of the network's basis fields.

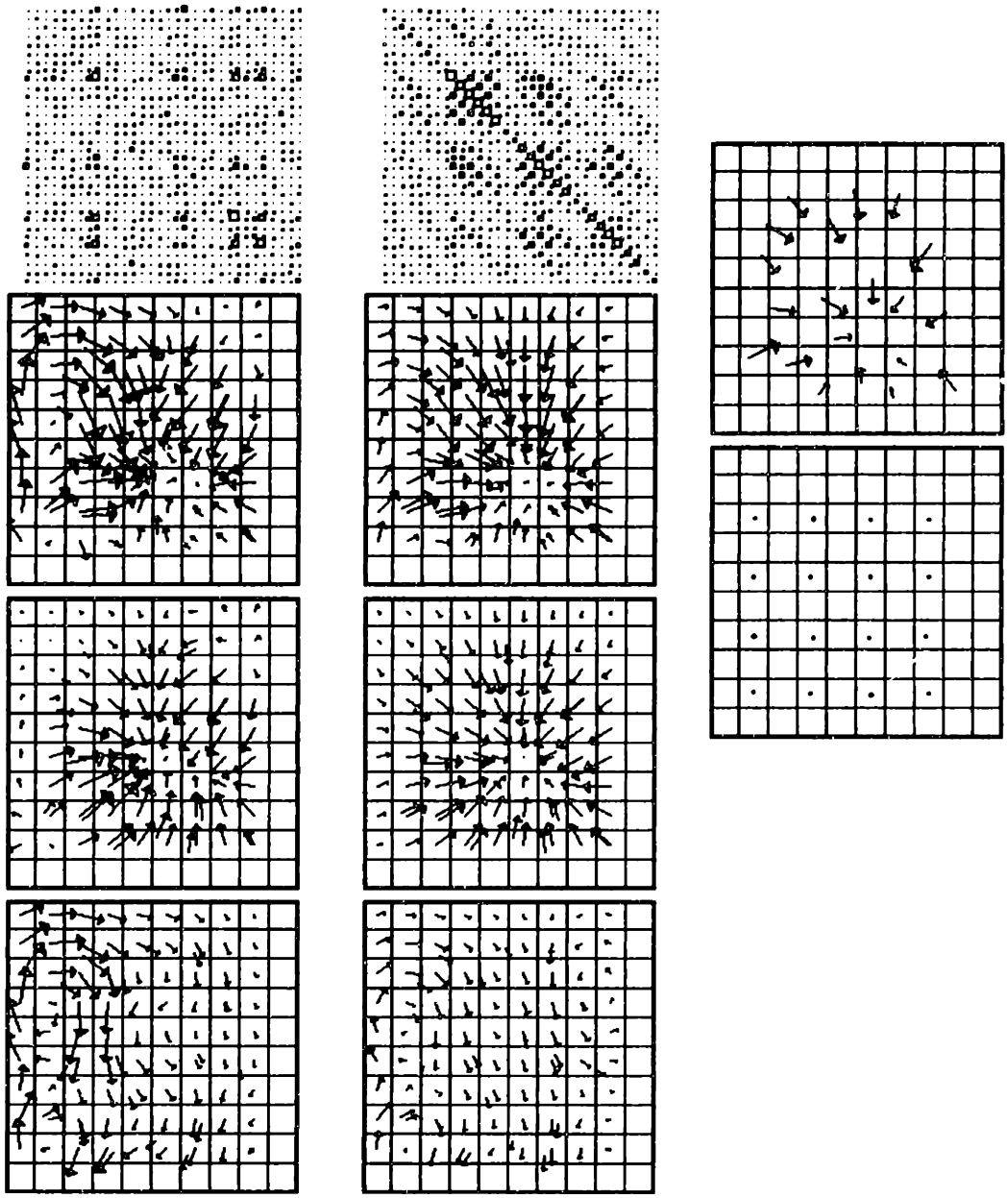

Figure 8-2: Simulation results.

Chapter 9

Conclusions

This thesis indicates that movement can be interpreted as a linear combination of motor primitives. Such primitives can be modeled as torque fields, which provide a mapping from the state of the limb to the torques needed to generate the desired behavior. This schema is consistent with psychophysical results, simulations, and physiological findings in the spinal cord.

We used adaptation to viscous loads as a paradigm to investigate how the central nervous system represents outside perturbations. Our psychophysical results are consistent with the hypothesis that the motor-control system builds a model of the environment as a map between experienced sensory input and the output forces necessary to counterbalance external perturbations.

In addition, we found that motor adaptation is local: subjects were able to compensate for perturbations not only over the experienced states, but the adaptation decayed smoothly and quickly with increasing distance from the locations where disturbances were sensed by the moving limb. We found that the extent of local adaptation could be tuned by training.

Furthermore, our experiments indicate that motor adaptation is encoded in intrinsic coordinates (muscles or joints). Consequently, a change in the arm configuration produced effects on learning even though the same end point posture was preserved.

Adaptation is by no means exclusive to humans. Our experiments showed that monkeys were able to adapt to viscous perturbations, and that their pattern of adap-

tation closely resembled what had been observed in humans.

We developed a model of adaptation based on the constraints of locality, smoothness and representation in intrinsic coordinates—which derived from psychophysics. We simulated the psychophysical experiments adding linearly the torques predicted by the model to the torques necessary to execute unperturbed movements. Simulations results showed that the identified constraints and linearity were enough to successfully reproduce the psychophysical results.

Having proposed a primitive-based schema, we have shown that it can be easily implemented as a superposition of spinal primitives. We have shown that the linearity is not a consequence of the limb biomechanics but an emergent property of the control. We proposed a neural network which solved the problem of mapping adaptation primitives onto spinal primitives.

In conclusion, this thesis indicates that adaptation and movement can be expressed as a superposition of motor primitives.

Bibliography

[1] E.D. Adrian. Afferent areas in the cerebellum connected with the limbs. *Brain*, 66:289–315.

[2] G.E. Alexander and M.D. Crutcher. Preparation for movement: Neural representations of intended direction in three motor areas of the monkey. *J. of Neurophys.*, 64(1):133–149, July 1990.

[3] H. Asanuma and I. Rosen. Topographical organization of cortical efferent zones projecting to distal forelimb muscles in the monkey. 1972.

[4] J. Baillieul. Kinematic programming alternatives for redundant manipulators. In *Proceedings of the IEEE International Conference on Robotics and Automation*, pages 722–728, St. Louis, MO, USA, 1985.

[5] C. Bishop. Improving the generalization properties of radial basis function neural networks. *Neural Computation*, 3:579 - 588, 1991.

[6] E. Bizzi, N. Accornero, W. Chapple, and N. Hogan. Posture control and trajectory formation during arm movement. *Journal of Neuroscience*, 4:2738 - 2744, 1984.

[7] E. Bizzi, F.A. Mussa-Ivaldi, and S.F. Giszter. Computations underlying the execution of movement: A biological perspective. *Science*, 253:287 - 291, 1991.

[8] E. Bizzi, F.A. Mussa-Ivaldi, and S.F. Giszter. Computations underlying the execution of movement: A biological perspective. *Science*, 253:287 - 291, 1991.

[9] T. Brashers-Krug. *Consolidation in human motor memory.* PhD thesis, Massachusetts Institute of Technology, 1995.

[10] T. Brashers-Krug, R. Shadmehr, and E. Todorov. Catastrophic interference in human motor learning. In *Advances in Neural Information Processing*, volume 7. 1995.

[11] K. Brodmann. *Vergleichende Localizationslehre der Grosshirnrinde in ihren Prinzipien dargestellt auf Grund des Zeelenbaues.* Barth, Lipzig, 1909.

[12] D.S. Broomhead and D. Lowe. Multi–variable functional interpolation and adaptive networks. *Complex Systems*, 2:321 – 355, 1988.

[13] W.R. Bruce. Conditions of transferof training. *J. of Exp. Psych.*, 16(3):343–361, 1933.

[14] H. Buelthoff and S. Edelman. Psychophysical support for a two-dimensional view intepolation theory of object recognition. *PNAS*, (89):60–64, 1992.

[15] H.H. Buelthoff, S.Y. Edelman, and M.J. Tarr. How are three-dimensional objects represented in the brain? *Cerebral Cortex*, 3:247–260, 1995.

[16] R Caminiti, P. B. Johnson, C. Galli, S. Ferraina, and Y. Burnod. Making arm movements within different parts of space: the premotor and motor cortical representation of a coordinate system for reaching to visual targets. *The Journal of Neuroscience*, 11(5):1182–1197, May 1991.

[17] E. Colgate and N. Hogan. An analysis of contact instability in terms of passive physical equivalents. In *IEEE Proc International Conference on Robotics and Automation*, pages 404 – 409, 1989.

[18] C. Desai, G. Garriga, S.L. McIntire, and H.R. Horovitz. A genetic pathway for the development of the caenorhabditis elegans hsn motor neurons. 1990.

[19] J.P. Donoghue, S. Leibovic, and J.N. Sanes. Organization of the forelimb area in squirrel monkey motor cortex: representation of digit, wrist and elbow muscles. *Exp. Brain Res.*, 89:1–19, 1992.

[20] R. Durbin and D.E. Rumelhart. Produc units: A computationally powerful and biologically plausible extension to backpropagation networks. *Neural Computation*, 1:133 - 142, 1989.

[21] D. Durlach. Auditory localization in teleoperator and virtual environment systems: ideas, issues and problems. *Perception*, 20:543–554, 1991.

[22] EW Evarts, C. Fromm, J Kroeller, and von Ayre Jennings. Motor cortex control of finely graded forces. *J. of Neurophysiology*, 49(5):1199–1215, May 1983.

[23] A.G. Feldman. Functional tuning of the nervous system during control of movement or maintenance of a steady posture. ii. controllable parameters of the muscles. iii. mechanographic analysis of the execution by man of the simplest motor task. *Biophysics*, 11:565 - 578, 766 - 775, 1966.

[24] A. Fiorentini and N. Berardi. Perceptual learning specific for orientation and spatial frequency. *Nature*, 28, Sept 1980.

[25] Fisher. Intersensory localisation in three modalities. *Bulletin British Psychological Society*, 4:24–25, 1960.

[26] J. R. Flanagan and A. K. Kao. Learning non-linear visuomotor mappings. In *ABSTRACTS*, volume 21, page 1922. Society for Neuroscience, 1995.

[27] T. Flash. The control of hand equilibrium trajectories in multi-joint arm movements. *Biological Cybernetics*, 57:257 - 274, 1987.

[28] T. Flash and I. Gurevich. Human motor adaptation to external loads. In *Annual International Conference of the IEEE Engineering in Medicine and Biology Society*, volume 13, pages 885–886, 1991.

[29] T. Flash and N. Hogan. The coordination of arm movements: An experimentally confirmed mathematical model. *Journal of Neuroscience*, 5:1688 - 1703, 1985.

[30] S.C. Gandevia, R.M. Enoka, D.G. Stuart A.J. McComas, and C.K. Thomas. Neurobiology of muscle fatigue: Advances and issues. *Advances in experimental medicine and biology.*, 384:515, 1995.

[31] F. Gandolfo, F.A. Mussa-Ivaldi, and E. Bizzi. Selectivity of adaptation in motor learning. In *ABSTRACTS*, volume 21, page 1922. Society for Neuroscience, 1995.

[32] A. P. Georgopoulos. Behavioral neurophysiology of the motor cortex. *J. Lab. Clin. Med.*, 124(6):766–774, December 1994. review paper.

[33] A. P. Georgopoulos, Smyrnis J. Ashe, and M. Tiara. The motor cortex and the coding of force. *Science*, 256:1692–1695, June 1992.

[34] A.P. Georgopoulos, J.F. Kalaska, R. Caminiti, and J. T. Massey. On the relations between the direction of two-dimensional arm movements and cell discharge in primate motor-cortex. *Journal of neuroscience*, 2:1527–1537, November 1982.

[35] Z. Ghahramani. *Computation and Psychophysics of Sensorimotor Integration.* PhD thesis, Massachusetts Institute of Technology, 1995.

[36] Z Ghahramani, D M Wolpert, and M I Jordan. Generalization to local remapping of the visuo-motor coordinate transformation. *J. of Neurosci.*, 1996, In Press.

[37] C. Ghez. *Principles of neural science. Voluntary Movement*, chapter 40, pages 609–625. Elsevier, third edition, 1991.

[38] M.F. Ghilardi, J. Gordon, and C. Ghez. Learning a visuomotor transformation in a local area of work space produces directional biases in other areas. 73(6):2535–2539, 1995.

[39] F. Girosi. On some extensions of radial basis functions and their applications in artificial intelligence. *International Journal of Computer and Mathematics with Applications*, 24(12):61–80, 1992.

[40] F. Girosi and T. Poggio. Networks and the best approximation property. *Biological Cybernetics*, 63:169 – 176, 1990.

[41] F. Girosi, T. Poggio, and B. Caprile. Extensions of a theory of networks for approximation and learning. *Advances in neural information processing systems*, 3:750–756, 1991.

[42] S.F. Giszter, E. Bizzi, and F.A. Mussa-Ivaldi. Motor organization in the frog's spinal cord. In D. C. Demo and F. H. Eeckman, editors, *Analysis and Modeling of Neural Systems*. Kluwer Academic Publishers, Norwell, MA, 1991.

[43] S.F. Giszter, F.A. Mussa-Ivaldi, and E. Bizzi. Equilibrium-point mechanisms in the spinal frog. In M. A. Arbib and J. P. Ewert, editors, *Visual Structures ad Integrated Functions*, pages 223 – 237. Springer-Verlag, 1991.

[44] S.F. Giszter, F.A. Mussa-Ivaldi, and E. Bizzi. Equilibrium-point mechanisms in the spinal frog. In M. A. Arbib and J. P. Ewert, editors, *Visual Structures ad Integrated Functions*, pages 223 – 237. Springer-Verlag, 1991.

[45] S.F. Giszter, F.A. Mussa-Ivaldi, and E. Bizzi. Convergent force fields organized in the frog's spinal cord. *Journal of Neuroscience*, 1993.

[46] A. Goswami and M.A. Peshkin. A task-space formulation of passive force control. In *Proceedings of the 1991 IEEE International Symposium on Intelligent Control*, pages 95–100, Arlington, VA, 1991.

[47] A.M. Graybiel, T. Aosaki, A.W. Flaherty, and M. Kimura. The basal ganglia and adaptive motor control. *Science*, 265:1826–1831, September 1994.

[48] M.S.A. Graziano and C.G. Gross. A bimodal map of space: somatosensory receptive fields in the macaque putamen with corresponding visual receptive fields. *Exp. Brain Res.*, 97:96–109, 1993.

[49] M.S.A. Graziano, G.S. Yap, and C.G. Gross. Coding for visual space by premotor neurons. *Science*, 266:1054–1057, Nov. 1994.

[50] C.G. Gross. *Handbook of sensory physiology*, chapter Visual functions of the inferotemporal cortex, pages 451–482. Springer, Berlin, 1973.

[51] W. Härdle. *Applied nonparametric regression*, volume 19 of *Econometric Society Monographs*. Cambridge University Press, 1990.

[52] R. Held. *Adaptation to rearrangement and visual-spatial aftereffects*, volume 6 of *Psychologische Beitraege*, pages 439–450. 1962.

[53] R. Held and J. A. Bauer. Development of sensorially-guided reaching in infant monkeys. *Brain Research*, 71:265–271, 1974.

[54] N. Hogan. An organizing principle for a class of voluntary movements. *Journal of Neuroscience*, 4:2745 - 2754, 1984.

[55] N. Hogan. Impedance control: an approach to manipulation: Parts i, ii, iii. *ASME Journal of Dynamic Systems, Measurement and Control*, 107:1 - 24, 1985.

[56] N. Hogan. The mechanics of multi-joint posture and movement control. *Biological Cybernetics*, 52:315 - 331, 1985.

[57] J. M. Hollerbach and K.C. Suh. Redundancy resolution of manipulators through torque optimization. In *Proceedings of the IEEE International Conference on Robotics and Automation*, pages 1016–1021, St. Louis, MO, USA, 1985.

[58] J. Ilmberger and E. Endrich. Motor learning, bimanual transfer and isochrony in a tracking task. In *ABSTRACTS*, volume 21, page 1922. Society for Neuroscience, 1995.

[59] H. Imamizu, Y. Uno, and M. Kawato. Adaptive internal model of intrinsic coordinates transformation during learning of a reaching task. In *ABSTRACTS*, volume 21. Society for Neuroscience, 1995.

[60] M. Ito. *The Cerebellum and Neural Control.* Raven Press, New York, 1984.

[61] J.H. Jackson. *Selected Writings of John Hughlings Jackson.* J. Taylor ed, London, 1931-1932.

[62] R.A. Jacobs, M.I. Jordan, S.J. Nowlan, and G.E. Hinton. Adaptive mixtures of local experts. *Neural Computation*, 3:79 - 87, 1991.

[63] M. Jordan and Rumelhart. Forward models: Supervised learning with distal teacher. *Cognitive Science*, 16:307–354, 1992.

[64] J.H. Kaas, M.M. Merzenich, and H.P. Killackey. The reorganization of somatosensory cortex following peripheral nerve damage in adult and developing mammals. *Annual Rev. Neurosci.*, 4:1–24, 1993.

[65] J.H. Kaas, R.J. Nelson, M. Sur, and M.M. Merzenich. Multiple representation of the body within the primary somatosensory cortex of primates. *Science*, 204:521–523, 1981.

[66] J.F. Kalaska, D.A.D. Cohen, and M.L.Hyde. A comparison of movement directio-related versus load direction-related activity in primate motor cortex, using a two-dimensional reaching task. *J.of Neurosci.*, 9(6):2080–2102, June 1989.

[67] E. R. Kandel, J. H. Schwartz, and T. M. Jessel. *Principles of neural science.* Elsevie, third edition, 1991.

[68] O. D. Kellogg. *Foundations of Potential Theory.* Dover, New York, NY, 1953.

[69] J.A.S. Kelso and K. G. Holt. Exploring a vibratory system analysis of human movement production. *Journal of Neurophysiology*, 43:1183 - 1196, 1980.

[70] C.A. Klein and C.H. Huang. Review of pseudoinverse control for use with kinematically redundant manipulators. *IEEE Transactions on System, Man and Cybernetics*, SMC–13:245–250, 1983.

[71] J.R. Lackner and P. Dizio. Rapid adaptation to coriolis force perturbations of arm trajectory. *J. of Neurophys.*, 72, July 1994.

[72] D. Lewis, A. Shepherd, and J. Adams. Evidence of associative interference in psychomotor performance. *Science*, 110:271–273, 1949.

[73] N.K. Logothetis and J. Pauls. Psychophysical and physiological evidence for viewer-centered object representations in the primate. *Cerebral Cortex*, 3:270–288, 1995.

[74] N.K. Logothetis and D.L. Sheinberg. Visual object recognition. *Annual review of neuroscience*, 19, 1996.

[75] G. Luppino, M. Matelli, and G. Rizzolatti. Cortico-cortical connections of two electrophysiologically identified arm representations in the mesial agranular frontal cortex. *Exp. Brain Research*, 82:214–218, 1990.

[76] W.H. Marshall, C.N. Woolsey, and P. Bard. Observations on cortical somatic sensory cortex. *J. Neurophisiol.*, 4:1–24, 1941.

[77] A J McComas. Is voluntary motor drive affected by fatigue of a synergic muscle. *Muscle and nerve*, 4//Supp:S49, 1996.

[78] C. Miall, D. Weir, D. Wolpert, and J. Stein. Is the cerebellum a smith predictor? *J. of Motor Behavior*, 25(3):203–216, 1993.

[79] B. Milner. Visual recognition and recall after right temporal excision in man. *Neuropsychologia*, 6:191–209, 1968.

[80] B. Milner. *Nerve cells, transmitters and behaviour*, chapter Complementary functional specialization of the human cerebral hemispheres, pages 601–625. Vatican City: Pontificiae Academiae Scientiarium Scripta Varia, 1980.

[81] P. Morasso. Spatial control of arm movements. *Exp. Brain Res.*, 42, 1981.

[82] F. A. Mussa-Ivaldi. From basis functions to basis fields: Using vector primitives to capture vector patterns. *Biological Cybernetics*, 1992.

[83] F. A. Mussa-Ivaldi, E. Bizzi, and S. F. Giszter. Transforming plans into actions by tuning passive behavior: A field-approximation approach. In *Proceedings of the 1991 IEEE International Symposium on Intelligent Control*, pages 101 - 109, Arlington, VA, 1991.

[84] F. A. Mussa-Ivaldi and N. Hogan. Integrable solutions of kinematic redundancy via impedance control. *The International Journal of Robotics Research*, 10:481 -491, 1991.

[85] F.A. Mussa-Ivaldi and F. Gandolfo. Networks that approximate vector-valued mappings. *IEEE Int. Conf. Neural Networks*, pages 1973–1978, 1993.

[86] F.A. Mussa-Ivaldi and S.F. Giszter. Vector field approximation: A computational paradigm for motor control and learning. *Biological Cybernetics*, 1992.

[87] F.A. Mussa-Ivaldi, N. Hogan, and E. Bizzi. Neural, mechanical and geometrical factors subserving arm posture in humans. *Journal of Neuroscience*, 5:2732 - 2743, 1985.

[88] E. A. Nadaraya. On estimating regression. *Theory prob. Appl.*, 10:186–190, 1964.

[89] W. Penfield and T. Rasmussen. *The Cerebral Cortex of Man: A Clinical Study of Localization of Function.* Macmillan, 1950.

[90] T. Poggio and S. Edelman. A network that learns to recognize 3d objects. *Nature*, 343:263 - 266, 1990.

[91] T. Poggio, M. Fahle, and S. Edelman. Fast perceptual learning in visual hyperacuity. *Science*, 256(5059):1018–1020, May 1992.

[92] T. Poggio and F. Girosi. Networks for approximation and learning. *Proc. of the IEEE*, 78:1481 - 1497, 1990.

[93] T. Poggio and F. Girosi. A theory of networks for learning. *Science*, 247:978–982, 1990.

[94] J. R. Rice. *The Approximation of Functions.* Addison-Wesley, Reading, MA, 1964.

[95] G. Rizzolatti, M. Gentilucci, R. Camarda, V. Gallese, G. Luppino, M. Matelli, and L. Fogassi. Neurons related to reaching-grasping arm movements in the rostal part of area 6 (area 6abeta). *Experimental brain research*, 82(2):337–350, October 1990.

[96] E. M. De Robertis, G. Oliver, and C.V.E. Wright. Homeobox genes and the vertebrate body plan. *Sci. Am*, 263(1):46–52, 1990.

[97] A. Roby-Brami and Y. Burnod. Learning a new visuo-motor transformation: error correction and generalization. *Cognitive Brain Research*, 2:229–242, 1995.

[98] R. L. Sainburg and C. Ghez. Limitations in the learning and generalization of multi-joint dynamics. In *ABSTRACTS*, volume 21, page 686. Society for Neuroscience, 1995.

[99] R.L. Sainburg, M.F. Ghilardi, H Poizner, and C. Ghez. Control of limb dynamics in normal subjects and patients without proprioception. 73(2):820–835, 1995.

[100] J.N. Sanes, S. Suner, and J.P. Doneghue. Dynamic organization of primary motor cortex output to target muscles in adult rats: I. long-term patterns of reorganization following motor or mixed peripheral nerve lesions. *Exp. Brain Res.*, 79:479–491, 1990.

[101] J.N. Sanes, S. Suner, and J.P. Doneghue. Dynamic organization of primary motor cortex output to target muscles in adult rats: Ii. rapid reorganization following motor nerve lesions. *Exp. Brain Res.*, 79:492–503, 1990.

[102] A.B. Schwartz, R. E. Kettner, and A. P. Georgopoulos. Primate motor cortex and free arm movements to visual targets in three-dimensional space. i. relations between single cell discharge and direction of movement. *The Journal of Neuroscience*, 8(8):2913–2927, August 1988.

[103] S H Scott and J F Kalaska. Changes in motor cortex activity during reaching movements with similar hand paths but different arm postures. *Journal of neurophysiology.*, 73(6):2563, 1995.

[104] R. Shadmehr, F. A. Mussa-Ivaldi, and E. Bizzi. Postural force fields of the human arm and their role in gener ating multijoint movements. *The Journal of neuroscience*, 13(1):45, January 1993.

[105] R. Shadmehr and F.A. Mussa-Ivaldi. Adaptive representation of dynamics during learning of a motor task. *J. of Neurosci.*, 14(5):3208–3224, May 1994.

[106] G.M. Shambes, J.M. Gibson, and W. Welcher. Fractured somatotopy in granule cells tactile areas of rat cerebellar hemispheres revealed by micromapping. *Brain Behav evol.*, 15:94–140.

[107] T. Shamir and Y. Yomdin. Repeatability of redundant manipulators: Mathematical solution of the problem. *IEEE Transactions on Automatic Control*, 33:1004 - 1009, 1988.

[108] J. Sutton and A. Barton. Toward a modern theory of adaptive networks: execution and prediction. *Psych. Review*, 88:135–170, 1981.

[109] W.T. Thach and S.A. Kane. *Cerebellar Output: Multiple Maps and Modes of Control in Movement Coordination.* Ramon-y Cayal Centennary. Springer, Berlin, 1991.

[110] A. N. Tikhonov and V. Y. Arsenin. *Solutions of Ill-posed Problems.* W. H. Winston, Washington, DC, 1977.

[111] Y. Uno, M. Kawato, and R. Suzuki. Formation and control of optimal trajectory in human multiple arm movement: minimum-torque-change model. *Biol. Cyb.*, 61:89–101, 1989.

[112] R.J. van Beers, A.C. Sitting, and J.J. Dernier van der Gon. The combination of visual and proprioceptive information about the position of the hand. In

Neural Control of Movement. Abstracts of the 6th annual meeting., page 18. Marco Island, Fl., April 1996.

[113] T. Vilis and J. Hore. Effects of changes in mechanical state of limb in cerebellar intention tremor. *J.Neurophysiol.*, 40:1214–1224, 1977.

[114] Y. Wada and M. Kawato. A neural network for arm trajecotry formation using. Technical Report 1992.5.21, ATR, 1992.

[115] G. Wahba. Vector splines on the sphere, with application to the estimation of vorticity and divergence from discrete noisy data. In W. Schempp and K. Zeller, editors, *Multivariate Approximation Theory*, pages 407 – 429. Birkhauser Verlag, 1982.

[116] C. W. Wampler. Inverse kinematics functions for redundant manipulators. In *Proceedings of the IEEE International Conference on Robotics and Automation*, pages 610–617, Raleigh, NC, USA, 1987.

[117] G.S. Watson. *Smooth regression analysis.* A. Sankya, 1964.

[118] R. Welch. *Handbook of perception and performance*, volume 1, chapter Adaptation to space perception. Wiley-Interscience, 1986.

[119] D. E. Whitney. Resolved motion rate control of manipulators and human prostheses. *IEEE Transactions on Man-Machine Systems*, MMS–10:47–53, 1969.

[120] M. A. Wilson and B. L. McNaughton. Dynamics of the hippocampal ensemble code for space. *Science*, 261:1055–1058, August 1993.

[121] M. A. Wilson and B. L. McNaughton. Reactivation of hippocampal ensemble memories during sleep. *Science*, 265(5172):676, 1994.

[122] D. M. Wolpert, Z. Ghahramani, and M. I. Jordan. Perceptual distortion contributes to the curvature of human reaching movements. *Experimental brain research.*, 98(1):153, 1994.

[123] C.N. Woolsey. *Organization of somatic sensory and motor areas of the cerebral cortex*, pages pp63–81. Biological and Biochemical Basis of Beahvior. University of Wisconsin Press, h.f. harlow and c.n. woolsey (ed) edition, 1958.

[124] T Yoshikawa. *Fundations of Robotics. Analysis and Control.* The MIT Press, 1990.